Final Technical Report

Project Title:	**Effects of Impurities on Fuel Cell Performance and Durability**
DOE AWARD NO.:	**DE-FG36-07GO17011**
Covering period:	**Feb. 15, 2007 to Sept. 30, 2011**
Date of Report:	**Nov. 14, 2011**
Recipient Organization:	**Clemson University**
Partners:	**Savannah River National Lab, John Deere**
Technical Contact:	**Dr. James G. Goodwin, Jr.** **Professor** **Department of Chemical & Biomolecular Engineering** **Clemson University** **Clemson, SC 29634-0909** **864-656-6614 (office)** **864-656-0784 (fax)** **jgoodwi@clemson.edu**
Business Contact:	**Bettie McGowan-Hudson, CRA** **Senior Sponsored Programs Administrator** **Clemson University** **Office for Sponsored Programs** **300 Brackett Hall** **Clemson, SC 29634-5702** **864 656 4305 voice** **864 656 0881 fax** **mcgowab@clemson.edu**

EXECUTIVE SUMMARY

The main objectives of this project were to investigate the effect of a series of potential impurities on fuel cell operation and on the particular components of the fuel cell MEA, to propose (where possible) mechanism(s) by which these impurities affected fuel cell performance, and to suggest strategies for minimizing these impurity effects. This project was carried out primarily at Clemson University and the Savannah River National Lab. Fuel cell investigations were done at SRNL while all investigations of the MEA components were carried out at Clemson. Meetings took place weekly at Clemson University and at SRNL with the respective project participants. Joint meetings between researchers at Clemson and SRNL took place quarterly, on average. In addition, frequent communications among project participants took place via e-mail and telephone discussions. On other occasions the researchers met with the technical staff of John Deere for discussions. At least one member of our team routinely participated in the DOE-Sponsored Joint Hydrogen Quality Task Force Meetings (usually conducted monthly).

The nature and concentrations of impurities investigated and their impact on fuel cell performance and individual components are given in the table below. The negative effect on Pt/C was to decrease hydrogen surface coverage and hydrogen activation at fuel cell conditions. The negative effect on Nafion components was to decrease proton conductivity, primarily by replacing/reacting with the protons on the Bronsted acid sites of the Nafion.

Even though already well known as fuel cell poisons, the effects of CO and NH_3 were studied in great detail early on in the project in order to develop methodology for evaluating poisoning effects in general, to help establish reproducibility of results among a number of laboratories in the U.S. investigating impurity effects, and to help establish lower limit standards for impurities during hydrogen production for fuel cell utilization.

New methodologies developed included (1) a means to measure hydrogen surface concentration on the Pt catalyst (HDSAP) before and after exposure to impurities, (2) a way to predict conductivity of a Nafion membranes exposed to impurities using a characteristic acid catalyzed reaction (methanol esterification of acetic acid), and, more importantly, (3) application of the latter technique to predict conductivity on Nafion in the catalyst layer of the MEA. H_2-D_2 exchange was found to be suitable for predicting hydrogen activation of Pt catalysts.

Using a combination of standard catalyst characterization techniques, a structure sensitive catalytic reaction technique (cyclopropane hydrogenolysis), and reaction and transport modeling led to the finding that in the catalyst layer (essentially Nafion/Pt/C) the following best describes the structure. Pt is highly dispersed on the C support, but primarily in the meso- and macro-pores. The Nafion (ca. 30 wt%) resides primarily on the external surface of the C support where it blocks significant numbers of micropores, but only partially blocks the pore openings of the meso- and macro-pores wherein lie the small Pt particles (crystallites). For this reason, even with 30 wt% Nafion on the Pt/C, few Pt sites are blocked and, hence, are accessible for hydrogen activation.

Of the impurities studied, CO, NH_3, perchloroethylene (also known as tetrachloroethylene), tetrahydrofuran, diborane, and metal cations had significant negative effects on the components in a fuel cell. While CO has no effect on the Nafion, it significantly poisons the Pt catalyst by adsorbing and blocking hydrogen activation. The effect can be reversed with time once the flow of CO is stopped.

NH_3 has no effect on the Pt catalyst at fuel cell conditions; it poisons the proton sites on Nafion (by forming NH_4^+ cations), decreasing drastically the proton conductivity of Nafion. This poisoning can slowly be reversed once the flow of NH_3 is stopped.

Perchloroethylene has a major effect on fuel cell performance. Since it has little/no effect on Nafion conductivity, its poisoning effect is on the Pt catalyst. However, this effect takes place primarily for the Pt catalyst at the cathode, since the presence of oxygen is very important for this poisoning effect.

Tetrahydrofuran was shown not to impact Nafion conductivity; however, it does affect fuel cell performance. Therefore, its primary effect is on the Pt catalyst. The effect of THF on fuel cell performance is reversible.

Diborane also can significant affect fuel cell performance. This effect is reversible once diborane is removed from the inlet streams.

H_2O_2 is not an impurity usually present in the hydrogen or oxygen streams to a fuel cell. However, it is generated during fuel cell operation. The presence of Fe cations in the Nafion due to system corrosion and/or arising from MEA production act to catalyze the severe degradation of the Nafion by H_2O_2.

Finally, the presence of metal cation impurities (Na^+, Ca^{2+}, Fe^{3+}) in Nafion from MEA preparation or from corrosion significantly impacts its proton conductivity due to replacement of proton sites. This effect is not reversible.

Not surprisingly, inert and relatively inert gases like He, Ar, N_2, CO_2 have little or no effect beyond acting as a diluents. Light paraffins (C3-C7) also do not seem to have any impact on Pt or Nafion at typical fuel cell conditions. More reactive hydrocarbons, such as ethylene, might be expected to affect Pt or Nafion but do not at a typical fuel cell temperature of 80^oC. In the presence of large quantities of hydrogen on the anode side, ethylene is converted to ethane which is very nonreactive. More surprisingly, even more reactive hydrocarbons such as formic acid and acetaldehyde do not appear to react enough with the strong Bronsted acid sites on Nafion at such low temperatures to affect Nafion's conductivity properties.

These results clearly identify a number of impurities which can have a detrimental impact on fuel cell performance, although some are reversible. Obviously, fuel cells exposed to impurities/poisons which are reversible can recover their original performance capabilities once the impurity flow is stopped. Impurities with irreversible effects should be either minimized in the feed streams, if possible, or new catalytic materials or ion conductors will need to be used to minimize their impact.

Impurities Studied	Max. Conc. Tested	Max. Partial Pressure (atm)	Effect on FC Performance	Component Studies	
				Effect on Pt/C	Effect on Nafion Conductivity
Inerts (N_2, Ar, He)	50 – 80%	1.0 – 1.6	No	No	No
CO_2	500 ppm	0.0005	*ND*	No	No
CO	2-50 ppm	to 0.00005	Major	Major	No
NH_3	10-5000 ppm	to 0.005	Major	Minimal	Major
Formic acid	400 ppm	0.0004	*ND*	*ND*	No
Ethylene	400 ppm	0.0004	*ND*	No	No
Acetaldehyde	250 ppm	0.00025	*ND*	*ND*	No
Perchloroethylene	30-400 ppm	0.0004	Major	Major	No
Tetrahydrofuran (THF)	400 ppm	0.0004	Yes –but reversible	*ND*	No
Propane (C_3H_8)	100 ppm	0.0001	No	Minimal	No
Butane (C_4H_{10})	100 ppm	0.0001	No	Minimal	No
Pentane (C_5H_{12})	100 ppm	0.0001	No	Minimal	No
Hexane (C_6H_{14})	100 ppm	0.0001	No	Minimal	No
Heptane (C_7H_{16})	100 ppm	0.0001	No	Minimal	No
Diborane (B_2H_6,)	50 ppm	0.00005	Yes –but reversible	*ND*	*ND*
hydrogen peroxide (H_2O_2)	30% H_2O_2 aq. soln. for 4–72 h	NA	*ND*	*ND*	Major
Cations (Na^+, Ca^{2+}, Fe^{3+})	NA	NA	Major [Ref. (1)-(3)]	Minimal	Major

ND = not determined
NA = not applicable
(1) B. S. Pivovar et al., *Handbook of Fuel Cells*. (Wiley, 2009)
(2) B. L. Kienitz et al., Electrochim. Acta 54 (2009) 1671
(3) T. A. Greszler et al., *Handbook of Fuel Cells*. (Wiley, 2009)

TABLE OF CONTENTS

1.0 INTRODUCTION

A fuel cell is an electrochemical energy conversion device that produces electricity during the combination of hydrogen and oxygen to produce water. Among the different types of fuel cells, proton exchange membranes fuel cells (PEMFC) are favored for portable applications as well as stationary ones due to their high power density, low operating temperature, and low corrosion of components [Fuel Cell Handbook 2000]. However, commercialization of proton exchange membrane fuel cell (PEMFC) technology requires cost-effective electrocatalysts used in the gas diffusion electrodes (GDEs). Current electrocatalysis for PEMFC research focuses on reducing loading, optimizing reactant diffusivity, ionic and electrical conductivity, and the level of hydrophobicity as well as the resiliency of catalysts [Litster 2004]. Various catalyst layer fabrication approaches such as PEFE-bound, thin-film, vacuum deposition, and electrodeposition methods have been developed. Currently, thin-film methods are widely employed for fabricating catalyst layers for PEMFCs with catalyst loadings less than 0.35 mg/cm^2 [Wilson 1993]. In this method, carbon-supported Pt is mixed with Nafion solution and other solvents to form an adequately viscous ink, which is then applied to both sides of a Nafion membrane. Recently, ultra thin catalysts with platinum loadings as low as 0.014 mg/cm^2 have been reported using novel sputtering methods [Cha 1999, O'Hayre 2002].

In real life operation, the use of pure fuel and oxidant gases results in an impractical system. A more realistic and cost efficient approach is the use of air as an oxidant gas and hydrogen from hydrogen carrier molecules (i.e., ammonia, hydrocarbons, hydrides). The short and long term effect of impurities in these gases may have an overriding effect on the fuel cell performance. Even though the hydrogen oxidation reaction occurs at higher rates than the oxygen reduction reaction at the cathode [Um 2000], the effect of impurities in the hydrogen fuel on fuel cell performance can be devastating.

Numerous impurities can be present in hydrogen and oxygen streams used in PEM fuel cells. The impurities in the hydrogen fuel come from the source of the hydrogen and how it is produced. These impurities often include water, hydrocarbons, CO_2, CO, sulfur-containing gases, and ammonia, especially. Impurities present in the environment around the fuel cell are often present in the oxygen stream being fed to the cathode of the fuel cell. These impurities can include, among other things, SO_2, NO_2, H_2S, chlorides, and O_3 [Veldhuis 1998]. Many of these impurities have detrimental effects on fuel cell operation, primarily by blocking sites on the metal catalyst of the electrodes for chemisorption or by interacting with the polymeric material used in the PEM. These trace amounts of impurities can result in a loss in the performance of the fuel cell that can be either permanent or reversible. However, little is known about their mechanisms of interaction with fuel cell components and how they precisely affect fuel cell operation.

References

Cha, S. Y.; Lee, W. M., Journal of the Electrochemical Society 146 (**1999**) 4055–4060.
Fuel Cell Handbook, 5th ed.; EG&G-Services, Parsons Inc., **2000**.

Litster, S., McLean, G., Journal of Power Sources 130 (**2004**) 61-76.
O'Hayre, R.; Lee, S. J.; Cha, S. W.; Prinz, F. B., Journal of Power Sources 109 (**2002**) 483–493.
Um, S., Journal of The Electrochemical Society, 147 (**2000**) 4485-4493.
Veldhuis, J. B. J.; de Bruijn, F. A.; Mallant, R. K. A. M., Proceedings of the Seminar on Fuel Cells, **1998**.
Wilson, M. S.,U.S. Patent 5234777, **1993**.

2.0 PROJECT OBJECTIVES

The project had the objective to investigate the effect of impurities in the hydrogen fuel stream on the operation and durability of fuel cells. The impurities proposed included water, hydrocarbons (including formaldehyde, formic acid), oxygen, inert gases (He, N_2, Ar), CO_2, CO, sulfur-containing gases, ammonia, halogenated compounds and particulates. As part of this study, it was also proposed to delineate the mechanisms of the impurities in affecting the components of the fuel cell catalyst and polymer membrane and, as a secondary objective, to suggest strategies/means to reduce their impact.

3.0 COMPARISON OF THE ACTUAL ACCOMPLISHMENTS WITH THE GOALS AND OBJECTIVES

It was originally proposed to study the effect of the following impurities: water, hydrocarbons (including formaldehyde, formic acid), oxygen, inert gases (He, N_2, Ar), CO_2, CO, sulfur-containing gases, ammonia, halogenated compounds and particulates. Table 3.0 presents a comparison of the impurities proposed to those actually studied. As one can see, by and large, most classes of impurities planned to be investigated were studied at least to some extent. Only two classes proposed were not studied (sulfur-containing gases and particulates). Instead, other investigations were carried out on the effects of metal cations (in Nafion, arising from system corrosion and/or MEA production), H_2O_2 (produced during FC operation and causing degradation of Nafion), diborane (a potential impurity from the decomposition of hydrogen storage boron compounds), and a cyclic hydrocarbon (tetrahydrofuran, a typical solvent) due to the need to better understand their effects. Fewer impurities were able to be investigated in the single fuel cell available to the project due to time spent (1) comparing impurity effects under similar conditions for a standard MEA in order to benchmark all the DOE funded projects on impurity effects for further comparisons and (2) making long term runs at low concentrations of several impurities at the behest of the DOE-Sponsored Joint Hydrogen Quality Task Force, attempting to set impurity level standards for industrial hydrogen generation for fuel cell applications.

Table 3.0: Impurities Proposed and Studied

Impurity Class	Impurities Studied	Fuel Cell Studies	Catalyst Studies	Nafion Studies
Proposed Impurities				
Ammonia	NH_3	studied	studied	studied
CO	CO	studied	studied	studied
CO_2	CO_2	-	-	studied
Water	H_2O	studied in conj. with all impurities	studied in conj. with CO and PCE	studied in conj. with all impurities
Oxygen	O_2	NR	studied in conj. with PCE	-
Inert Gases	N_2	studied	studied	studied
	He/Ar	studied	studied	-
Hydrocarbons	ethane	-	studied	studied
	ethylene	-	studied	studied
	C3-C7 paraffins	-	-	studied
	acetaldehyde	-	-	studied
	formic acid	-	-	studied
Halogenated Compounds	perchloroethylene	studied	studied	studied
S-Containing Gases	-	-	-	-
Particulates	-	-	-	-
Additional Impurities (not originally proposed)				
Metal Cations	Na^+, Ca^{2+}, Fe^{3+}	-	-	studied
Hydrogen Peroxide	H_2O_2	-	-	studied
Hydrocarbon	tetrahydrofuran	studied	studied	studied
Diborane	B_2H_6	studied	-	-

As part of this study, it was also proposed to delineate the mechanisms of the impurities in affecting the components of the fuel cell catalyst and polymer membrane and to suggest strategies/means to reduce their impact. This was done for most of the detrimental impurities studied.

4.0 PROJECT FINDINGS

4.1 Pt/C Catalyst Fundamentals

4.1.1 The Effect of Low Concentrations of CO on H_2 Adsorption and Activation on Pt/C: Part 1 – In the Absence of Humidity

4.1.1.1 Motivation

While the poisoning effect that CO has on PEMFC performance is well documented, there exists differing opinions between the surface science and electrochemical communities regarding the extent and fundamental characteristics of this poisoning. For example, results from high pressure scanning tunneling microscopy (HP STM) and density functional theory (DFT) calculations of adsorption of CO on Pt(111) over the pressure range (P_{CO}) of 10^{-6} to 760 Torr at room temperature show an increase in the ratio of amount of surface CO to Pt_S (CO/Pt_S), where Pt_S indicates exposed surface atoms of Pt, from 0.5 to 0.7 [Longwitz 2004, Andersen 2005, Davies 2004]. In contrast, electrochemical results on Pt electrodes via cyclic voltammetry (CV) suggest a completely covered Pt surface ($\theta_{CO/Pt} = 1$) at much lower CO concentrations of 100 ppm CO in the presence of H_2 [Igarashi 2001, Papageorgopoulos 2002]. However, calculation of surface coverage based on CV measurement of peak currents is imprecise and is not an ideal quantitative technique [Bard 2001].

Due to the number of ambiguities regarding CO poisoning on Pt, such as the ones outlined above, research was carried out to investigate the fundamental effect of CO on H_2 activation on a commercial Pt/C catalyst used in fuel cells. This effect was studied utilizing H_2-D_2 exchange (as a probe reaction related to hydrogen activation) and surface concentration measurements of hydrogen and CO at conventional PEMFC operating conditions (80^oC, 2 atm) and in the absence of humidity. While the presence of humidity would have a notable effect on the adsorption of CO on Pt, as shown qualitatively via ATR-IR and Raman spectroscopy by Ebbesen et al. [Ebbesen 2007] and Ren et al. [Ren 2003], respectively, quantitative measurement of CO surface coverage on Pt using the new methodology involving H_2-D_2 must first be established in the absence of humidity before the additional effects of Nafion and water can be investigated. In addition, measurements in the absence of water vapor permit a more direct comparison to the results on this topic in the surface science literature. Comparison and verification of the exchange reaction as a valid test reaction for the electrocatalytic oxidation of H_2 on Pt can be found elsewhere [Ross 1974].

4.1.1.2 Experimental

A commercial Pt fuel cell catalyst, 20 wt% Pt supported on carbon black (Vulcan XC-72, Cabot Co.) (Pt/C), was purchased from BASF. Nominal composition was confirmed via elemental analysis (performed by Galbraith Laboratories) and energy dispersive x-ray spectroscopy (EDX) (STEM-Hitachi HD2000 equipped with an Oxford INCA Energy

200 EDS). Other characterizations of the catalyst include: BET, static H_2/CO chemisorption, TEM, XRD, FTIR, and TPD.

Results for H_2-D_2 exchange reaction and H_2-D_2 Switch with Ar Purge [HDSAP, see (Zhang 2010) for details of the method] were obtained at 80°C and 2 atm absolute in a conventional plug flow, micro-reactor system. Prior to reaction experiments, all catalyst samples were pretreated at 80°C in H_2 for 3 h.

4.1.1.3 Results and Discussion

Catalyst Characterization

BET surface area, pore size, and pore volume were 225 ± 12 $m^2\ g^{-1}$, 16.4 ± 1.8 nm, and 0.63 ± 0.04 $cm^3\ g^{-1}$ for the carbon support (XC-72), respectively; and 186 ± 5.6 $m^2\ g^{-1}$, 19.7 ± 4.2 nm, and 0.57 ± 0.01 $cm^3\ g^{-1}$ for Pt/C, respectively. Results for XC-72 correspond well to values in the literature [10,11]. While little change was observed for pore size and volume, the addition of Pt to the carbon support reduced the BET surface area by ca. 17%.

Analysis of TEM images indicated a fairly even distribution of Pt particles on XC-72 in the Pt/C catalyst. Average Pt particle size for the as-received Pt/C was determined to be 4.0 ± 0.9 nm. Exposure of Pt/C to H_2 and H_2/Ar at 80°C for 24 h had no effect on its average particle size, suggesting that the sintering process is very slow at 80°C. Similar results were obtained via XRD using the Debye-Scherrer equation and the full width at half maximum (FWHM) of the Pt(111) diffraction peak for both the as-received and pretreated Pt/C (ca. 3 nm and 4 nm, respectively).

Regardless of analysis temperature (35 – 80°C), the amount of CO uptake remained relatively constant (Table 4.1.1-1). This suggests that CO does not spill over onto the carbon support. Average Pt particle size calculated from CO chemisorption is higher than that from the TEM images; the difference in the results is due to the existence of linear and bridge-bonded CO on Pt, such that the overall stoichiometry CO:Pt_S is actually < 1.

Contrary to CO chemisorption results, depending on the analysis temperature (35°C vs. 80°C), the amount of H_2 uptake during H_2 chemisorption varied from 215 μmol H $g.cat^{-1}$ to 255 μmol H $g.cat^{-1}$, respectively. Although both concentrations yield average Pt particle sizes (4.2 – 4.9 nm) within the range observed by TEM, the former is closer to the estimated average size. Thus, due to the probability of H_2 spillover at higher temperatures, especially on a carbon support [Leuking 2004], and considering the CO chemisorption results, the actual concentration of surface Pt atoms on Pt/C is estimated to be approximately 215 μmol H $g.cat^{-1}$. The additional 40 μmol H $g.cat^{-1}$ uptake at 80°C is likely due to hydrogen spillover.

Table 4.1.1-1: Static H_2 and CO chemisorption results at 35 and 80°C for 20 wt% Pt/C[a].

Adsorption Gas	Analysis Temp. (°C)	Amount of CO/H Adsorbed[b] (μmol g.cat^{-1})	Metal Dispersion (%)	Avg. Pt Particle Size (nm)[c]
CO	35	190	19	5.7
	80	200	20	5.4
H_2	35	215	22	4.9
	80	255	26	4.2

[a]Pt/C was pretreated in H_2 at 80°C for 3 h.
[b]Experimental error for all results was ca. ± 3%.
[c]Avg. Pt particle size calculated from:
Avg. Pt Particle Size (nm) $= \frac{1.08}{\text{Metal Dispersion}}$, assuming $CO/Pt_S = 1$ and $H/Pt_S = 1$ [Coloma 1995].

H_2-D_2 Exchange Reaction

In the absence of CO or other impurities, the exchange reaction is equilibrium-limited on even small quantities of Pt catalyst, even at 35°C. For this reason, in the absence of impurities, the hydrogen oxidation reaction (HOR, $H_2 \leftrightarrow 2H^+ + 2e^-$) is rarely the rate-limiting step in fuel cell operation, even at high current densities [Bellows 1996]. Such was the case here even using 0.5 mg of Pt/C for the conditions employed. For an equal molar flow of H_2 and D_2 at 80°C, equilibrium is approximately 45% conversion of H_2.

The activation energy, E_a, for H_2 activation (H_2-D_2 exchange) in the absence of CO was not able to be obtained due to the reaction being limited by equilibrium at the experimental conditions used in this study, even for extremely small amounts of catalyst (ca. 0.5 mg). However, surface science studies of H_2-D_2 exchange on Pt(111) [Bernasek 1975, Montano 2006] have reported apparent E_a of 4.5 kcal mole^{-1} and 5.3 kcal mole^{-1} between a temperature range of 25°C and 300°C using molecular beam and low pressure experiments, respectively.

Introduction of even 10 ppm CO significantly increased the apparent activation energy of the exchange reaction in the surface science studies. In the present study, values for E_a of 19.3 kcal mol^{-1} and 19.7 kcal mol^{-1} were measured for Pt/C in the presence of 10 and 70 ppm CO, respectively. These results agree well with the value measured by Montano et al. [Montano 2006] of 17.4 kcal mol^{-1} (200 mTorr H_2, 20 mTorr D_2, 5 mTorr CO) on Pt(111), overlooking the slight potential curvature of their Arrhenius plot.

The increase in E_a may be influenced by a restructuring of the Pt surfaces by CO [Montano 2006, Thostrup 2003, Somorjai 1999, Somorjai 1997], which can occur even at room temperature [Thostrup 2003, Mallat 1999]. In addition, molecular beam studies show that the H_2-D_2 exchange reaction is structure sensitive at low pressures (~10^{-7} torr) of H_2 and D_2 [Somorjai 1986]. However, the authors theorized that the exchange reaction is not structure sensitive at high pressures (1 atm) due to the reaction being so fast that equilibrium is usually achieved (in the absence of an impurity). The combination of (1)

blocking of Pt sites, (2) surface restructuring, and (3) structure sensitivity of the H_2-D_2 exchange reaction could explain why even a small amount of CO can have such a significant effect on the apparent activation energy for H_2 activation on Pt. Increase in CO concentration (70 ppm) did not seem to affect the apparent activation energy further. This suggests that an increase in CO concentration beyond 10 ppm does not affect the exchange mechanism significantly.

H_2 and CO Surface Concentration Measurements

Effect of CO on Hydrogen Surface Concentration

-ure 4.1.1-1 shows TOS measurements using HDSAP of hydrogen surface concentration on 100 mg of Pt/C in the presence of 10–200 ppm CO in 20% H_2 and 80% Ar. Table 4.1.1-2 gives the steady-state surface concentrations. As the CO concentration increased, the time required to reach steady-state coverage decreased. This is understandable as higher CO concentrations allowed for higher initial uptakes. However, what primarily dictated the rate of decline with TOS was that, for ppm concentrations of CO, it took a long time to populate the surface of 100 mg Pt/C to steady-state coverage, even if every molecule adsorbed. For example, at the calculated loading of Pt, it would have taken at least 8.8 h in the presence of 10 ppm CO for all of the available surface Pt atoms to have undergone full coverage with CO.

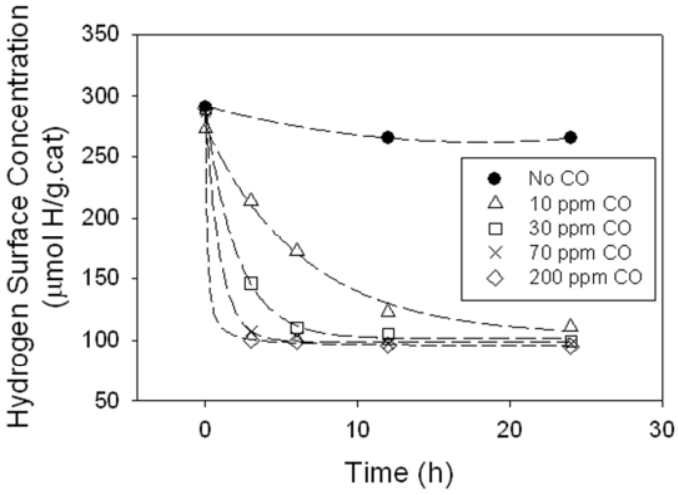

Figure 4.1.1-1: TOS measurement of hydrogen surface concentration as a function of CO concentration (10 – 200 ppm) on Pt/C at 80°C.

Due to adsorption/desorption equilibrium of CO at 80°C, the surface concentration of hydrogen never approached 0 at steady-state, even in as high a concentration as 200 ppm CO. Increasing CO concentration to 200 ppm, from 70 ppm, did not appear to significantly further decrease steady-state hydrogen surface concentration or exchange conversion.

Table 4.1.1-2: Steady-state H_2-D_2 exchange conversion and surface coverage of Pt/C by CO and hydrogen (from HDSAP and TPD).[a]

CO Conc. (ppm)	Steady-State H_2-D_2 Exchange Conversion[b]	Surface H Concentration at Steady-State (μmol H $g.cat^{-1}$) [HDSAP][c]	Surface CO Concentration (μmol CO $g.cat^{-1}$) [TPD][d]	Surface Coverage of Pt by CO based on HDSAP (ML)[e,f]	Surface Coverage of Pt by CO based on TPD (ML)[f,g]
0	45% Equil.	265	-	-	-
2	45% Equil.	121	51	0.44	0.24
10	42%	111	64	0.48	0.30
30	34%	99	70	0.54	0.33
70	26%	97	74	0.55	0.34
200	22%	95	72	0.56	0.33

[a]100 mg Pt/C

[b]Experimental error for all results was ca. ± 3%.

[c]Experimental error for all results was ca. ± 8%.

[d]Experimental error for all results was ca. ± 5%.

[e]Calculated from: $\text{CO Surface Coverage (HDSAP)} = \frac{215\ \mu\text{mol Pt}_S\ g.cat^{-1} - (\text{Surface H})_{x\ \text{ppm CO}}}{215\ \mu\text{mol Pt}_S\ g.cat^{-1}}$

[f]Calculated from: $\text{CO Surface Coverage (TPD)} = \frac{(\text{Surface CO})_{x\ \text{ppm CO}}}{215\ \mu\text{mol Pt}_S\ g.cat^{-1}}$

[g]Calculations are based on a Pt surface concentration of 215 μmol Pt_S $g.cat^{-1}$ obtained from static H_2 chemisorption at 35°C and assuming a stoichiometry of (1:1) for both H:Pt and CO:Pt.

While steady-state hydrogen surface concentration is a function of CO concentration regardless of the amount of catalyst, H_2 activation or H_2-D_2 exchange conversion is not. Even though a large loss in hydrogen surface concentration was observed for 100 mg of Pt/C in the presence of 10 ppm CO, H_2-D_2 exchange at steady-state was still very close to equilibrium (ca. 42% vs 45% at equilibrium). Exposure of 100 mg of Pt/C to 200 ppm CO further decreased H_2-D_2 exchange conversion at steady-state to 22%. This result suggests that, although CO is blocking a large portion of the sites, there are still sufficient available Pt surface atoms remaining in the 100 mg of catalyst to cause the H_2-D_2 exchange reaction to achieve high conversions at steady-state.

If, according to electrochemical results, the CO were completely covering the Pt ($\theta_{CO/Pt}$ = 1) in the presence of 100 ppm CO [Igarashi 2001, Papageorgopoulos 2002], the steady-state conversion of H_2-D_2 exchange at 200 ppm CO should be 0%. In addition, because steady-state CO coverage on Pt_S is not 100%, even at relatively high concentrations (i.e., 200 ppm) of CO, increasing the total amount of Pt/C also increases the total number of free Pt_S sites unoccupied by CO, such that higher concentrations of CO are required before the poisoning effect can be observed. This is the reason why increasing the Pt loading in fuel cells has the false effect of increasing its CO tolerance [Bellows 1996]. This is important because, regardless of how much of the Pt surface is poisoned by CO, as long as there exists enough unpoisoned Pt surface atoms such that the HOR is not the rate-limiting step, no effect of CO poisoning is observed.

Even after 108 h of exposure to CO, equilibrium conversion was still observed for H_2-D_2 exchange. Surprisingly, a reduction of CO from 10 to 2 ppm, which should shift the adsorption/desorption equilibrium of CO, had only a small effect on the concentration of surface hydrogen at steady-state (Table 4.1.1-2). Analysis of CO coverage results on Pt(111) as a function of CO pressure also showed very little change between the equivalent 2 – 10 ppm partial pressure range (10^{-3} – 10^{-2} Torr) [Longwitz 2004].

Surface Coverage of CO on Pt

Due to the ambiguity of surface coverage, the definition that will be employed in this section is based on the coverage of Pt_S by CO, such that if we have two nondissociated CO molecules bridge-bonded to four Pt_S atoms on the surface of a unit cell, we have a CO surface coverage of one monolayer ($\theta_{CO/Pt} = 1$). In other words, we are focused on surface coverage by CO as blocked surface atoms of Pt (Pt_S).

Actual surface Pt concentration is speculated to be between 190 – 215 μmol Pt_S $g.cat^{-1}$ from static CO and H_2 chemisorption results at 35°C, respectively. The reason for this difference can be attributed to the fact that a portion of the CO is bridge-bonded to two Pt_S atoms, which is evident from IR obtained at 80°C as well as literature [Andersen 2005]. Because the stoichiometric ratio of (1:1) for H:Pt_S is much more likely than that of CO:Pt_S, the Pt_S concentration of 215 μmol Pt_S $g.cat^{-1}$ obtained from static H_2 chemisorption at 35°C was used as the basis for the surface coverage analysis. These results are also tabulated in Table 4.1.1-2.

As expected, CO surface coverage calculated from HDSAP and TPD results both increase with CO concentration. The difference between these two results is due, in large part, to a portion of the CO being bridge-bonded such that the stoichiometric ratio of CO:Pt is less than 1. Thus, the true surface coverage of Pt_S by CO is most likely closer to the values calculated based on hydrogen surface concentration [HDSAP] than that of CO [TPD]. These results show a maximum coverage of Pt_S by CO to be approximately 0.44 ML (monolayer) and 0.56 ML for the CO concentrations of 2 and 200 ppm, respectively, at 80°C and 0.4 atm of H_2. Further increases in CO concentration may alter CO coverage due to phenomena such as restructuring, formation of surface carbonyls, and other unforeseen variables.

Reversibility of CO Poisoning

In contrast to NH_3 on Nafion, the adsorption of CO on Pt is not permanent but rather reversible at 80°C. This is illustrated very clearly from the adsorption/desorption equilibrium (less than one monolayer) that is achieved even when Pt is exposed to relatively high concentrations of CO.

From electrochemical results obtained by Uribe et al. [Uribe 2002], it was found that the performance of a fuel cell, previously poisoned with CO, was able to be fully regenerated within a few minutes of purging the anode with pure H_2, which appears to suggest a complete removal of adsorbed CO. Jimenez et al. [Jimenez 2005] utilized this apparent

fast reversibility of CO in a fuel cell by continuously cycling between feed streams of pure H_2 and CO/H_2 mixture every couple of minutes to improve CO tolerance. Similar to the results obtained by Uribe et al. [Uribe 2002], the authors also concluded that the poisoning process is reversible with only the injection of pure H_2. However, due to the high Pt loadings (20 wt% Pt/C, 0.5 mg Pt cm^{-2}) employed and the short duration of their experiments (110 min), the system was most likely not at steady-state and would not have adsorbed enough CO to shift the HOR away from being equilibrium limited. In addition, it is again pertinent to point out that as long as there exists enough unpoisoned Pt surface atoms such that the HOR is not the rate-limiting step, no effect of CO poisoning should be observed.

Figure 4.1.1-2 shows the hydrogen surface concentrations of Pt/C sequentially exposed to 30 ppm CO followed by regeneration in H_2, both for 12 h. The process was repeated a second time on the same catalyst to see if poisoning of a previously poisoned Pt surface would yield different results. After an initial 12 h exposure to 30 ppm CO, steady-state was reached (35% H_2-D_2 conversion). Regeneration capacity (ca. 150 μmol H $g.cat^{-1}$). However, the amount of CO-free Pt surface atoms, even after 6 h of regeneration, was enough to allow the H_2-D_2 exchange reaction to achieve equilibrium conversion (~45%). Re-exposure of the regenerated catalyst to 30 ppm CO again resulted in a hydrogen surface concentration similar to that following the initial exposure to CO.

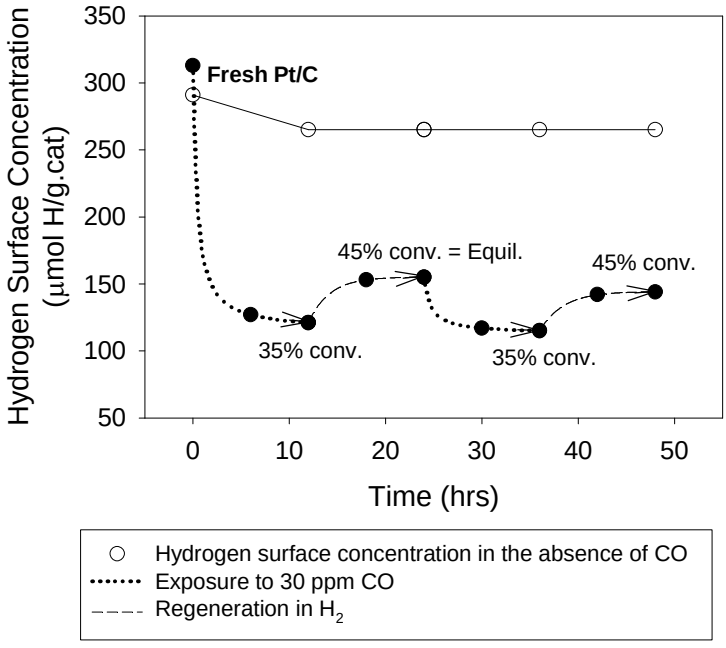

Figure 4.1.1-2: Reversibility of CO poisoning after exposure of Pt/C to 30 ppm CO for 12 h. Steady-state H_2-D_2 exchange conversion was at 35% in the presence of CO and at equilibrium (~45%) for all points following regeneration.

These results suggest that the adsorption/desorption equilibrium of CO on Pt is not affected by whether or not the surface is fresh or pre-poisoned and regenerated. However, while only a partial recovery was again achieved, H_2-D_2 exchange conversion after 6 h regeneration was at equilibrium under the conditions employed.

Therefore, purging with H_2 may appear to initially restore fuel cell performance, but this apparent recovery is not due to the complete removal of CO from the Pt sites. Rather, it appears that there is only a partial recovery of sites – but sufficient CO-free Pt sites are recovered to allow H_2 activation not to be the rate-limiting step any longer. Based on these results, the addition of a H_2 purge between CO exposures may help in slowing its poisoning effect, but it by no means totally reverses this poisoning, unless perhaps if extremely long purge times are used.

4.1.1.4 Conclusions

Comparison of HDSAP results to those of static H_2/CO chemisorption at 80^{o}C and CO TPD show excellent agreement, thus validating HDSAP as an excellent technique for the measurement of hydrogen surface concentration on Pt in the absence and presence of CO at the experimental conditions employed. While the H_2-D_2 exchange reaction (a model for H_2 activation) is able to reach equilibrium very easily on Pt in the absence of CO, introduction of CO is able to shift the reaction away from equilibrium. This shift from reaction equilibrium is supported by the increase in apparent activation energy of H_2-D_2 exchange from 4.5 – 5.3 kcal mole^{-1} [Bernasek 1975, Montano 2006] (in the absence of CO) to 19.3 – 19.7 kcal mole^{-1} (in the presence of 10 – 70 ppm CO). Apparent activation energy results, in the presence of CO, agree well with those reported by Montano et al. [Montano 2006] within experimental error.

Results from the H_2-D_2 exchange reaction, HDSAP, and TPD show that the catalyst surface is not fully saturated by CO in the presence of as high as 200 ppm CO in H_2 under the experimental conditions used (80^{o}C and 0.4 atm H_2), which suggest that surface coverage estimations via cyclic voltammetry (CV) are inaccurate. Furthermore, comparisons of hydrogen surface concentration and CO measurements with that of static H_2 chemisorption at 35^{o}C show a CO surface coverage of ca. 0.44–0.56 ML in 2–200 ppm of CO in H_2, respectively. Surface science results of CO surface coverage obtained via HP STM on Pt(111) for the range of CO studied were consistently ~0.1 ML higher than the values obtained in this study. However, considering the differences in experimental conditions (i.e., room temperature, in the absence of hydrogen, and single crystal surface), CO surface coverage obtained from HDSAP show good agreement with those obtained from surface science.

Regeneration of Pt/C in H_2, at fuel cell conditions, after exposure to 30 ppm CO shows only a partial recovery of surface Pt sites. However, the amount of CO-free sites available from removal of CO in the gas stream can still be enough to achieve equilibrium conversion for H_2-D_2 exchange. This explains why a complete recovery of performance is observed in a fuel cell – not because all of the surface CO has been

removed, but because enough has been removed to make H_2 activation not be the rate-limiting step. In addition, surface coverage of hydrogen and CO results at steady-state appear to imply a limiting effect on hydrogen spillover by CO, perhaps due to CO adsorption at Pt-C interface.

HDSAP was established as a valid technique for the measurement of hydrogen surface concentration on Pt.

For further details about this study, please refer to:
"The Effect of Low Concentrations of CO on H_2 Adsorption and Activation on Pt/C," ***Journal of Power Sources*** 195 (2010) 3060-3068 (Jack Z. Zhang, Zhiming Liu, and James G. Goodwin, Jr.).

References

Andersen, M.; M. Johansson, I. Chorkendorff, J. Phys. Chem. B 109 (**2005**) 10285.
Bard, A.J.; and L.R. Faulkner, Electrochemical Methods: Fundamentals and Applications, second ed., John Wiley & Sons, New York, **2001**.
Bellows, R.J.; E.P. Marucchi-Soos, D.T. Buckley, Ind. Eng. Chem. Res. 35 (**1996**) 1235.
Bernasek, S.L.; and G.A. Somorjai, J. Chem. Phys. 62 (**1975**) 3149.
Coloma, F.; A. Sepulveda-Escribano, F Rodriguez-Reinoso, J. Catal. 154 (**1995**) 299.
Davies, J.C.; R.M. Nielsen, L.B. Thomsen, I. Chorkendorff, A. Logadottir, Z. Lodziana, J.K. Norskov, W.X. Li, B. Hammer, S.R. Longwitz, J. Schnadt, E.K. Vestergaard, R.T. Vang, F. Besenbacher, Fuel Cells (Weinheim, Ger.) 4 (**2004**) 309.
Ebbesen, S.D.; B.L. Mojet, L. Lefferts, J. Catal. 246 (**2007**) 66.
Igarashi, H.; T. Fujino, Y. Zhu, H. Uchida, M. Watanabe, Phys. Chem. Chem. Phys. 3 (**2001**) 306.
Jia, R.L.; C.Y. Wang, S.M. Wang, J. Mater. Sci. 41 (**2006**) 6881.
Jimenez, S.; J. Soler, R.X. Valenzuela, L. Daza, J. Power Sources 151 (**2005**) 69.
Leuking, A.D.; R.T. Yang, Appl. Catal., A 265 (**2004**) 259.
Longwitz, S.R.; J. Schnadt, E.K. Vestergaard, R.T. Vang, E. Lægsgaard, I. Stensgaard, H. Brune, F. Besenbacher, J. Phys. Chem. B 108 (**2004**) 14497.
Mallat, T.; S. Frauchiger, P.J. Kooyman, M. Schurch, A Baiker, Catal. Lett. 63 (**1999**) 121.
Montano, M.; K. Bratlie, M. Salmeron, G.A. Somorjai, J. Am. Chem. Soc. 198 (**2006**) 13229.
Papageorgopoulos, D.C.; M. Keijzer, J.B.J. Veldhuis, F.A. de Bruijin, J. Electrochem. Soc. 149 (**2002**) A1400.
Ren, B.; L. Cui, X.F. Lin, Z.Q. Tian, Chem. Phys. Lett. 376 (**2003**) 130.
Ross, P.N.; and P. Stonehart, J. Res. Inst. Catal., Hokkaido Univ. 22 (**1974**) 22.
Somorjai, G.A.; and J. Carrazza, Ind. Eng. Chem. Fund. 25 (**1986**) 63.
Somorjai, G.A.; Appl. Surf. Sci. 121/122 (**1997**) 1.
Somorjai, G.A.; X. Su, K.R. McCrea, K.B. Rider, Top. Catal. 8 (**1999**) 23.
Thostrup, P.; E.K. Vestergaard, T. An, E. Lægsgaard, F. Besenbacher, J. Chem. Phys. 118 (**2003**) 3724.
Uribe, F.A.; S. Gottesfeld, T.A. Zawodzinski, J. Electrochem. Soc. 149 (**2002**) 293.

Zhang, J.Z.; Z. Liu, and J.G. Goodwin, Jr., J. *of Power Sources* 195 (**2010**) 3060-3068.
Zhou, Z.; W. Zhou, S. Wang, G. Wang, L. Jiang, H. Li, G. Sun, Q. Xin, Catal. Today 93-95 (**2004**) 523.

4.1.2 The Effect of Low Concentrations of CO on H_2 Adsorption and Activation on Pt/C: Part 2 – In the Presence of H_2O Vapor

4.1.2.1 Motivation

In this study, H_2-D_2 exchange and a simple H_2-D_2 switch with an Ar purge in between (HDSAP) technique was employed to quantitatively investigate the effect of CO on H_2 dissociation and on the hydrogen surface concentration on Pt/C catalysts in the presence of water vapor. The HDSAP methodology, developed earlier [Zhang 2010], has proven to be a powerful approach for the time-on-stream (TOS) measurements of hydrogen surface concentrations on Pt in the absence of humidity. This convenient non-destructive approach has many benefits over other conventional performance tests, for example, simple material preparation, low cost, and time efficiency. It provides valuable information (hydrogen surface concentration on Pt catalysts) which could be reasonably used to predict performance of a partially poisoned-fuel cell. The knowledge of the effect of water vapor (humidity) and CO on the amount of hydrogen adsorbed on Pt/C obtained in this work provides fundamental insight for future investigations of the effect of humidity and CO on Nafion-Pt/C in the catalyst layer of the fuel cell.

4.1.2.2 Experimental

A commercial Pt fuel cell catalyst, 20 wt% Pt supported on carbon black (Vulcan XC-72, Cabot Co.) (Pt/C), was purchased from BASF. Nominal composition was confirmed via elemental analysis (performed by Galbraith Laboratories) and energy dispersive x-ray spectroscopy (EDX) (STEM-Hitachi HD2000 equipped with an Oxford INCA Energy 200 EDS). Other characterizations of the catalyst include: BET, static H_2/CO chemisorption, TEM, XRD, FTIR, and TPD.

Results for H_2-D_2 exchange reaction and H_2-D_2 Switch with Ar Purge (HDSAP) were obtained at 80^{o}C and 2 atm abs. in a conventional plug flow, micro-reactor system. Prior to reaction experiments, all catalyst samples were pretreated at 80^{o}C in H_2 for 3 h.

In order to provide a shorthand designation for the various treatment and adsorption conditions to which the catalyst was exposed, the following designations are used throughout this section:

Designation	**Treatment**
/:	TOS = 0 h. The nomenclatures given before and after "/" were treatment or adsorption conditions prior to and after TOS = 0 h, respectively.
w:	in the presence of 10%RH; P_{H2O} = 0.023 atm
C:	30 ppm CO

H: H_2; P_{H2} = 1 atm balanced with P_{Ar} = 1 atm
D: D_2; P_{D2} = 1 atm balanced with P_{Ar} = 1 atm
Hw: H_2 and H_2O; P_{H2} = 1 atm balanced with P_{Ar} = 0.977 atm and P_{H2O} = 0.023 atm
A: Ar; P_{Ar} = 2 atm
Aw: Ar and H_2O; P_{Ar} = 1.977 atm balanced with P_{H2O} = 0.023 atm

The total pressure and temperature in the reactor were always kept at 2 atm and 80°C, respectively. Ar was used as an inert gas balance to maintain a total flow rate of 100 sccm and total pressure of 2 atm. The treatment and experimental conditions for each set of results are given in the legend of each figure. For clarification purposes, the nomenclature, for example, "Hw / HwC", means that the Pt/C catalyst, after reduction, was equilibrated in a 100 sccm stream with P_{H2} = 1 atm, P_{Ar} = 0.977 atm, and P_{H2O} = 0.023 atm (equal to 10%RH) overnight at 80°C prior to the first (TOS = 0 h) hydrogen surface concentration measurement via HDSAP. The catalyst was then subsequently exposed to 30 ppm CO in the presence of 1 atm P_{H2} with 10%RH for further TOS measurements of hydrogen surface concentration. While most of the experiments involving water vapor were performed in the presence of both H_2 and water, in order to isolate the amount of surface hydrogen attributed to the water, a few of the experiments investigated the hydrogen surface concentration on Pt/C in the absence of H_2. The nomenclature, for example, "Aw / AwC", means that the Pt/C catalyst, after reduction, was equilibrated in a 100 sccm gas stream with P_{Ar} = 1.977 atm and P_{H2O} = 0.023 atm (10%RH) overnight at 80°C before the first (TOS = 0 h) hydrogen surface concentration of Pt/C was measured with subsequent exposure to 30 ppm CO at 10%RH Ar (in the absence of H_2).

4.1.2.3 Results and Discussion

Catalyst Characterization

BET surface area, pore size, and pore volume were 225 ± 12 $m^2 g^{-1}$, 16.4 ± 1.8 nm, and 0.63 ± 0.04 $cm^3 g^{-1}$ for the carbon support (XC-72), respectively; and 170 $m^2 g^{-1}$, 15.9 nm, and 0.44 ± 0.01 $cm^3 g^{-1}$ for Pt/C, respectively.

Table 4.1.2-1 summarizes the hydrogen and CO chemisorption results for the Pt/C catalyst. It can be observed that the amount of hydrogen adsorbed at 35°C was slightly less than that of 80°C due most likely to an increased amount of spillover of the chemisorbed hydrogen onto the carbon support at the higher temperature. However, the amounts of CO adsorbed on Pt/C at 35°C and 80°C were similar and equal within experimental error to the hydrogen uptake at 35°C. Images from TEM have shown that Pt was well-dispersed on the carbon support with an average Pt particle size of 2.6 ± 0.4 nm, comparable to the average Pt particle size predicted by hydrogen or CO chemisorption.

Table 4.1.2-1: Static H_2 and CO Chemisorption results at 35 and 80°C for 20 wt% Pt/C.

Chemisorption	Adsorption temperature (°C)	Total H atoms or CO chemisorbed[a] (μmol g^{-1})	D_{Pt} (%)[b]	Avg. Pt particle size[c] (nm)
H_2	35	316	35	3.1
H_2	80	361	40	2.7
CO	35	292	33	3.3
CO	80	297	33	3.3

[a]Determined by extrapolating the isotherm for total H/CO chemisorption in the linear region at high pressure to zero pressure; experimental error = ± 6%. Hydrogen chemisorbed is given as μmol of H atoms per g catalyst.
[b]Pt %dispersion obtained by assuming $H:Pt_s = 1$ or $CO/Pt_s = 1$.
[c]Average Pt particle sizes calculated from $(1.08 \times 100)/D_{pt}$ [Coloma 1995].

Effect of Water Vapor on the Amount of Hydrogen Adsorbed on Pt/C in the Absence of CO

Figure 4.1.2-1 illustrates the hydrogen surface concentration on Pt/C at 80°C as a function of time-on-stream (TOS) exposure to H_2 and/or water vapor in the absence of CO. It shows that the steady-state, strongly-bound hydrogen surface concentration of the Pt/C catalyst treated with H_2 [H / H] was ca. 321 (μmol H) $(g)^{-1}$, which is within the range of values obtained by static chemisorption (Table 4.1.2-1). Exposure of the catalyst to a mixture of both H_2 and water vapor [H / Hw] (10%RH) resulted in an increase in the amount of exchangeable strongly-bound hydrogen by ca. 221 (μmol H) $(g)^{-1}$. Surprisingly, the amount of exchangeable hydrogen from water, in the absence of H_2, [A / Aw] was the same, within experimental error, as the increase from the addition of water to H_2. [A / Aw] refers to the experiments where hydrogen surface concentration were measured after exposure only to water vapor.

It can be seen in Figure 4.1.2-1 that the total amount of strongly-bound hydrogen surface concentration on Pt/C exposed to [H / Hw] at steady-state was ca. 221 μmol H g^{-1} higher than in the absence of any water vapor [H / H], which appeared to be essentially identical to the amount of strongly-bound hydrogen adsorbed on Pt/C (223 μmol H g^{-1}) after exposure to only water at 10%RH [A / Aw] in the absence of H_2. This direct increase in hydrogen surface concentration, attributed most likely to the (strong) adsorption of H_2O, appears to imply that, in the absence of any impurities, the adsorption of H_2 and H_2O on the Pt/C catalyst results in a total hydrogen surface concentration that is the summation of the amount of exchangeable strongly-bound hydrogen contributed by each species. The additional hydrogen surface concentration on Pt after exposure to [Hw] {221 (μmol H) $(g)^{-1}$}, observed in this study, was most likely due to the isotopic exchange of H_2O and D_2 on surface Pt during the switch to D_2 for HDSAP measurements. This is because it has been reported that the complete exchange reaction between H_2O and D_2 on surface Pt can take place rapidly even at 100 K [Fisher 1980], and water dissociation on a Pt surface is

not thermodynamically favorable [Jimenez 2005, Ishikawa 2002] under the conditions of this study.

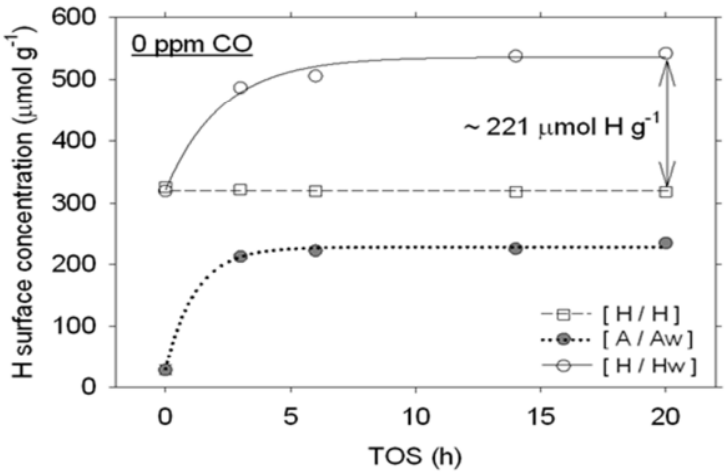

Figure 4.1.2-1: Variation of strongly-bound hydrogen surface concentration on Pt/C with TOS at various conditions and 80°C in the absence of CO.

Effect of CO Poisoning and Its Reversibility on Hydrogen Surface Concentration in the Presence/Absence of H_2 and Water Vapor

Figure 4.1.2-2 illustrates the hydrogen surface concentration on Pt during CO exposure and regeneration under various conditions at 80°C. The designation used in this section was slightly modified. The nomenclatures given before, between, and after "/" correspond to treatment conditions prior to TOS = 0 h, CO exposure conditions after TOS = 0 h, and regeneration conditions after TOS = 33 h, respectively. After the steady-state CO poisoning was obtained (TOS = 33 h), CO flow was stopped and regeneration was initiated by flowing a gas mixture of H_2, water vapor, and/or Ar {[H], [Hw], and [Aw]} through the catalyst bed. In Figure 4.1.2-2, the filled and unfilled symbols illustrate the hydrogen surface concentration on Pt/C during 30 ppm CO exposure (TOS = 0-33 h) and regeneration phase (TOS = 33–97 h), respectively.

These results show that the presence of CO significantly affected the amount of exchangeable strongly-bound hydrogen on Pt/C regardless of whether the adsorbing gas consists of H_2 + H_2O, H_2, or just H_2O. The pseudo steady-state hydrogen surface concentrations measured on Pt/C after CO exposure in the presence of only H_2 (no H_2O, squares) and only H_2O (no H_2, stars) were ca. 96 μmol H g^{-1} and 131 μmol H g^{-1}, respectively. The pseudo steady-state hydrogen surface concentration measured on Pt/C after CO exposure in the presence of both H_2 and H_2O (circles) was ca. 239 μmol H g^{-1}, which is the same, within experimental error, as the summation of the amount of exchangeable hydrogen contributed from H_2 and H_2O adsorption individually and again exhibits the perfectly additive nature of the exchangeable hydrogen from the two species, even in the presence of CO. Also, it can be seen in Figure 4.1.2-2 that the kinetics of CO

adsorption (reflected in the rate of decrease of the hydrogen surface concentration) at 10%RH in the presence/absence of H_2 appeared to be slower than that at 0%RH.

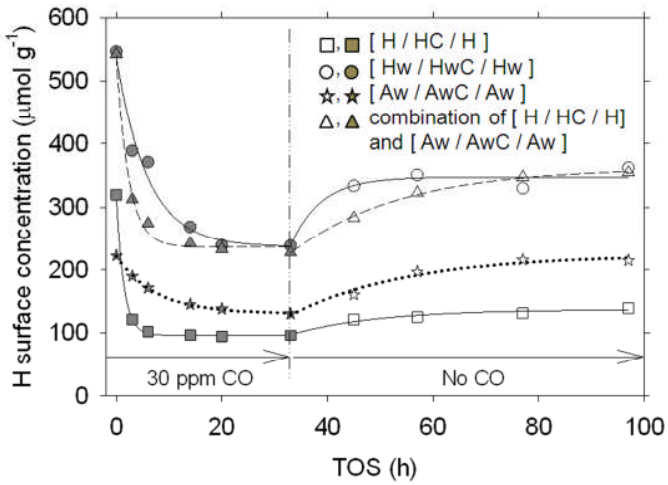

Figure 4.1.2-2: CO poisoning and regeneration of Pt/C in the presence/absence of H_2 and water vapor (10%RH) at 80°C. (Filled symbols and unfilled symbols represent the hydrogen surface concentration on Pt/C exposed to 30 and 0 ppm CO, respectively.).

Regeneration of the catalysts was initiated by stopping the flow of CO, which ultimately resulted in an increase in the amount of hydrogen surface concentration observed for all conditions. The steady-state hydrogen surface concentration of the catalyst regenerated in a flow of H_2 at 0%RH [H / HC / H] was ca. 136 μmol H g^{-1}, which is in agreement with results obtained previously [Zhang 2010]. Regeneration of CO-poisoned Pt/C catalyst in a flow of H_2 at 10%RH [Hw / HwC / Hw] resulted in a hydrogen surface concentration of ca. 345 μmol H g^{-1} at steady-state. It is clear that regeneration of the CO-poisoned catalysts in the presence of H_2 at 0% or 10%RH {[H / HC / H] and [Hw / HwC / Hw]} for long periods of time (64 h) yields incomplete recovery of the strongly-bound hydrogen uptake capacity and hydrogen surface concentration.

These results suggest that, even in the presence/absence of CO, the effects of H_2 and H_2O on the hydrogen uptake capacity of Pt/C at steady state are additive and the sites for H and H_2O adsorption could be somehow different. Because there exist no evidence suggesting that hydrogen cannot adsorb on certain surfaces of Pt, a plausible solution to this question may be due to the induction of a hydrophobic surface observed from TPD and reflective absorption infrared spectroscopy (RAIRS) results on the interaction of water and deuterium on this stepped Pt(533) [van der Niet 2008]. However, while water does not appear to have much of an equilibrium effect on the adsorption/poisoning of Pt by CO, its presence apparently helps in the faster desorption of CO during regeneration of the poisoned Pt/C catalyst, probably due to electronic interactions between adsorbed (strong) H_2O and CO.

It is important to note that this study used higher ppm levels of CO than expected in an operating fuel cell to create a greater effect of the impurity that would be more easily

investigated. The degree of CO poisoning (e.g., kinetics, steady-state θ_{CO}) observed in this study should be more severe than in a real fuel cell because of (a) the high CO impurity level used (30 ppm) and (b) the fact that, during fuel cell operation, the anode potential enhances CO electro-oxidation and helps clean the Pt surface during fuel cell operation [Jimenez 2005]. It is unlikely that oxidative removal of CO_{ads} by OH_{ads} occurs during HDSAP measurements because CO oxidation is not thermodynamically favorable [Jimenez 2005, Liao 2000, Ishikawa 2000] at the low potential (in the absence of an electric current) conditions extant in this study. The slower kinetics of CO poisoning and faster kinetics of CO desorption on the hydrogen uptake capacity in the presence of water vapor observed in this study suggest that higher CO tolerance would be expected for PEMFCs operating at higher relative humidity.

4.1.2.4 Conclusions

In this study, direct measurements of the strongly-bound hydrogen surface concentration on Pt/C, used as a typical anode catalyst, exposed to CO and water vapor were performed via an H_2-D_2 switch with an Ar purge (HDSAP technique). Surprisingly, hydrogen surface concentration results from the co-adsorption of H_2 and H_2O on Pt/C showed that the total amount of strongly-adsorbed surface hydrogen to be the sum of the exchangeable amount of hydrogen attributed to each individual species. This additive nature observed for the strongly-bound hydrogen surface concentration associated with H_2 and H_2O on Pt/C was consistent regardless of whether in the presence/absence of CO, which suggests that the adsorption (strong) of H_2 and H_2O occurs entirely on the Pt and may be due to the induction of a hydrophobic Pt surface as suggested by surface science results.

It was found that the amount of strongly-bound hydrogen adsorbed on the Pt surface decreased with TOS CO exposure at both 0% and 10%RH. While the presence of water vapor helped to decrease the kinetics of CO adsorption during TOS, it only affected the steady-state CO surface coverage of Pt (θ_{CO}) at most slightly, as the steady-state θ_{CO} values were found to be 0.70 and 0.66 ML for Pt catalysts exposed to 30 ppm CO at 80°C in the presence of H_2 (P_{H2} = 1 atm) and H_2/H_2O (P_{H2} = 1 atm and P_{H2O} = 0.023 atm), respectively. These experimental results suggest that the presence of H_2O has little effect on the adsorption on/poisoning of Pt/C by the CO at steady-state.

Reversibility of CO poisoning of the Pt catalyst during regeneration in gas containing H_2, water, or a combination of H_2/H_2O was also investigated. It was found that the kinetics of CO poisoning reversibility were significantly faster when the catalyst was regenerated in a humidified H_2 stream than in a dry H_2 stream. This increase in the rate of CO desorption in the presence of water may be due to electronic interactions between CO and strongly-bound H_2O on the Pt surface. Accordingly, greater CO tolerance is expected for PEMFCs operating at high relative humidity due to a slower rate of CO poisoning and faster rate of CO desorption during regeneration (or after removal of CO from the gas stream). After regeneration, the remaining CO surface coverages on Pt treated in a H_2 stream [H / HC / H] vs. a mixture of both H_2/H_2O [Hw / HwC / Hw], after accounting for

the extra hydrogen surface concentration due to adsorbed water, were ca. 0.56 and 0.54 ML, respectively.

For further details about this study, please refer to:
"The Effect of Low Concentrations of CO on H_2 Adsorption and Activation on Pt/C: Part 2 – in the Presence of H_2O Vapor," ***Journal of Power Sources*** 196 (2011) 6186-6195 (Jack Z. Zhang, Kitiya Hongsirikarn, James G. Goodwin, Jr.).

References

Coloma, F.; A. Sepulvedaescribano, and F. Rodriguezreinoso, J. Catal. 154 (**1995**) 299-305.
Fisher, G.B.; and J.L. Gland, Surf. Sci. 94 (**1980**) 446-455.
Ishikawa, Y.; M.S. Liao, and C.R. Cabrera, Surface Science 463 (**2000**) 66-80.
Ishikawa, Y.; M.S. Liao, and C.R. Cabrera, Surf. Sci. 513 (**2002**) 98-110.
Jimenez, S.; J. Soler, R.X. Valenzuela, and L. Daza, J. Power Sources 151 (**2005**) 69-73.
Liao, M.S.; C.R. Cabrera, and Y. Ishikawa, Surface Science 445 (**2000**) 267-282.
van der Niet, M.J.T.C.; I. Dominicus, M.T.M. Koper, and L.B.F. Juurlink, Phys. Chem. Chem. Phys. 10 (**2008**) 7169-7179.
Zhang, J.Z.; Z.M. Liu, and J.G. Goodwin, Jr., J. Power Sources 195 (**2010**) 3060-3068.

4.1.3 Structure Sensitivity of Cyclopropane Hydrogenolysis on Carbon-Supported Platinum

4.1.3.1 Motivation

This investigation was carried out in order to have a tool for exploring how Nafion sits on the Pt/C in the MEA. Its applicability will become apparent in Section 4.1.4.

There has been debate in the past as to whether or not cyclopropane hydrogenolysis is a structure sensitive reaction. This study addresses, for the first time, the structure sensitivity of cyclopropane hydrogenolysis on Pt using a series of K^+-doped Pt/C catalysts prepared via sequential impregnation of the pre-reduced supported metal catalyst to prevent modification of the particle size distribution. Potassium was chosen due to evidence suggesting the promoter-metal interactions to be limited to simple site blocking on Pt and other noble metals if impregnated sequentially [Bajusz 1997, Hoost 1991]. The methodology of this investigation is similar to that of Hoost and Goodwin [Hoost 1991] and utilizes the statistical dependence of the rate of structure-sensitive reactions on simple site blockage originally established and reviewed in detail by Martin [Martin 1988] in determining the approximate ensemble size required for reaction. In addition, results for the hydrogenation of CO, a classic structure-insensitive reaction, on the K^+-modified Pt/C catalysts are also presented to contrast to those for cyclopropane hydrogenolysis. Due to the low temperature required for cyclopropane hydrogenolysis, if this reaction were shown to be structure sensitive, it could be used to characterize Pt

catalyst surfaces in catalysts not stable at higher temperatures, such as Nafion-Pt/C, which is used as the anode catalyst in proton exchange membrane fuel cells (PEMFCs).

4.1.3.2 Experimental

A commercial Pt fuel cell catalyst, 20 wt% Pt supported on carbon black (Vulcan XC-72, Cabot Co.) (Pt/C), was purchased from BASF. Unless specified otherwise, the Pt/C catalyst used here is the same as the one used in the study investigating the effect of H_2O on H_2 adsorption and activation.

A portion of the purchased Pt/C catalyst were impregnated sequentially via incipient wetness with aqueous KNO_3 solutions of varying concentrations to prepare a series of K^+-doped catalysts with theoretical $(K/Pt_T)_{atom}$ ratios of 0, 0.1, 0.2, 0.4, and 0.8, where Pt_T stands for the total amount of Pt available. In order to obtain a more uniform distribution of the potassium for each batch, the KNO_3 (Sigma Aldrich, 99.999% purity) was dissolved in 30 mL of distilled water and added drop-wise to the catalyst until incipient wetness was achieved. The wet catalyst was then placed in a static oven at 90°C for ca. 20 min to dry and the process was repeated until the entire solution has been used. The K^+-free Pt/C catalyst was treated with only distilled water to check for possible effects from the impregnation process. After impregnation, the material was dried at 90°C overnight in a static air oven, then crushed, and sieved to obtain a catalyst particle size distribution of 60 – 180 μm. Nominal Pt and K compositions were confirmed via elemental analysis (performed by Galbraith Laboratories) for all catalysts. The K^+-modified Pt/C catalysts are designated as *xx*K/Pt to indicate $(K/Pt_T)_{atom}$ = *xx*/100. It should be noted that the $(K/Pt_T)_{atom}$ ratio is based on the total amount of Pt in the catalyst.

Cyclopropane hydrogenolysis reaction rate results were obtained at 30°C and 1 atm utilizing a conventional plug flow, micro-reactor system with a tubular quartz reactor with an internal diameter of ca. 5 mm. Due to the high activity of Pt for this reaction [Dalla Betta 1997], 1.5–5 mg of the xxK/Pt catalysts (depending on activity) were diluted uniformly with 38.5–35 mg of XC-72, respectively, to achieve a catalyst bed of ca. 1 cm in thickness. Prior to reaction, the catalysts were reduced in 100 sccm of H_2:Ar (50:50) (National Specialty Gases, UHP) for 3 h at 80°C and 1 atm. After reduction, the temperature was decreased from 80°C to 30°C and stabilized. Reaction was initiated by flowing a gas mixture of C_3H_6:H_2:Ar (1:50:149) (total flow = 200 sccm) through the catalyst bed and allowing the reaction to stabilize for 5 min before sampling the gas effluent with a Varian 3800 GC equipped with FID and a Restek RT-QPLOT column (30 m, 0.53 mm ID). All reaction rates reported were those for initial reaction (TOS = 5 min) to avoid possible complications from catalyst deactivation due to carbon deposition [Hegedus 1973].

The hydrogenation of CO on Pt was done to contrast to cyclopropane hydrogenolysis. Rate measurements of methanation on the Pt/C catalysts were taken at 392°C due to evidence indicating the dominant role of K^+ on Pt for this reaction to be simple site-blockage in this higher temperature range [Bajusz 1997]. The reaction temperature of 392°C was also required due to the low activity of Pt for this reaction. The reaction rate

measurements were made using 100 mg of catalyst loaded in a fixed-bed differential reactor (316 stainless steel) with a length of ca. 300 mm and an internal diameter of ca. 5 mm. Prior to reaction, the catalyst was first reduced in 22 sccm H_2 for 3 h at 80°C and 1.8 atm. After reduction, the temperature was ramped at 5°C/min from 80°C to 392°C, still in the flow of H_2. Once the temperature was stabilized, reaction was initiated by flowing a H_2:CO (12:1) mixture with a total flow rate of 22 sccm through the catalyst bed to achieve the same partial pressures of H_2 and CO used by Bajusz et al. [Bajusz 1997]. The high relative partial pressure of H_2 to CO was employed to produce primarily methane as the product to simplify analysis.

4.1.3.3 Results and Discussion

Catalyst Characterization

The effects of the impregnation process on the physical characteristics of the catalyst were minimal as the BET surface area, average pore size, and pore volume measured for 00K/Pt were the same as those for the as-received Pt/C (Table 4.1.3-1). However, with the addition of K^+, a noticeable decrease in BET surface area with increasing K^+ concentration was evident. The loss of such a large amount of surface area (up to ca. 37%) is most likely due to blockage of some of the smaller pore structures in the support by K^+ species. This is substantiated by the increase in the average pore size from ca. 16 to 19 nm. The effect of K^+-loading on the total pore volume of the catalysts appears to have been minimal, but this parameter is mainly a function of the larger pores.

Table 4.1.3-1: BET surface area, average pore size, and pore volume of K^+-doped Pt/C.

Catalyst	BET SA* (m^2/g.cat)	Pore Size* (nm)	Pore Volume* (cm^3/g.cat)
Pt/C	170	15.9	0.44
00K/Pt	171	16.4	0.45
10K/Pt	159	16.2	0.44
20K/Pt	151	17.2	0.43
80K/Pt	107	19.1	0.48

*Experimental error was less than ± 6%.

Results from TEM and XRD spectra of the as-received Pt/C, 00K/Pt, 40K/Pt, and 80K/Pt catalysts showed no differences in the average Pt particle size (2.6 ± 0.4 nm, 2.6 ± 0.4 nm, 2.7 ± 0.3 nm, and 2.7 ± 0.4 nm, respectively) determined for these catalysts. This was expected as the mild conditions used during the sequential impregnation process should not alter the metal particle size or dispersion of the Pt.

Elemental analysis results from Galbraith Laboratories showed an actual Pt loading of ca. 18 wt% for all catalysts, compared to the nominal loading of 20 wt%. The amount of K measured was 0.0, 0.24, 0.54, 1.02, and 1.82 wt% for the 00–80K/Pt catalysts, respectively. Based on these Pt and K loadings, consequent calculation of the actual $(K/Pt_T)_{atom}$ ratios for the K^+-doped catalysts resulted in ratios of 0.07, 0.15, 0.29, and 0.53

for the 10–80K/Pt catalysts, respectively (Table 4.1.3-2). Even though subsequent rinsing with distilled water of the KNO_3 solution containers were done to impregnate as much of the K^+ as possible, it appears that a portion of the K^+ was inevitably lost during the impregnation process.

Table 4.1.3-2: Surface coverage of Pt by K^+.

Catalyst	K/Pt_T[a] (atomic)	$K^+_{impreg.}$[a] (μmol/g.cat)	Pt_S[b,c] (μmol/g.cat)	θ_{Pt}[d]
Pt/C	0.00	0	286	-
00K/Pt	0.00	0	278	1.0
10K/Pt	0.07	63	270	0.97
20K/Pt	0.15	135	264	0.95
40K/Pt	0.29	260	252	0.90
80K/Pt	0.53	475	177	0.64

[a]Based on elemental analysis results from Galbraith Laboratories.
[b]From static H_2 chemisorption at 35°C using the total adsorption isotherm and assuming (1:1) H:Pt_S.
[c]Experimental error was less than ±5%.
[d]Based on Pt_S of the 00K/Pt catalyst determined from static H_2 chemisorption at 35°C.

While more than enough K^+ was added to completely block all Pt surface atoms available, results from static hydrogen chemisorption (Table 4.1.3-2) and a plot of available surface Pt vs. the amount of K^+ added (Figure 4.1.3-1) clearly show that only a small portion (ca. 12%) of the K^+ impregnated on the Pt/C to be associated with surface Pt (i.e., blocking it) for the 10–40K/Pt catalysts. This increased to ca. 21% for 80K/Pt. Repeat analyses of specific samples show the experimental error to be well below ±5%, suggesting the K^+ to be more or less well distributed throughout each sample of catalyst.

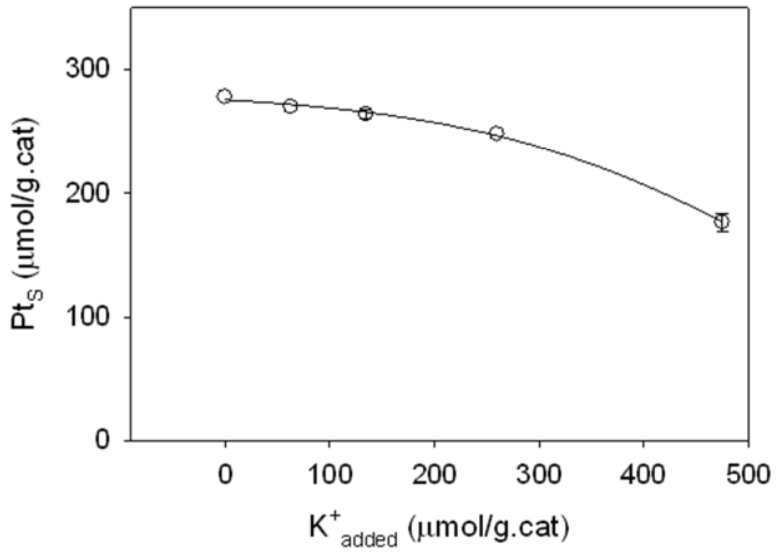

Figure 4.1.3-1: Relationship of amount of K^+ impregnated to the amount of surface Pt (based on static H_2 chemisorption, 35°C).

Cyclopropane Hydrogenolysis

Table 4.1.3-3 shows the initial (5 min) reaction rate data obtained for cyclopropane hydrogenolysis on the various K^+-doped Pt/C catalysts and Figure 4.1.3-2 shows a plot of initial rate of this reaction as a function of K^+-coverage on Pt ($1 - \theta_{Pt}$). Initial reaction rate results for cyclopropane hydrogenolysis on the as-received Pt/C and 00K/Pt catalysts were the same, within experimental error. For the xxK/Pt catalysts, rate decreased with increasing K^+-loading. As can be seen from Figure 4,1.3-2, most of the significant reduction in initial reaction rate data was before a K^+-coverage of 0.15, with rate leveling off as K^+-coverage increased further. Calculation of the TOF for cyclopropane hydrogenolysis based on the amount of exposed Pt surface atoms (Pt_S) obtained from static H_2 chemisorption showed an overall decrease of ca. a factor of 6 ($0.34\ s^{-1}$–$0.06\ s^{-1}$) for the range of K^+-coverage investigated. Comparison of TOF of Pt/C with those of other supported Pt catalysts reported in literature (Pt/Al_2O_3 [Boudart 1966] and Pt/SiO_2 [Boudart 1966, Oteroschipper 1977]) show the values to be in agreement within the same order of magnitude, which is very good considering differences in catalyst preparation, composition, and reaction conditions.

Table 4.1.3-3: Initial reaction results[a] of cyclopropane hydrogenolysis on K^+-modified Pt/C catalysts.

Catalyst	Initial R_P[b] (μmol/g.cat-s)	TOF[c] (s^{-1})	E_{app}[d] (kcal/mol)
00K/Pt	96	0.34	11.9
10K/Pt	81	0.30	11.7
20K/Pt	69	0.26	10.9
40K/Pt	41	0.16	10.1
80K/Pt	10	0.06	10.4

[a] 30^oC, 1 atm, $H_2/C_3H_5/Ar$ = 50/1/149 sccm.
[b] Initial reaction rate for the formation of propane: Error < ±7% .
[c] Based on Pt_S from static H_2 chemisorption.
[d] Apparent activation energy: Error < ±10%.

The apparent activation energy (E_{app}) of 11.9 kcal/mol measured for the non-modified Pt/C catalyst is in agreement with what has been reported in the literature [Kahn 1974] for Pt catalysts. The relatively constant E_{app}, within experimental error, with the addition of K^+ suggests the lack of electronic and/or promotion effects between the Pt and K^+-species for cyclopropane hydrogenolysis, such that the reaction mechanism and heats of adsorption remain relatively essentially the same. Thus, K^+ appears to act only as a blocking agent for this reaction.

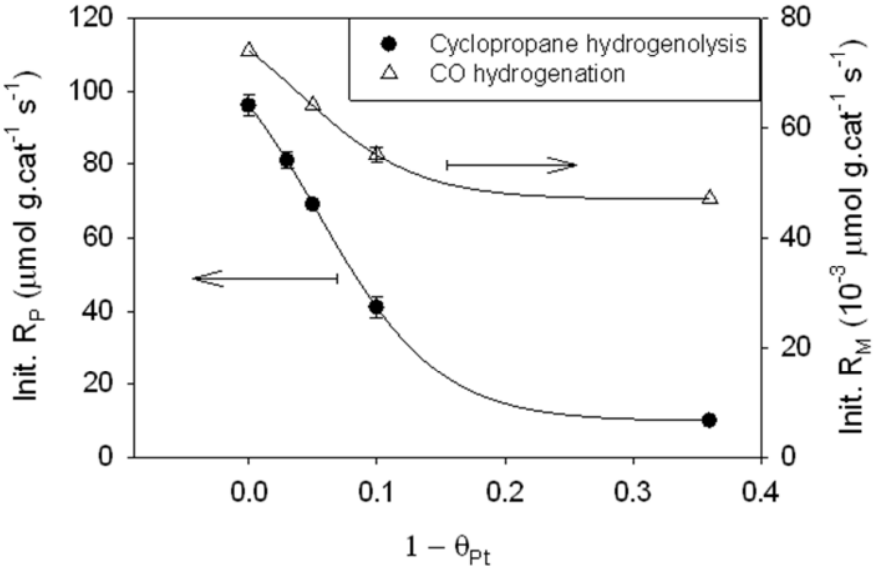

Figure 4.1.3-2 Initial rates of cyclopropane hydrogenolysis and CO hydrogenation as a function of K^+-coverage on Pt surface.

CO Hydrogenation

Table 4.1.3-4 lists the initial reaction rate data and surface kinetic parameters, as determined by SSITKA, for CO hydrogenation on the various K^+-doped Pt/C catalysts. Figure 4.1.3-2 gives a plot of the initial rate of CO hydrogenation as a function of K^+-coverage on Pt ($1 - \theta_{Pt}$).

Table 4.1.3-4: Initial reaction rates and SSITKA results for CO hydrogenation on K^+-doped Pt/C catalysts.

Catalyst	R_M[a] (10^{-3} μmol/g.cat-s)	τ_{CO}[b] (s)	N_{CO}[c] (μmol/g.cat)	τ_M[b] (s)	N_M[d] (μmol/g.cat)	$1/\tau_M$ (s^{-1})	E_{app} (kcal/mol)
00K/Pt	74	2.4	30	5.0	0.37	0.20	26.3
20K/Pt	64	2.3	29	4.8	0.31	0.21	28.5
40K/Pt	55	2.4	30	4.8	0.25	0.20	27.9
80K/Pt	47	2.5	32	4.8	0.20	0.21	28.2

[a]Rate of CH_4 formation: Error = ± 2 × 10^{-3} μmol/g.cat s.
[b]Average surface residence time of rev. ads. CO: Error = ± 0.2 s.
[c]Surface concentration of rev. ads. CO: Error = ± 5%.
[d]Surface concentration of carbon-containing intermediates leading to CH_4: Error = ± 4%.

As seen in Figure 4.1.3-2, decrease in the initial reaction rate was relatively proportional to the increase in K^+-coverage from 0–0.1 and began to level off as K^+-coverage increases to 0.36. Thus, the overall subtle decrease in rate with increasing fraction of Pt surface covered by K^+ suggests that this reaction is less sensitive to surface structure than cyclopropane hydrogenolysis. Surface parameters measured by SSITKA for CO

hydrogenation show that, considering the large amount of surface Pt atoms available based on static H_2 chemisorption, only a small portion (ca. 10%) appeared to be occupied by reversibly adsorbed CO (N_{CO}) at 392°C and even less (ca. 1%) for the formation of active intermediates (in terms of carbon atoms) that led to the production of CH_4 (N_M). The fact that the average residence time of the carbon-based intermediates leading to the formation of CH_4 (τ_M) remained constant with K^+-coverage suggests that the decrease in the activity of the catalyst was solely attributable to the blockage of the sites that were active for the formation of CH_4. Furthermore, the relatively constant value of $1/\tau_M$ for the various K^+-doped catalysts suggests either uniform poisoning or, more likely, the lack of variation in activity among the different sites available, which is what would be expected for a structure insensitive reaction. The reason for the decrease in rate is clearly due to a loss in surface intermediates (sites), N_M, with increasing amounts of K^+, since $Rate = (1/\tau_M)N_M$. Similar to what was observed for cyclopropane hydrogenolysis, comparison of TOF ($1/\tau_M$) obtained for CO hydrogenation on Pt/C to that for Pt/SiO_2 [Bajusz 1997] shows the values to be similar with an order of magnitude.

The E_{app} of 26.3 kcal/mol measured for CO hydrogenation on the non-doped (bare) Pt/C is similar to the literature value of 27 kcal mol^{-1} [Bajusz 1997]. Similar to cyclopropane hydrogenolysis results, the lack of variation (within experimental error) in E_{app} between the bare and K^+-doped Pt/C catalysts observed for this reaction also indicates the absence of any electronic or promotion effects caused by K^+. All results suggest that the effect of K^+ as a Pt modifier for both reactions appears to have been limited to simply blocking active sites.

Structure Sensitivity Analysis

While the variation in the TOF for cyclopropane hydrogenolysis is an indication of structure sensitivity, that evidence alone is not enough as confirmation. Utilizing the simplified exponential expression relating the statistical dependence of rate on site blockage by a blocking agent presented by Hoost and Goodwin [Hoost 1991] and originally proposed by Martin [Martin 1988], the ensemble size required for a specific reaction can be approximated by the following equation:

$$\frac{R}{R_{P=0}} = (1 - \theta_P)^{N_E} \quad (1)$$

where R is the reaction rate of the doped catalyst (K^+-doped Pt/C), $R_{P=0}$ is the rate of the non-doped (non-blocked) catalyst (Pt/C), N_E is the ensemble size required for the reaction, and θ_P is the fraction of the surface metal blocked by the blocking agent or poison P. This simplified expression is only valid when the number of available surface atoms on a particle is greater than the site ensemble size, which is usually the case for supported catalysts.

Figure 4.1.3-3 shows the semi-logarithmic plot of the normalized initial rates of reaction ($R/R_{P=0}$) as a function of fraction of Pt surface exposed (θ_{Pt}) for both cyclopropane hydrogenolysis and CO hydrogenation. The slopes of the individual curves should yield

the value for N_E or ensemble size required for reaction. As one would expect for a structure insensitive reaction, data points for CO hydrogenation on the semi-log plot follow the same trend as that of a uniformly poisoned reaction with an ensemble size requirement of ca. 1 (single-atom ensemble model). While there is some slight deviation from the theoretical line, the difference is minimal. Similarly, interpretation of the decrease in initial rate with K^+-coverage for θ_{Pt} = 1–0.8 suggests the ensemble size required for cyclopropane hydrogenolysis to be ca. 7 (7-atom ensemble model). As the K^+-coverage increased to give $\theta_{Pt} < 0.8$, a deviation from the 7-atom ensemble theoretical line predicted by Martin's model can be observed. This variation, as clearly shown by the modeling results of Hoost and Goodwin [Hoost 1991], is indicative of preferential blockage of certain surface planes of the metal by the blocking agent (in this case K^+).

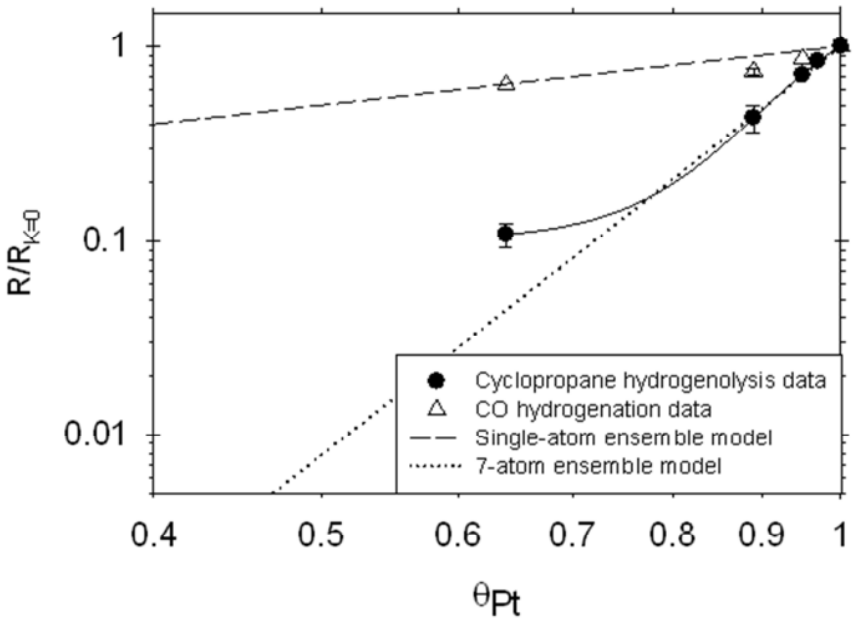

Figure 4.1.3-3: Fraction of Pt surface exposed vs. normalized initial reaction rates for cyclopropane hydrogenolysis and CO hydrogenation.

Given the large decrease in rate with K^+-coverage and the existence of probable preferentially blockage of certain Pt surface structures with higher activities, it can be concluded that cyclopropane hydrogenolysis on Pt is definitely structure sensitive. The ensemble size required for cyclopropane hydrogenolysis of Pt is possibly less than 7, however, but likely greater than 2, the value found for cyclopropane hydrogenolysis on Ni-Cu/SiO_2 by Cale and Richardson [Cale 1985]. Specific possibilities for the required ensemble size will not be discussed here as more data is needed.

4.1.3.4 Conclusions

The structure sensitivity of cyclopropane hydrogenolysis on Pt was investigated via a series of K^+-doped Pt/C catalysts. While the BET surface area and average pore diameter decreased with K^+-loading, sequential impregnation of the alkali species had no effect on

the average Pt particle size as determined from TEM and XRD. Static H_2 chemisorption results confirm that, of the large amount of K^+ added, only a small portion (ca. 10–20%) was associated with surface Pt atoms.

Based on the surface parameters, as determined from SSITKA, and apparent activation energies, the effect of K^+ on the Pt for both reactions appear to be limited to simple site blockage. No evidence indicating promotion or true poisoning effects were observed at the reaction conditions employed. Initial reaction rate results for cyclopropane hydrogenolysis on the as-received Pt/C and 00K/Pt catalysts were the same, within experimental error, indicating also no effect due to aqueous impregnation.

The value for the site ensemble size required for cyclopropane hydrogenolysis on Pt, based on Martin's model [Martin 1988], was estimated to be ca. 7, whereas, CO hydrogenation, a classic structure insensitive reaction, appears to require a site ensemble size of ca. 1, as might be expected. In addition, calculation of TOF (based on H_2 chemisorption) for cyclopropane hydrogenolysis show a decrease with increasing K^+-loading, while the TOF (based on $1/\tau_M$ from SSITKA) for CO hydrogenation remained essentially constant. Based on these results and the extremely high probability of non-uniform distribution of K^+ on specific Pt surfaces, as suggested by Monte Carlo simulations for bimetallic systems [Strohl 1989], reaction results for K^+-modified Ru/SiO_2 [Hoost 1991], and the deviation observed from the ensemble model at the higher K^+ coverages, it can be concluded that the significant loss of rate with increasing K^+-coverage for cyclopropane hydrogenolysis is dependent not only on the number of Pt surface atoms exposed, but also on the Pt surface planes exposed and the availability of sites with higher numbers of contiguous atoms for reaction. The evidence clearly shows that cyclopropane hydrogenolysis on Pt is structure sensitive.

For further details about this study, please refer to:
"Structure Sensitivity of Cyclopropane Hydrogenolysis on Carbon-Supported Platinum," ***Journal of Catalysis*** 280 (2011) 89-95 (Jack Z. Zhang, Yu-Tung Tsai, Khunya Leng Sangkaewwattana, and James G. Goodwin, Jr.).

<u>References</u>

Bajusz, I.G.; D.J. Kwik, and J.G. Goodwin, Jr., Catal. Lett. 48 (**1997**) 151-157.
Boudart, M.; A. Aldag, J.E. Benson, N.A. Dougharty, and C.G. Harkins, J. Catal. 6 (**1966**) 92.
Cale, T.S.; and J.T. Richardson, J. Catal. 94 (**1985**) 289-291.
Dalla Betta, R.A.; J.A. Cusumano, and J.H. Sinfelt, J. Catal. 19 (**1970**) 343.
Hegedus, L.L.; and E.E. Petersen, J. Catal. 28 (**1973**) 150-156.
Hoost, T.E.; and J.G. Goodwin, Jr., J. Catal. 130 (**1991**) 283-292.
Kahn, D.R.; E.E. Petersen, and G.A. Somorjai, J. Catal. 34 (**1974**) 294-306.
Martin, G.A.; Catal. Rev. 30 (**1988**) 519-562.
Oteroschipper, P.H.; W.A. Wachter, J.B. Butt, R.L. Burwell, and J.B. Cohen, J. Catal. 50 (**1977**) 494-507.

Strohl, J.K.; and T.S. King, J. Catal. 116 (**1989**) 540-555.

4.1.4 The Effect and Siting of Nafion® in a Pt/C PEM Fuel Cell Catalyst

4.1.4.1 Motivation

As a continuation of our previous work , where the fundamental effects of CO poisoning on hydrogen activation on Pt/C catalysts were investigated utilizing the H_2-D_2 exchange reaction [Zhang 2010], research was carried out to investigate the interaction of Nafion on the properties of Pt in a commercial Pt/C catalyst commonly used in fuel cells. In addition to general catalyst characterization by BET, TEM, and static H_2/CO chemisorption, experiments were performed utilizing the H_2-D_2 exchange reaction for kinetic measurements of hydrogen activation in the presence of CO (a catalyst poison). In the absence of CO, the exchange reaction was at equilibrium and kinetic measurements could not be made. A modified H_2 to D_2 switch procedure, H_2-D_2 switch with Ar purge (HDSAP), was also used to measure in-situ the surface concentrations of hydrogen and CO with time-on-stream (TOS). Furthermore, a structure sensitive reaction, cyclopropane hydrogenolysis, was employed as a characterization technique to magnify the obstructing effect, if any, of surface Pt sites by Nafion. All experimental results presented in this paper were obtained at conditions where reaction equilibrium was not a contributing factor. In addition, unlike the electrochemical studies, all reaction results were obtained for the catalysts exposed only to the gas-phase, where solution effects can be ignored.

4.1.4.2 Experimental

A commercial Pt fuel cell catalyst, 20 wt% Pt supported on carbon black (Vulcan XC-72, Cabot Co.) (Pt/C), was purchased from BASF. Unless specified otherwise, the Pt/C catalyst used here is the same as the one used in the study investigating the effect of H_2O on H_2 adsorption and activation.

Nafion supported on Pt/C (Nfn-Pt/C) catalysts were prepared via incipient wetness impregnation of the commercial 20 wt% Pt/C with a Nafion ionomer solution (LQ-1105, DuPont, 5 wt% Nafion) to give a target weight loading of 30 wt% for the Nafion. The 30 wt% loading of Nafion has been shown in the literature to be the optimum Nafion content in a PEMFC catalyst layer [Easton 2005, Li 2003, Passos 2006, Santarelli 2007]. The impregnated material was dried at 90^{o}C overnight in a static air oven, crushed, and sieved to obtain a particle size of 60 – 150 μm. The catalyst was then stored in the dark prior to use. Nominal Pt composition was confirmed via elemental analysis (performed by Galbraith Laboratories) for both Pt/C and Nfn-Pt/C.

Results for H_2-D_2 exchange reaction and H_2-D_2 Switch with Ar Purge (HDSAP) were obtained at 80^{o}C and 2 atm abs. in a conventional plug flow, micro-reactor system with a total flow rate of 100 sccm. Prior to reaction experiments, all catalyst samples were pretreated at 80^{o}C in H_2 for 3 h. Cyclopropane hydrogenolysis were performed at 30^{o}C

and 1 atm with a total flow rate of 150 sccm [C_3H_6:H_2:Ar (1:49:150)] in order to achieve differential conversion conditions.

4.1.4.3 Results and Discussion

Catalyst Characterization

BET surface area, pore size, and pore volume were 225 ± 12 $m^2 g^{-1}$, 16.4 ± 1.8 nm, and 0.63 ± 0.04 $cm^3 g^{-1}$ for the carbon support (XC-72), respectively; and 170 $m^2 g^{-1}$, 15.9 nm, and 0.44 ± 0.01 $cm^3 g^{-1}$ for Pt/C, respectively. Impregnation of Pt/C with Nafion resulted in a reduction of BET surface area and pore volume from 170 $m^2 g^{-1}$ and 0.44 $cm^3 g^{-1}$ to 38 $m^2 g^{-1}$ and 0.28 $cm^3 g^{-1}$, respectively, while increasing the average pore size to 32.7 nm. Analysis of pore size distribution for XC-72, Pt/C, and Nfn-Pt/C, based on the desorption differential distribution confirms, more or less, a substantial filling/blocking of the smaller pores by Nafion while the larger sized pores appears to be less significantly blocked.

Elemental analysis results for Pt/C and Nfn-Pt/C from Galbraith Laboratories showed Pt loadings of 17.3 wt% and 13.7 wt%, respectively, and sulfur contents of 0.5 wt% and 1.2 wt%, respectively. The amount of sulfur obtained for Pt/C is similar to that of the carbon support (XC-72). While the residual sulfur (ca. 0.5 wt%) in the Pt/C is most likely due to the vulcanization process used in producing the activated carbon support, the additional sulfur obtained for Nfn-Pt/C (ca. 0.7 wt%) can be directly attributed to the sulfonic sites present in the polymer. Calculation of Nafion-loading based on the sulfur content shows a Nafion content of ca. 22 wt% and a sulfonic site concentration of ca. 231 μmol H^+-SO_3^- per g of Nfn-Pt/C or 1688 μmol H^+-SO_3^- per g of Pt.

Analysis of TEM images indicated an even distribution of Pt particles on the carbon support (XC-72) for both Pt/C and Nfn-Pt/C catalysts. Average Pt particle sizes for the as-received Pt/C and the as-prepared Nfn-Pt/C were determined to be 2.6 ± 0.4 nm and 2.8 ± 0.5 nm, respectively, indicating no apparent change in Pt particle size (within experimental error) during Nafion loading.

Due to differing Pt loadings for Pt/C and Nfn-Pt/C, static chemisorption results were scaled to “per g of Pt” rather than “per g of catalyst” in order for a valid comparison (see Table 4.1.4.1). Surprisingly, the amounts of hydrogen uptake (on a Pt basis) for both Pt/C and Nfn-Pt/C were identical, within experimental error. Even the effect of analysis temperature on hydrogen spillover was roughly the same for both catalysts, suggesting that Nafion did not inhibit the hydrogen adsorption capability of Pt through either physical blocking or chemical interactions, even though such a large amount of Nafion was present. The actual slight reduction in CO uptake for Nfn-Pt/C reaffirms this.

Table 4.1.4-1: Static H_2 and CO chemisorption results at 35°C and 80°C for Pt/C and Nfn-Pt/C.

Catalyst[a]	Adsorption Gas	Analysis Temp. (°C)	Amount of CO or H Adsorbed[b] (μmol (g Pt)$^{-1}$)	Metal Dispersion (%)	Avg. Pt Particle Size (nm)[c]
Pt/C	H_2	35	**1806**	35	3.1
		80	2063	40	2.7
	CO	35	1669	33	3.3
		80	1697	33	3.3
Nfn-Pt/C	H_2	35	**1861**	36	3.0
		80	2160	42	2.6
	CO	35	1452	28	3.9
		80	1452	28	3.9

[a]Catalysts were pretreated in H_2 at 80°C for 3 h.
[b]Experimental error for all results was ca. ± 5%.
[c]Avg. Pt particle size calculated from:
Avg. Pt Particle Size (nm) $= \frac{1.08}{\text{Metal Dispersion}}$, assuming $CO/Pt_S = 1$ and $H/Pt_S = 1$ [Coloma 1995].

H_2-D_2 Exchange Reaction

Similar to the results presented in our previous study [Zhang 2010], exposure of Pt/C to the CO resulted in an apparent E_a of 20.3 ± 0.5 kcal mol^{-1} for the poisoned Pt surface compared to an apparent E_a of 4.5 – 5.4 kcal mol^{-1} reported for an unpoisoned Pt surface [Bernasek 1975, Montano 2006]. Exposure of Nfn-Pt/C to 30 ppm CO resulted in an apparent E_a of ca. 21.5 ± 1.0 kcal mol^{-1}. No difference was observed in the rate of HD formation from H_2-D_2 exchange for Pt/C [1080 ± 50 μmol HD (g Pt)$^{-1}$ sec^{-1}] and Nfn-Pt/C [1065 ± 63 μmol HD (g Pt)$^{-1}$ sec^{-1}], both in the presence of 30 ppm CO. This similarity in both apparent activation energy and reaction rate between the two catalysts reaffirms that the Pt particles are most likely in the larger pore structures of the carbon support and that the Nafion does not appear to be inhibiting the adsorption of either hydrogen or CO on the Pt surface via any physical and/or chemical interactions.

In-situ TOS Surface Hydrogen Concentration via HDSAP

Figure 4.1.4.1 shows the amount of hydrogen surface concentration as a function of purge time used for HDSAP measurements. The addition of Nafion to Pt/C appeared to increase the purge time required from 30 min (for Pt/C) to 50 min (for Nfn-Pt/C), due most likely to the Nafion clusters acting as a barrier to the diffusion of gas-phase H_2 away from the catalyst. Furthermore, the presence of the Nafion also appeared to increase the amount of exchangeable surface hydrogen from the protonated sulfonic sites [SO_3^- - H^+ ≈ 1688 μmol H (g Pt)$^{-1}$]. This increase in purge time required was also observed for samples of Nfn-Pt/C exposed to NH_3 (gas), which increased the amount of exchangeable surface hydrogen from Nafion from 1 hydrogen atom per sulfonic site to 4 hydrogen atoms due to the formation of SO_3^- - NH_4^+. In contrast, exposure of Pt/C to NH_3 (gas) prior to HDSAP showed a negligible effect on the surface hydrogen concentration.

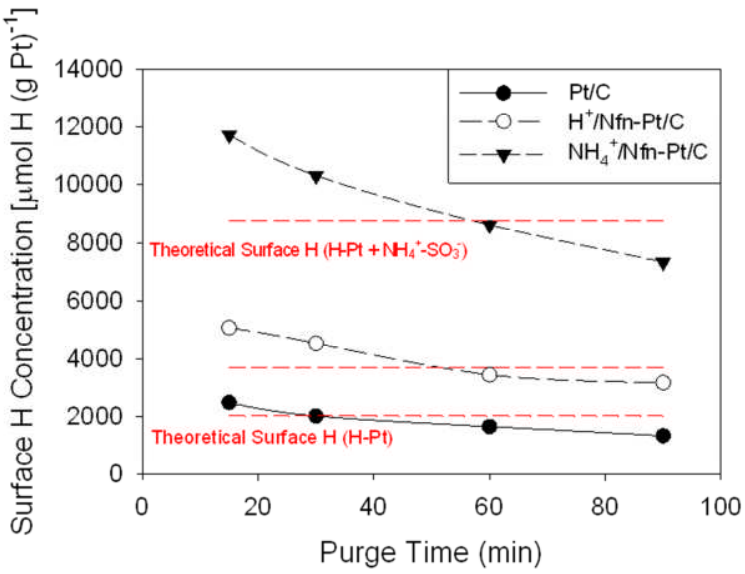

Figure 4.1.4-1: Effect of purge time on hydrogen surface concentration measurements on Pt/C, Nfn-Pt/C, and the NH_4^+ form of Nfn-Pt/C.

In order to verify whether the excess hydrogen is indeed from the sulfonic sites in the Nafion, separate samples of Nfn-Pt/C were poisoned by ion-exchanging the H^+ cations with a non-proton containing cation, Na^+. From these results, poisoning of sulfonic sites with Na^+ cations (Figure 4.1.4-2) significantly decreased the hydrogen surface concentration for Na^+-Nfn-Pt/C compared to Nfn-Pt/C, giving values close to those of Pt/C. The slightly higher surface hydrogen concentration found for Na^+-Nfn-Pt/C than for Pt/C is due to a portion of the sulfonic sites being not fully exchanged with Na^+ but still being in the protonated form (H^+/Na^+-Nfn-Pt/C). Exposure of H^+/Na^+-Nfn-Pt/C to NH_3 (gas) resulted in the conversion of just the protonated sulfonic sites to the ammonium form (NH_4^+/Na^+-Nfn-Pt/C); calculations from the results suggest that ca. 4.5 out of 5.5 sulfonic sites had been poisoned with Na^+. The Pt/C catalyst treated with NaCl in an identical fashion yielded surface hydrogen concentration results similar to those of untreated Pt/C, which confirmed that the Na^+ was associated only with the Nafion. The poisoning results involving NH_3 and Na^+ clearly show the excess surface hydrogen concentration measured for H^+/Nfn-Pt/C to be from the protonated sulfonic sites in the Nafion.

In addition, these results also confirm the rapid transport of protons from the surface Pt atoms to nearby Nafion clusters and vice versa, which is the desired intent of having such a high weight loading of Nafion. Thus, contrary to the previous thought that contact must be maintained between the Pt particles and the polymer electrolyte in order for proton transport to take place [Uchida 1996, Uchida 1995], surface diffusion of protons on the carbon support, while slower than on Pt [Robell 1964], proves to be adequate for the reaction. The poisoning of the sulfonic sites by NH_3 did not appear to have an effect on this transport process (where D exchanges with NH_4^+).

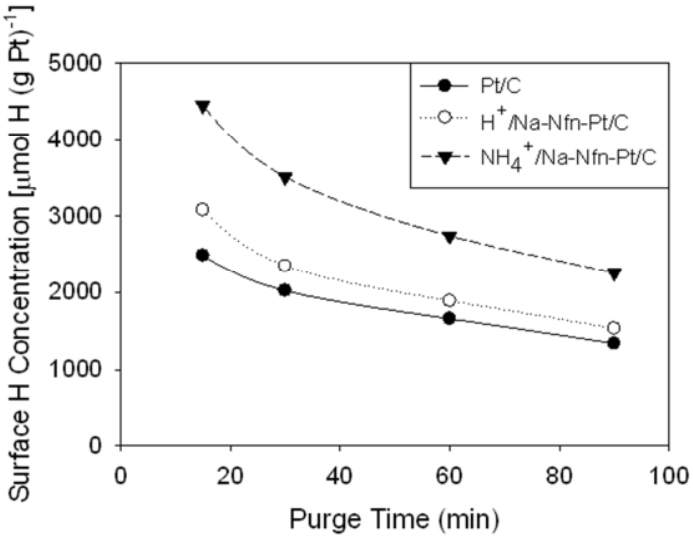

Figure 4.1.4-2: Effect of sulfonic sites exchanged with Na^+ ions on hydrogen surface concentration on Nfn-Pt/C.

Effect of Nafion on the Surface Coverage of ppm CO in H_2 on Pt

Possible effects of Nafion on the surface coverage of CO on Pt from ppm quantities of CO in H_2 were investigated indirectly via hydrogen surface concentration measurements. Similar to the CO surface coverage experiments performed on Pt/C in our previous work [Zhang 2010], TOS measurements of hydrogen surface concentration were measured for both Pt/C and Nfn-Pt/C over a 24 h period of exposure to 30 ppm CO in H_2.

From Figure 4.1.4-3, the poisoning behavior of 30 ppm CO on Nfn-Pt/C, after adjusting for the excess surface hydrogen from the sulfonic sites in Nafion, is similar to that for Pt/C. The hydrogen surface concentration for Nfn-Pt/C, after 24 h of exposure to 30 ppm of CO, was somewhat higher than that for Pt/C, 660 µmol H $(g\ Pt)^{-1}$ vs. 570 µmol H $(g\ Pt)^{-1}$, respectively. Upon closer inspection, it can be observed that the addition of Nafion resulted in an apparent slightly slower approach to steady-state than for Pt/C at the same concentration of CO, which may account for the difference in the surface hydrogen measured. While this may be argued to be related to the longer purge time required for HDSAP measurements for Nfn-Pt/C versus for Pt/C, the more likely possibility is that of the large Nafion clusters interfering with the rate at which CO reaches the surface Pt atoms as it was confirmed that the increase in required purge time between Pt/C and Nfn-Pt/C did not have an effect on the surface coverage of strongly-bound CO. Thus, the hydrogen surface concentration for Nfn-Pt/C was most likely not at steady-state at 24 h, and further exposure of Nfn-Pt/C to CO would have resulted in a hydrogen surface concentration even more similar to that of Pt/C. Regardless, the CO surface coverage for Nfn-Pt/C and for Pt/C after 24 h of exposure is the same (0.69 vs. 0.71, respectively), within experimental error. The CO surface coverage results show that the Nafion does not, in general, appear to affect significantly the adsorption of CO on Pt at steady state.

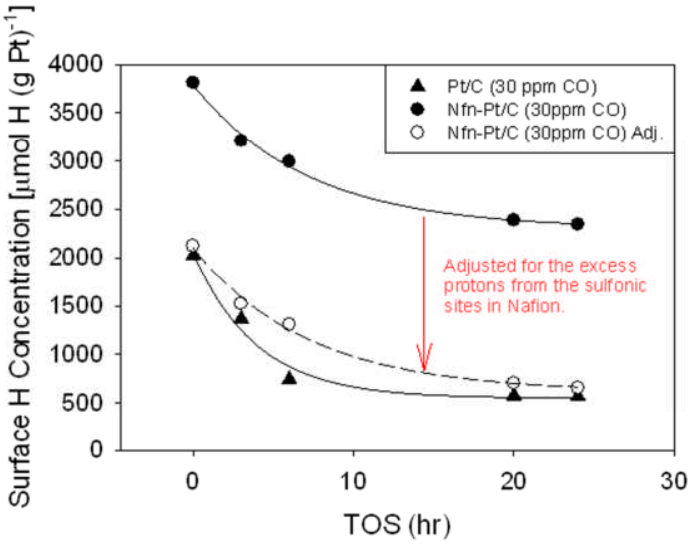

Figure 4.1.4-3: Effect of Nafion on the surface coverage of CO on Pt/C and Nfn-Pt/C from 30 ppm of CO in H_2.

Effect of Nafion on the Activity of Pt/C for Cyclopropane Hydrogenolysis

Up until this point, the presence of such a high weight loading of Nafion has appeared to have a lack of effect on the activity of Pt for the adsorption of hydrogen and CO, which is extremely surprising considering the significant reduction in BET surface area from the impregnation of the Nafion and the large amount of Nafion present. Even if the majority of the surface Pt resided in the larger pore structures of the carbon support, one would think that the presence of such a large amount of Nafion would have at least some effect on the Pt via physical and/or chemical interactions. Because the results given so far have all involved the activation of hydrogen in one form or another, this apparent lack of effect from the Nafion may be due to the fast kinetics of hydrogen diffusion and activation and the structure insensitive characteristic of activation. To probe this issue further, a more structure sensitive reaction was employed to provide further insight. Use of a "demanding" or "structure sensitive" reaction is often very useful for investigating metal dispersion and metal decoration effects on specific activity in heterogeneous catalysts [Hoost 1991].

For this study, the hydrogenolysis of cyclopropane was chosen as a structure sensitive reaction mainly due to its lower reaction temperature requirement for Pt-based catalysts (0-80^{o}C [Hegedus 1973]). Other structure sensitive reactions, such as ethane hydrogenolysis, require operating temperatures in excess of 300^{o}C and above [Cortright 1999, Martin 1998], which is problematic for the catalysts employed due to Nafion degradation at temperatures above 120^{o}C. In addition, at temperatures below 150^{o}C, only one product (propane) is formed from the reaction of cyclopropane with hydrogen over Pt catalysts, which greatly simplifies analysis [Kahn 1974, Schwank 1987].

In order to compare the rates, given the different wt% of Pt before and after loading Nafion, rates were calculated on a per weight Pt basis. Observed rates were calculated to

be 557 μmol C_3H_8 (g Pt)$^{-1}$sec^{-1} and 373 μmol C_3H_8 (g Pt)$^{-1}$sec^{-1} for Pt/C and Nfn-Pt/C, respectively. Furthermore, determination of E_a from Arrhenius plots show the value for Nfn-Pt/C (5.4 kcal mol^{-1}) to be almost exactly half that of Pt/C (11.6 kcal mol^{-1}). This difference in E_a, where the measured (Nfn-Pt/C) is ca. half that of the intrinsic (Pt/C), is a very strong indication for the possibility of internal diffusion limitations, such that the reaction rate is shifted from being reaction-limited to diffusion-limited.

In this case, because no signs of internal diffusion limitations are evident for Pt/C, it can only be concluded that the presence of internal diffusion limitations observed for Nfn-Pt/C is due to the Nafion. Based on the lack of evidence suggesting the filling of these pores by the Nafion, it can be proposed that the main cause of internal diffusion limitations observed for Nfn-Pt/C is probably due to the partial blocking of pore openings by the polymer, such that the diameter of the entrance into a pore (δ) is smaller than the diameter of the pore (d) itself (as illustrated by Figure 4.1.4-4).

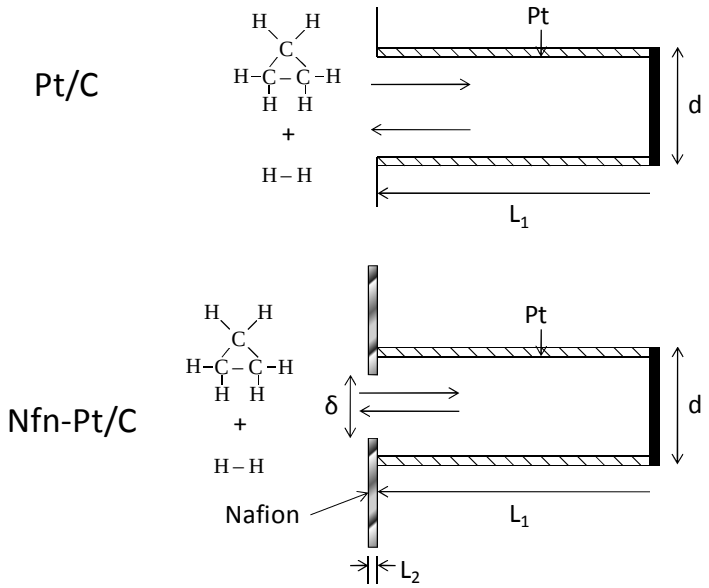

Figure 4.1.4-4: Simplified scenario of blocking of pore opening by the Nafion in Nfn-Pt/C.

Theoretical modeling of the effect of δ on the E_a was performed using a single one-dimensional ideal cylindrical pore with a length of L_1 and a diameter of d; factors such as tortuosity, pore porosity, and constriction factor were all assumed to be unity. Using a similar scenario depicted by El-Kady and Mann [El-Kady 1981] in their work regarding the deactivation of catalyst due to pore-mouth plugging from coke deposition, the Nafion was assumed to form a membrane as an impenetrable barrier of thickness L_2 with an opening to the pore of diameter δ. Please refer to that paper for further details regarding the assumptions and equations used in the model.

The Arrhenius plot of the rate resulting from the concentration in the pore is plotted in Figure 4.1.4-5 with varying values for the diameter of the opening in the membrane. It can be observed from the figure that in the case where opening in the membrane is equal

to pore diameter (i.e., $\delta = d = 10$ nm), the theoretical E_a is the intrinsic value and no evidence of internal diffusion limitations exists. As the value of δ decreases, the concentration in the pore and the resulting E_a does not start to be affected until δ is as low as 0.7 nm. Further decreases in δ beyond that point shifts the theoretical E_a farther from its intrinsic value of 11.5 kcal mol^{-1}, until finally, at a value of 0.5 nm, the δ was so small that almost no solute, in this case cyclopropane with a critical diameter of ca. 0.49 nm, is able to diffuse into the pore, thus yielding an E_a close to zero. It should be noted that for all values of δ, the concentration gradient, at steady-state, remained relatively constant throughout the pore. Even at a δ value of 0.55 nm, where the E_a showed clear diffusion limitations, the steady-state concentration of cyclopropane in the pore was ca. a factor 0.6 that of the bulk and varied no more than 0.02% from one end of the pore to the other. This lack of a concentration gradient in the pore is counterintuitive for a supposedly diffusion-influenced reaction. But this is just because most people are used to the effect of decreasing diameter of the pore. The real diffusion barrier is the membrane in the current case.

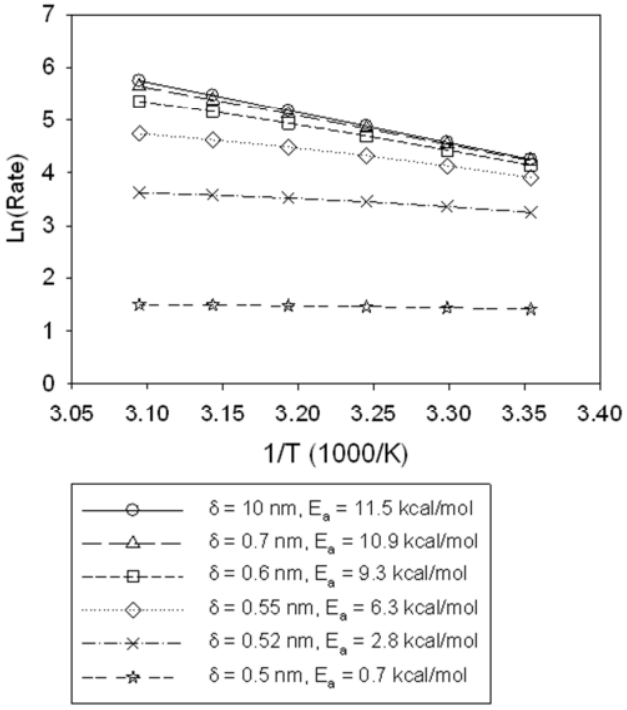

Figure 4.1.4-5: Effect of membrane opening on E_a for cyclopropane hydrogenolysis on Pt/C using an idealized cylindrical pore model with the pore mouth partially covered by a (Nafion) membrane.

It is important to note that the model is based upon a simple mass-balance and does not take into account wall effects and other electronic interactions on diffusion. In the presence of these effects, the effect of membrane diameter may be even larger.

Based on these and all previous results, it can be concluded that the effect of Nafion on Pt/C for cyclopropane hydrogenolysis appears to be limited to the induction of internal diffusion limitations by virtue of decreasing the effective diameter of the openings of the pores in the carbon support. The similar values of E_a observed for H_2-D_2 exchange reaction on both catalysts, poisoned with ppm CO, suggests that either the openings of the pores or the openings in the Nafion structure itself overlaying the pores were wide enough so that hydrogen diffusion was not affected. No blocking of Pt surface atoms by the Nafion via either physical and/or chemical interactions was observed. It is important to note that while the Nafion in this study was in the dry or unswelled state. Due to the apparent lack of interactions between the polymer and Pt surface and the minimal impact water vapor has for H_2 adsorption and activation on Pt/C [Zhang 2011], the effect that humidity would have on the this Nafion-Pt system of this study should also be minimal.

4.1.4.4 Conclusions

While the impregnation of 30 wt% Nafion on Pt/C had dramatic effects on the physical characteristics of Pt/C, such as the reduction of BET surface area from 170 m^2 $g.cat^{-1}$ to 37 m^2 $g.cat^{-1}$, the overall effect of the Nafion on the adsorption capabilities of Pt for hydrogen and CO were minimal, based on both static chemisorption and in-situ surface hydrogen concentration results. Likewise, the similar rates of H_2-D_2 exchange for Pt/C and Nfn-Pt/C poisoned with ppm CO suggests that the effect of Nafion on the poisoning behavior of CO on the reaction is also minimal. However, for cyclopropane, a molecule larger than CO, a clear decrease in the rate of hydrogenolysis was observed in going from Pt/C to Nfn-Pt/C. While this decrease might be thought to be attributable to the blocking of Pt surface atoms by Nafion, due to the lack of evidence suggesting such an interaction exists from static chemisorption, H_2-D_2 exchange and hydrogen surface concentration results, the decrease in reaction rate is most likely due to internal diffusion limitations caused by the Nafion.

Results from the modeling of a membrane (the Nafion in this case) over an idealized cylindrical pore show the effect of decreasing the size of the membrane opening, while keeping the pore diameter constant, to effectively decrease the value of E_a as a result of diffusion limitations through the membrane but not in the pore. In contrast, the similar values of E_a observed for H_2-D_2 exchange reaction on both Pt/C and Nfn-Pt/C suggests that the smaller effective pore openings in Nfn-Pt/C were not small enough to affect the smaller hydrogen molecules, as compared to cyclopropane. No blockage of Pt surface atoms by the Nafion via either physical and/or chemical interactions was observed. Based on all the measurements made, it appears that most of the Nafion is probably on the external surface of the carbon support, where it blocks micro pores significantly and partially blocks meso-macro pores. Most of the Pt particles appear to reside in the meso-macro pores.

Results from hydrogen surface concentration measurements on Pt/C and Nfn-Pt/C using H_2-D_2 exchange suggest a rapid diffusion of hydrogen and deuterium across the carbon surface at 80^{o}C. The increase in the amount of total exchangeable hydrogen going from Pt/C to Nfn-Pt/C was confirmed to be from the protonated sulfonic sites in the Nafion. It

should be noted that while contact between the polymer and Pt particles is not required for proton transport, recent results from a new evaluation method for the effectiveness of Pt/C electrocatalysts clearly show the benefits of ionic contact in improving the apparent utilization of Pt available [Lee 2010].

For further details about this study, please refer to:
"Effect and Siting of Nafion® in a Pt/C PEM Fuel Cell Catalyst," ***Journal of Power Sources*** 196 (2011) 7957-7966 (Jack Z. Zhang, Kitiya Hongsirikarn, and James G. Goodwin, Jr.).

References

Bernasek, S.L.; and G.A. Somorjai, J. Chem. Phys. 62 (**1975**) 3149-3161.
Coloma, F.; A. Sepulvedaescribano, and F. Rodriguezreinoso, J. Catal. 154 (**1995**) 299-305.
Cortright, R.D.; R.M. Watwe, B.E. Spiewak, and J.A. Dumesic, Catal. Today 53 (**1999**) 395-406.
Easton, E.B.; T.D. Astill, and S. Holdcroft, J. Electrochem. Soc. 152 (**2005**) A752-A758.
El-Kady, F.Y.A.; and R. Mann, J. Catal. 69 (**1981**) 147-157.
Hegedus, L.L.; and E.E. Petersen, J. Catal. 28 (**1973**) 150-156.
Hoost, T.E.; and J.G. Goodwin, Jr., J. Catal. 130 (**1991**) 283-292.
Kahn, D.R.; E.E. Petersen, and G.A. Somorjai, J. Catal. 34 (**1974**) 294-306.
Lee, M.; M. Uchida, H. Yano, D.A. Tryk, H. Uchida, and M. Watanabe, Electrochim. Acta 55 (**2010)** 8504-8512.
Li, G.C.; and P.G. Pickup, J. Electrochem. Soc. 150 (**2003**) C745-C752.
Martin, G.A.; R. Dutartre, S. Yuan, C. Marquez-Alvarez, and C. Mirodatos, J. Catal. 177 (**1998**) 105-112.
Montano, M.; K. Bratlie, M. Salmeron, and G.A. Somorjai, J. Am. Chem. Soc. 128 (**2006**) 13229-13234.
Passos, R.R.; V.A. Paganin, and E.A. Ticianelli, Electrochim. Acta 51 (**2006**) 5239-5245.
Robell, A.J.; E.V. Ballou, and M. Boudart, J. Phys. Chem. 63 (**1964**) 2748-2753.
Santarelli, M.G.; and M.F. Torchio, Energ. Convers. Manage. 48 (**2007**) 40-51.
Schwank, J.; J.Y. Lee, and J.G. Goodwin, Jr., J. Catal. 108 (**1987**) 495-500.
Uchida, M.; Y. Aoyama, N. Eda, and A. Ohta, J. Electrochem. Soc. 142 (**1995**) 4143-4149.
Uchida, M.; Y. Fukuoka, Y. Sugawara, N. Eda, and A. Ohta, J. Electrochem. Soc. 143 (**1996**) 2245-2252.
Zhang, J.Z.; Z.M. Liu, and J.G. Goodwin, Jr., J. Power Sources 195 (**2010**) 3060-3068.
Zhang, J.Z.; K. Hongsirikarn, and J.G. Goodwin Jr., J. Power Sources 196 (**2011**) 6186-6195.

4.1.5 The Effect of Low Concentrations of Tetrachloroethylene on H_2 Adsorption and Activation on Pt in a Fuel Cell Catalyst

4.1.5.1 Motivation

This study is a follow-up to the fuel cell work by Martínez-Rodríguez et al. [Martínez-Rodríguez 2011] to further delineate the effect of TTCE on the H_2 activation and surface coverage of Pt in order to better understand the poisoning mechanism of the impurity. It is important to note that the impurity was chosen as a model chlorinated compound that may present poisoning effects similar to chlorinated cleaning and degreasing agents. While these types of impurities are not directly associated with the production of fuel cell feed streams (i.e., hydrocarbon reformation), the use of cleaning and degreasing agents between the fueling station and the vehicle during everyday maintenance can inadvertently introduce these contaminants into the fuel. Due to the fast reaction rate of H_2 activation on Pt, kinetic measurements of the reaction could not be made at typical fuel cell operating conditions. Instead, a modified H_2-to-D_2 switch procedure, H_2-D_2 switch with Ar purge (HDSAP) [Zhang 2011a, Zhang 2010], was used to measure in-situ the surface concentrations of hydrogen on Pt/C and on Nafion-Pt/C with time-on-stream (TOS) in the presence of varying concentrations of TTCE (150-540 ppm). Chlorine elemental analyses were performed subsequently on the TTCE poisoned catalysts. Furthermore, in order to mimic conditions at the cathode, Pt/C was also exposed to 150 ppm TTCE under mixed redox conditions.

4.1.5.2 Experimental

A commercial Pt fuel cell catalyst, 20 wt% Pt supported on carbon black (Vulcan XC-72, Cabot Co.) (Pt/C), was purchased from BASF. Unless specified otherwise, the Pt/C catalyst used here is the same as the one used in the study investigating the effect of H_2O on H_2 adsorption and activation.

Nafion supported on Pt/C (Nfn-Pt/C) catalysts were prepared via incipient wetness impregnation of the commercial 20 wt% Pt/C with a Nafion ionomer solution (LQ-1105, DuPont, 5 wt% Nafion) to give a target weight loading of 30 wt% for the Nafion. The Nfn-Pt/C catalyst used here is the same as the one used in the study investigating the effect and siting of Nafion on Pt/C.

Results for H_2-D_2 exchange reaction and H_2-D_2 Switch with Ar Purge (HDSAP) were obtained at 80^{o}C and 2 atm abs. in a conventional plug flow, micro-reactor system with a total flow rate of 100 sccm. Prior to reaction experiments, all catalyst samples were pretreated at 80^{o}C in H_2 for 3 h. Time-on-stream (TOS) measurements of the effect of TTCE exposure of Pt/C and Nfn-Pt/C on hydrogen surface concentration were taken sequentially such that one sample could be used for the entire experiment. Preliminary results showed that the Ar purge periodically did not have any effect on the poisoning behavior of TTCE compared to an uninterrupted exposure of Pt/C to either 150 or 540 ppm TTCE for 12 h (non-sequential).

Specific concentrations of TTCE were obtained by flowing 10 sccm of either H_2 or Ar through a KIN-TEK Trace Source^{TM} permeation tube type LFH filled with approximately 30 mL of the liquid component. Based on the emission rate of the membrane inside the tube, control of the TTCE concentration at the outlet was maintained by placing the permeation tube in an insulated oven and adjusting its temperature accordingly.

4.1.5.3 Results and Discussion

Catalyst Characterization

Because both catalysts (Pt/C and Nfn-Pt/C) are the same as the ones used in the study investigating the effect and siting of Nafion on Pt/C, please refer to that study for details regarding the characterizations of the catalysts.

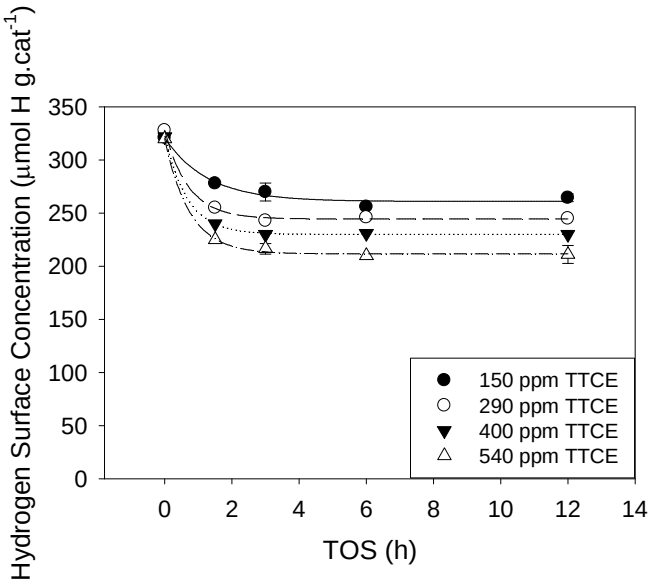

Figure 4.1.5-1: Effect of TTCE exposure on the hydrogen surface concentration on Pt/C in the presence of only H_2.

Effect of TTCE Poisoning on Pt in H_2 for Pt/C

Figure 4.1.5-1 shows the TOS measurements of hydrogen surface concentration on 100 mg of Pt/C in the presence of 150–540 ppm TTCE in a (50/50) H_2/Ar mixture at 60^{o}C and 2 atm. Even in the presence of such high concentrations of TTCE, the hydrogen surface concentration, at steady-state, showed a loss of only 18% when exposed to 150 ppm TTCE over a 12 h period. Increase in the TTCE concentration resulted in a further decrease in hydrogen surface concentration such that at 290, 400, and 540 ppm TTCE, the reductions in hydrogen surface concentration were ca. 24%, 29%, and 35%, respectively. While the loss in hydrogen surface concentration is not minor, it should be noted that, due to the extremely high activity Pt has for adsorbing and activating hydrogen, a much more substantial loss in Pt surface atoms (ca. 66%) is required to shift

the reaction away from equilibrium for the conditions used and to start inhibiting the performance of a PEMFC [Zhang 2010]. Because of this, the conversion of H_2-D_2 exchange on Pt, even in the presence of 540 ppm TTCE, remained at equilibrium at steady-state. This result can also be observed from fuel cell hydrogen pump experiments, where polarization scans using a H_2(anode)/N_2(cathode) setup, with 30 ppm TTCE in the anode feed, showed that the impurity had no effect on the overpotential of the hydrogen oxidation reaction (HOR) over a 4 h period [Martínez-Rodríguez 2011]. However, introduction of the same TTCE concentration to a H_2(anode)/O_2(cathode) fuel cell for 3 h showed almost a complete degradation in fuel cell performance.

Elemental analysis of Cl concentration (performed by Galbraith Laboratories) using ion chromatography for Pt/C samples exposed to 150, 290, 400, or 540 ppm TTCE for 12 h resulted in a retention of only ca. 13, 20, 23, and 26 µmol Cl $g.cat^{-1}$, respectively. While this low concentration of Cl would not account for the reduction in hydrogen surface concentration on a 1:1 Cl:Pt_S basis, surface science results for Cl adsorption on Pt(100) single crystals suggest that the stoichiometric ratio of Cl to Pt_S is actually closer to 1:2 [Gutleben 1990]. Furthermore, results from low-energy electron diffraction (LEED) for the adsorption of Cl on Pt(110) and Pt(111) single crystals show clear evidence of surface reconstruction [Schennach 1997]. Thus, based on this and the steady-state behavior of TTCE poisoning on the hydrogen surface concentration of Pt in the presence of excess H_2, it can be concluded that the poisoning effect of the impurity, at the lower reaction temperatures, is mainly due to the deposition of Cl-species on the Pt surface, resulting in Pt_S blockage, effects on the chemisorption of hydrogen on neighboring Pt surface atoms, and/or Pt surface reconstruction.

Reversibility of TTCE Poisoning on Pt in H_2 for Pt/C

Figure 4.1.5-2 shows the regeneration of Pt/C after exposure to 150 ppm TTCE in H_2 for 12 h. The regeneration was performed by flowing a mixture of (50/50) H_2/Ar over the poisoned catalyst at 60°C and 2 atm for a period of 22 h with hydrogen surface concentration measurements at 1.5, 3, 6, and 22 h of regeneration. As can be observed from the figure, some partial recovery of the Pt surface is evident after only 1.5 h of regeneration. However, similar to the results observed for the regeneration of CO poisoning on Pt/C [Zhang 2010], complete recovery of hydrogen surface concentration could not be achieved, even after 22 h of exposure to H_2. Elemental analysis of Cl on the poisoned Pt/C, after 22 h of regeneration, shows a concentration of ca. 7 µmol Cl $g.cat^{-1}$ remaining of the original 13 µmol Cl $g.cat^{-1}$. This lack of a complete recovery may be due to the difficulty in removing adsorbed Cl and/or in reconstructing at 60°C the surface modified by the adsorption of Cl-species.

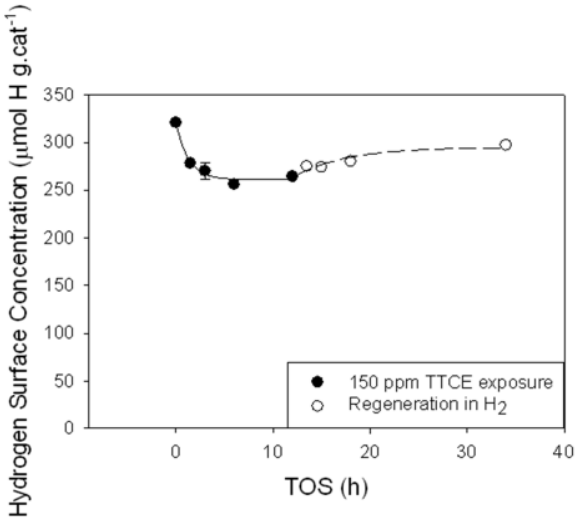

Figure 4.1.5-2: Regeneration in H_2 after TTCE poisoning for Pt/C.

Effect of Nafion on TTCE Poisoning on Pt/C in H_2 for Nfn-Pt/C

The effect of Nafion on the poisoning behavior of TTCE on Pt is shown in Figure 4.1.5-3. It should be noted that, based on the effect Nafion has for obstructing the diffusion of gas-phase H_2 away from the catalyst, the purge time used for the hydrogen surface concentration measurements for Nfn-Pt/C was increased to 50 min [Zhang 2011b].

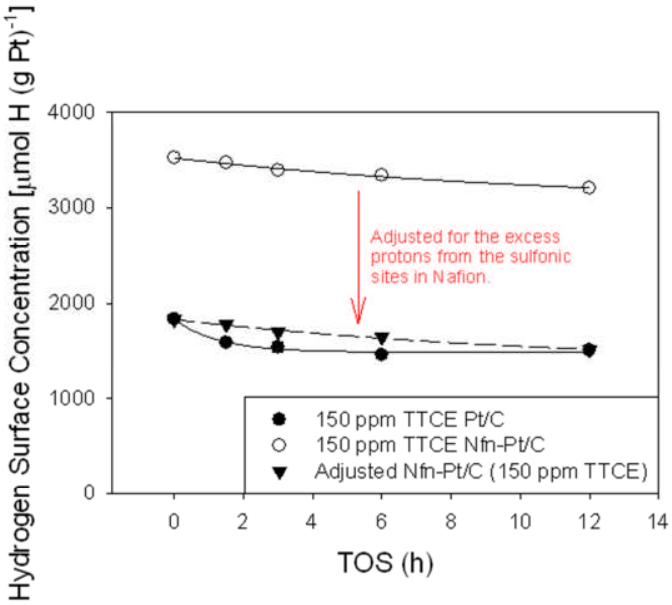

Figure 4.1.5-3: Effect of Nafion on the poisoning behavior of TTCE in H_2 on Pt.

Similar to the effect Nafion has in obstructing the rate of diffusion of CO to the Pt surface [Zhang 2011b], the presence of the polymer apparently also decreased the diffusion of TTCE to the Pt surface. After taking into account the excess protons available from the sulfonic sites in the Nafion, the effect of Cl on the strongly adsorbed hydrogen surface concentration on the Pt surface for Nfn-Pt/C was the same as for Pt/C, within experimental error. No evidence of physical and/or chemical interaction between the Nafion and the Pt surface atoms exists based on these results, as also previously found [Zhang 2011b].

Co-adsorption of TTCE and CO on Pt in H_2 for Pt/C

The poisoning effect of 150 ppm TTCE + 30 ppm CO on Pt/C was investigated via hydrogen surface concentration measurements, with the results plotted in Figure 4.1.5-4. While the poisoning effect of two impurities is always interesting due to possible synergistic effects, the co-poisoning experiment was further motivated by FT-IR results suggesting that the presence of Cl on the Pt surface may block similar sites for CO adsorption. In a study by Gracia et al. [Gracia 2002], two batches of Pt/SiO_2 catalysts were prepared with one using a Pt-precursor containing Cl (H_2PtCl_6) and the other using a Pt-precursor without Cl [$Pt(NH_3)_4(NO_3)_2$]. Results from FT-IR obtained by exposing each catalyst to 0.3% CO in He at varying temperatures (45-200°C) show a significant reduction in the absorbance for the IR band corresponding to the linear-bonded CO, especially at the lower temperatures.

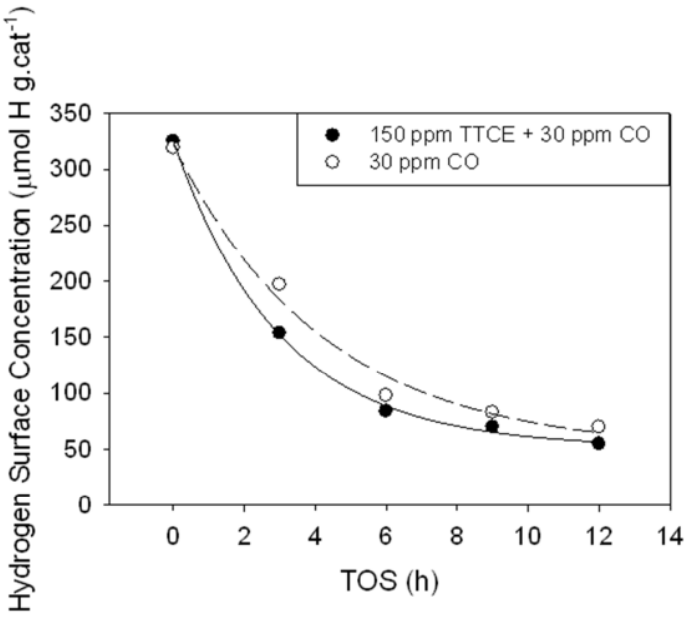

Figure 4.1.5-4: Effect of 30 ppm CO + 150 ppm TTCE in H_2 on the hydrogen surface concentration on Pt/C.

Based on Figure 4.1.5-4, the poisoning behavior of 150 ppm TTCE + 30 ppm CO on the hydrogen surface concentration of Pt/C appears to have been relatively similar to that of 30 ppm CO by itself, suggesting that the poisoning effect of CO is more dominant over that of Cl. This result is somewhat surprising, especially considering the highly electronegative nature of Cl. Furthermore, theoretical surface science studies of electrostatic adsorbate-adsorbate interactions show that an adsorbing molecule like CO, which extracts electrons from the surface, will be destabilized by nearby electronegative atoms like Cl [Holloway 1987, Nørskov 1987]. This result suggests that the presence of Cl should decrease the adsorption behavior of CO and is in agreement with what was observed from the FT-IR results mentioned above. So why then is CO the dominant poison in our CO + TTCE study? While the presence of such large amounts of H_2 may have some effect on the adsorption of the two impurities, the reason is more likely due to the method of Cl deposition or, more specifically, the hydrodechlorination of TTCE. In other words, unlike the Pt/SiO_2 study [Gracia 2002], where Cl was directly deposited on the catalyst using a Pt-precursor containing Cl, the surface Cl in our study is from the decomposition reaction of TTCE.

Effect of TTCE Poisoning on Pt in O_2 and H_2+O_2

While the exposure of Pt/C to TTCE in a reducing environment (H_2) has been shown to have a negligible effect on the activity of Pt for adsorbing and activating H_2 and only a small effect on hydrogen surface coverage, the detrimental effect the impurity has on the performance of a fuel cell still remains to be answered. While no TTCE was detected at the cathode outlet during any of the fuel cell tests, this does not eliminate the possibility of chlorinated species being present at the cathode. In fact, it was hypothesized by Martínez-Rodríguez et al. [Martínez-Rodríguez 2011] based on their results that the poisoning effect observed in their fuel cell was most likely due to the migration of a chlorinated compound, resulting from the decomposition of TTCE, across the membrane to the cathode where the oxygen reduction reaction (ORR) was poisoned.

In order to fully investigate the effect chlorinated compounds might have on the ORR, it is important to duplicate the mixed redox conditions present (hydrogen + O_2) at the cathode of a fuel cell, where water vapor is also produced. To this end, the poisoning effect of 150 ppm TTCE on Pt/C was investigated in a mixture of 4% H_2 and 1.8% O_2 in Ar. Besides being below the flammability range of a H_2 + O_2 mixture, the 2:1 ratio of H_2:O_2 was chosen due to evidence suggesting a reasonably high conversion of TTCE in this stoichiometric mixture at low temperatures (ca. 20% at 75^{o}C) [Orbay 2008]. In addition, the combination of both H_2 and O_2 on Pt also allows for the investigation of the effect that water vapor might have on the TTCE poisoning, which, at the partial pressures of H_2 and O_2 used would be equivalent to ca. 30 %RH, assuming 100% conversion.

From Figure 4.1.5-5, it can be observed that the exposure of Pt/C to the mixture of 4% H_2/1.8% O_2 in Ar for 3 h resulted in a slight increase in the hydrogen surface concentration measured. This excess surface hydrogen was most likely contributed by the formation and retention of some H_2O on the catalyst surface, and should not be

confused with an increase in Pt surface atom availability [Zhang 2011a]. In contrast to the lack of effect observed in the presence of H_2, exposure of Pt/C to 150 ppm TTCE in the H_2-O_2 mixture for 3 h resulted in a substantial decrease in Pt surface atom availability. The effect of this poisoning was repeated 5 times at the same conditions on fresh samples of Pt/C, with reproducibility being < ±5%. Furthermore, based on the fuel cell hydrogen pump results [H_2(anode)/N_2(cathode)] of Martínez-Rodríguez et al. [Martínez-Rodríguez 2011], with 30 ppm TTCE in the humidified anode feed, no decrease in the overpotential of the HOR was observed over a 4 h period in the presence of H_2 + H_2O. This suggests that the significant loss in the hydrogen surface concentration on Pt/C, from the exposure of TTCE in the H_2-O_2 mixture, was not due to either H_2 or H_2O, but clearly shows the role O_2 plays in enhancing the deactivation process of the catalyst. It should be re-emphasized that, in the absence of H_2, no effect from Cl poisoning was observed due to the TTCE being unable to decompose in O_2 at the lower reaction temperatures, resulting in little or no deposition of Cl on the Pt surface.

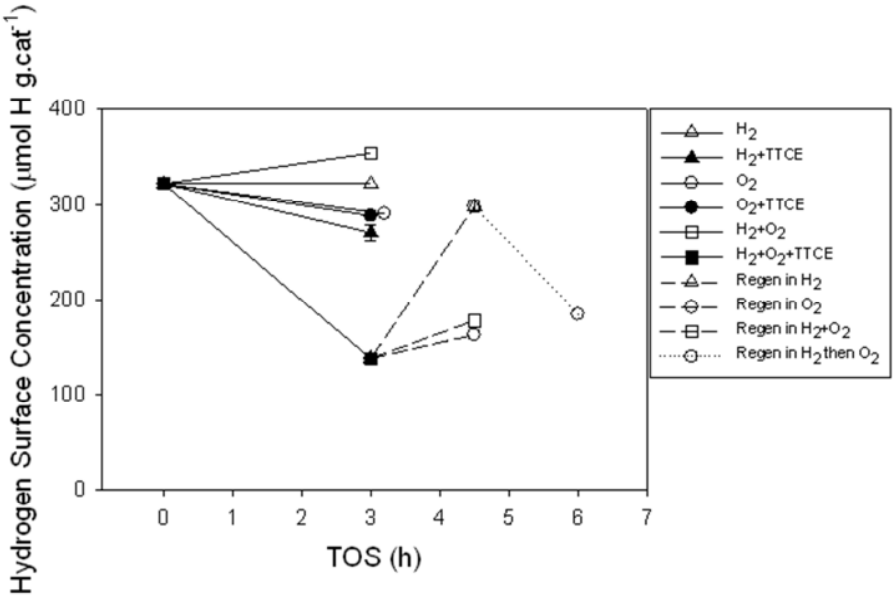

Figure 4.1.5-5: Comparison of exposure and 150 ppm TTCE poisoning of Pt/C in different gases (H_2, O_2, and H_2 + O_2). Effect of different regeneration gases. The data point for exposure to O_2 for 3 h has been moved slightly to the right due to overlapping with the data point for exposure to O_2+TTCE.

Thus, the poisoning effect of TTCE on the performance of a fuel cell is really the combination of processes that are occurring at both the anode and the cathode. In other words, while the addition of TTCE to the anode has a minor effect on the Pt surface atom availability, the presence of the H_2 plays a crucial role in initiating the poisoning process by facilitating the decomposition of TTCE to ethane and HCl. Once formed, the HCl then migrates from the anode to the cathode, where the presence of O_2 enhances the poisoning effect from the halogen. Without the H_2 being present to first decompose the TTCE via hydrodechlorination, the poisoning effect from the TTCE would most likely

not be as severe, as O_2 + TTCE had no further effect on the Pt surface atom availability compared to O_2 by itself. This is again due to the fact that the decomposition of TTCE on Pt in O_2 is nearly 0% at the lower temperatures (< 100^{o}C) [Orbay 2008].

Similar to the results observed in the performance recovery studies of a fuel cell poisoned with TTCE [Martínez-Rodríguez 2011] and what was shown in Figure 4.1.4-5, regeneration of the poisoned Pt/C in 4% H_2 showed an almost complete recovery of Pt surface atom availability (based on hydrogen uptake) in 1.5 h. In contrast, regeneration of the poisoned Pt/C in 1.8% O_2 or 4% H_2 + 1.8% O_2 resulted in little recovery in the same period of time. Interestingly, subsequent exposure to 1.8% O_2, with no TTCE, following regeneration in 4% H_2 showed a re-poisoning (i.e., loss of Pt surface atom availability) of the catalyst. This re-poisoning effect from subsequent exposure to O_2, after regenerating in H_2, was also observed by Martínez-Rodríguez et al. [Martínez-Rodríguez 2011] and was suggested to be from residual TTCE desorbing from the gas lines. However, due to the fact that all gas lines were heated to 100^{o}C with heating tape in our experimental system and the long time since TTCE was removed from the feed stream, a more likely reason may be associated with a study by Garcia et al. [Garcia 2002], where it was suggested that O_2 facilitates the migration of adsorbed Cl from the support to the metal surface, a process which H_2 helps reverse. However, more work is needed to validate this hypothesis.

4.1.5.4 Conclusions

The poisoning effect of TTCE on the ability of Pt to activate and adsorb H_2 was investigated at 60^{o}C and 2 atm using hydrogen surface concentration measurements on both Pt/C and Nfn-Pt/C catalysts exposed to varying concentrations of the impurity (150-540 ppm). Even at as high as 540 ppm TTCE, the reduction in hydrogen surface concentration was observed to be only ca. 33%, which was not enough to shift the H_2-D_2 exchange reaction away from being equilibrium limited. Decrease in the concentration of TTCE resulted in a decrease in the amount of surface hydrogen lost. As expected, the addition of Nafion to Pt/C decreased the rate of TTCE poisoning, due to the polymer inhibiting the rate of diffusion [Zhang 2011b], but had very little/no effect on the poisoning behavior of TTCE at steady-state. Considering the high activity Pt has for the adsorption and activation of H_2, these results suggest that the presence of TTCE should have no observable effects on the HOR, due to not being able to shift the reaction away from equilibrium. These results also suggest that the detrimental loss in fuel cell performance in the presence of TTCE is not from the anode but most likely from the cathode.

Co-adsorption of CO and TTCE (30 ppm CO + 150 ppm TTCE) on Pt/C in H_2 showed that the poisoning effect from the mixture to be primarily dominated by the CO. This result is surprising considering overwhelming evidence from FT-IR [Gracia 2002] and surface science studies [Holloway 1987, Nørskov 1987, Lang 1985, Nørskov 1984] suggesting that the presence of Cl should actually destabilize the adsorption of CO due to electrostatic adsorbate-adsorbate interactions. However, because the deposition of Cl on the Pt surface is from the hydrodechlorination of TTCE, it can be speculated that the

structure sensitivity of the reaction plays a role. The presence of CO, which has a much more direct method of adsorption, would then severely poison the reaction and limit the deposition of Cl. It should be emphasized that this is only speculation at this point as data regarding the structure sensitivity of the hydrodechlorination of TTCE is extremely limited.

While only a slight reduction in amount of available Pt surface atoms (measured based on H_2 uptake from HDSAP) was observed from the exposure of TTCE to Pt/C in a H_2-only environment, a much more significant loss of available Pt surface atoms was observed when the catalyst was exposed to TTCE in the presence of both H_2 and O_2. This increase in the poisoning effect of TTCE was found to be contributed by the combination of H_2 and O_2, as the absence of either one resulted in little/no poisoning at the experimental conditions studied (60^{o}C and 2 atm). This enhancement in the poisoning effect of TTCE in the presence of O_2 clearly shows the role O_2 plays in enhancing the deactivation process of the catalyst and further confirms that the actual poisoning of fuel cell performance by TTCE is at the cathode, rather than the anode. Similar to the recovery results obtain in a fuel cell [Martínez-Rodríguez 2011], regeneration of Pt surface atoms (based on hydrogen surface concentration measured) of a poisoned Pt/C showed the highest level of recovery when regenerated in only H_2, followed distantly by H_2+O_2 and O_2.

For further details about this study, please refer to:
"The Effect of Low Concentrations of Tetrachloroethylene on H_2 Adsorption and Activation on a Pt Fuel Cell Catalyst," ***Journal of Power Sources*** 196 (2011) 8391-8397 (Jack Z. Zhang, Hector Colon-Mercado, and James G. Goodwin, Jr.).

<u>References</u>

Gracia, F.J.; J.T. Miller, A.J. Kropf, and E.E. Wolf, J. Catal. 209 (**2002**) 341-354.
Gutleben, H.; and E. Bechtold, Surf. Sci. 236 (**1990**) 313-324.
Holloway, S.; J.K. Nørskov, and N.D. Lang, J. Chem. Soc.-Faraday Trans. I 83 (**1987**) 1935-1943.
Lang, N.D.; S. Holloway, and J.K. Nørskov, Surf. Sci. 150 (**1985**) 24-38.
Martínez-Rodríguez, M.J.; E.B. Fox, W.D. Rhodes, C.S. McWhorter, S. Greenway, and H.R. Colón-Mercado, J. Electrochem. Soc. 158 (**2011**) 1-5.
Nørskov, J.K.; S. Holloway, and N.D. Lang, Surf. Sci. 137 (**1984**) 65-78.
Nørskov, J.K.; and P. Stoltze, Surf. Sci. 189 (**1987**) 91-105.
Orbay, O.; S. Gao, B. Barbaris, E. Rupp, E. Saez, R.G. Arnold, and E.A. Betterton, Appl. Catal. B-Environ. 79 (**2008**) 43-52.
Schennach, R.; and E. Bechtold, Surf. Sci. 380 (**1997**) 9-16.
Zhang, J.Z.; Z.M. Liu, and J.G. Goodwin, Jr., J. Power Sources 195 (**2010**) 3060-3068.
Zhang, J.Z.; K. Hongsirikarn, and J.G. Goodwin, Jr., J. Power Sources 196 (**2011a**) 6186-6195.

Zhang, J.Z.; K. Hongsirikarn, and J.G. Goodwin, Jr., J. Power Sources 196 (**2011b**) 7957-7966.

4.2 Nafion Fundamentals

4.2.1 Influence of Ammonia on the Conductivity of Nafion® Membranes

4.2.1.1 Motivation

Polymer electrolyte membrane fuel cells (PEMFCs) have high power density [Wei 2006; Collier 2006] and have been proposed for automotive, portable, and stationary applications [Xia 2008; Slade 2002]. However, high system costs and durability to impurities in the H_2 fuel and/or oxidant streams have limited the adoption of PEMFC technologies [Kundu 2006].

Currently, the majority of hydrogen used in industrial processes is generated by reforming methane or other hydrocarbons [Farrell 2007]. These processes unavoidably generate small amounts of contaminants such as CO, CO_2, CH_4, NH_3, H_2S, and organic compounds [Cheng 2007]. It is known that NH_3 is one of the most detrimental impurities to proton transport in the Nafion membrane and ionomer layers of PEMFCs [Uribe 2002; Halseid 2004; Soto 2003].

Up to the present, most research groups have studied the effects of impurities on the overall fuel cell performance. However, very few have examined the effect on each component in the fuel cell, especially Nafion, under conditions similar to fuel cell operation. The goal of the research reported here was to measure the conductivity of a Nafion membrane when it was exposed to ammonia in a controlled way, thereby permitting the ohmic losses in the membrane and potentially in the ionomer layer to be better understood. The effects of NH_4^+ ions and of NH_3 on liquid-phase conductivity at ambient temperature and on gas-phase conductivity at typical fuel cell conditions of Nafion membranes were investigated via electrochemical impedance spectroscopy.

4.2.1.2 Experimental

The Nafion membranes with 1100 EW (DuPont Inc.), having nominal thicknesses of 183 μm (N-117, 360 g m^{-2}) and 25.4 μm (N-211, 50 g m^{-2}), were purchased from Ion Power, Inc. and pretreated to keep the membranes in a fully acidic form, free of contaminants. All membranes were pretreated to eliminate organic contaminants, to fully protonate the membrane, and to remove any residual acid. For certain studies, membranes with known concentrations of ammonium ions were prepared.

In order to determine sulfur leaching, chlorine adsorption, and ammonium uptake in the Nafion membranes, elemental analyses of the membranes and the exchange solutions were carried out by Galbraith Laboratories in Knoxville, Tennessee.

The IECs of the membranes (2.5 cm x 1 cm) were determined by ion-exchange with NaOH (Acros Organics). The ionic conductivities in the lateral direction of the membranes were determined by a two-probe technique using a frequency response analyzer (Gamry Potentiostat Reference 600). A portion of membrane (5.5 cm × 1 cm) was fixed in a custom-made polyetheretherketone (PEEK) sample holder that had a 2.5 cm x 2.5 cm working window with 2 Pt foil electrodes. Conductivity measurements of the pre-exchanged N-211 in liquid electrolyte (DI water) were carried out at room temperature. Conductivity measurements of the pre-exchanged N-211 in the gas phase as a function of humidity under a flow of 130 sccm of He (UHP, National Specialty Gases) at various %RH, and temperatures (60 – 90°C, standard 80°C) for 8 hr until there was no change in conductivity. Conductivity measurements of fresh N-211 in the gas phase containing low concentrations of ammonia were also carried out.

The ammonium ion content of N-211 (y_{NH4+}) was determined both for membranes prepared with a fixed ammonium concentration and after exposure of a membrane to the He gas phase containing ppm concentrations of ammonia. This was carried out using an aqueous solution with an excess of protons. The concentration of ammonium ions in the exchanged solution was analyzed by an ion selective electrode (ammonia electrode Thermo Scientific 9512 and Orion 4 Star pH benchtop meter).

4.2.1.3 Results and Discussion

Influence of Ammonium Composition in Ammonium Ion-Poisoned Nafion on Conductivity in DI Water and in Gas-Phase He

Figure 4.2.1-1 presents the conductivities of Nafion membranes that had been ion-exchanged with specific fractions of ammonium ions and equilibrated in deionized (DI) water at room temperature. It can be seen that the conductivities of both N-211 and N-117 decreased linearly with increasing ammonium concentration (y_{NH4+}) from 115 mS cm^{-1} with no ammonium ions to 24 mS cm^{-1} in the fully exchanged ammonium form. However, it was found that ammonium ion content affects the conductivity of N-211 differently when it is measured in a gas phase at 80°C versus in an aqueous phase at room temperature.

Figure 4.2.1-2 shows that the ionic conductivity of N-211 decreased more dramatically with increasing ammonium ion content in the membrane when it was measured in the gas phase as opposed to in the aqueous phase. The fully NH_4^+-form of Nafion, the ionic conductivity was reduced by 66% and 98% compared to the H^+-form at 100 %RH and 30 %RH, respectively. This finding suggests that ammonia has a lesser effect on the conductivity at higher humidity. Therefore, operating a PEMFC at high humidity should help increase ammonia tolerance.

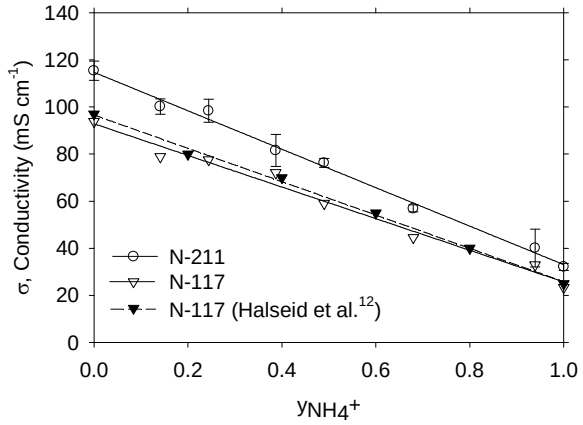

Figure 4.2.1-1: Conductivity at room temperature in DI water for Nafion membrane (N-117 and N-211) containing various ammonium compositions (y_{NH4+}=1 for 877 ± 7 µmol NH_4^+ g^{-1}).

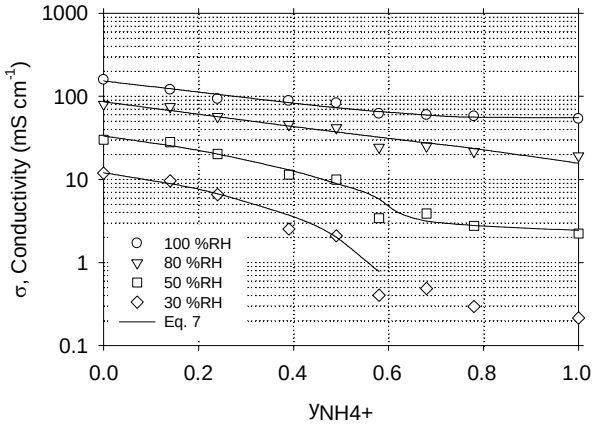

Figure 4.2.1-2: Conductivity at 80°C in a He gas phase for N-211 as a function of ammonium ion fraction (y_{NH4+}).

The explanation for the difference in ammonium ion effect on the conductivity in gas vs. liquid phase is probably due to the lower water content, lack of complete swelling, and poorly connected water network in the Nafion structure in the gas phase compared to in the aqueous solution. The water uptake of the membrane at a particular humidity and an elevated temperature (80°C; λ_{H2O} = 2.2 – 9.6 mol H_2O / mol $–SO_3^-$) was less than that in DI water at room temperature (λ_{H2O} = 21 mol H_2O / mol $–SO_3^-$) because the condensation of water vapor on the hydrophobic fluorocarbon surface is less favorable than in an excess of liquid water [Zawodzinski 1993; Onishi 2007; Weber 2003]. This lower water sorption in the gas phase in the pores and channels of the Nafion membrane causes non-continuous proton transport pathway and contracted structure, which increased the strength of the hydrogen-bonded networks between ammonium ions and neighboring water molecules leading to a more rigid structure.

Influence of Gas-Phase Ammonia Impurity on the Conductivity of a Fresh Nafion Membrane

The conductivity of fresh membranes in the presence of gas-phase ammonia was also studied. Figure 4.2.1-3 shows the real time conductivity of Nafion membranes exposed to 20 ppm NH_3 at various humidities and 80°C. The ammonia adsorption at high humidity was much slower than at low humidity and the steady-state conductivity was much greater, although the uptake of ammonia at final conductivity was still about the same (ca. 877 ± 23 μmol g^{-1}). It is conclusive that the ionic conductivity of N-211 is strongly affected by the level of humidity and the ammonium content in the Nafion membrane, and an increase in the PEMFC's performance and impurity tolerance would be expected at high humidity, which is consistent with our other results.

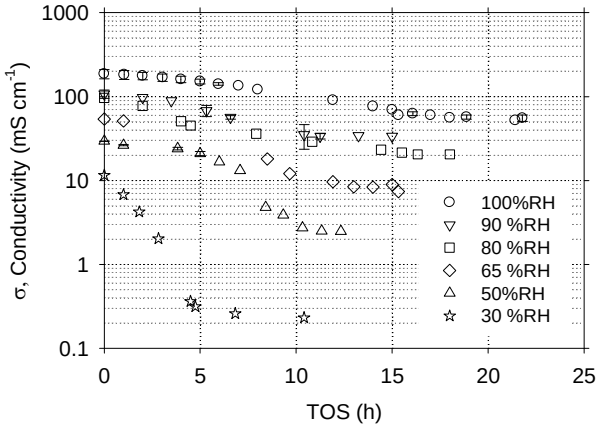

Figure 4.2.1-3: Ionic conductivity of N-211 at different humidities and 80°C in the presence of 20 ppm NH_3 as a function of time-on-stream (TOS).

4.2.1.4 Conclusions

Conductivity measurements of N-211 membranes exchanged with ammonium ions were performed both in an aqueous solution and in gas phase. In the liquid phase, the conductivity in DI water at room temperature in the NH_4^+ -form decreased linearly by a factor of 4 compared to that in the H^+-form. In the gas phase, the conductivity also decreased with increasing ammonium content in the membrane and with decreasing relative humidity. However, the impact of relative humidity on the ionic conductivity of N-211 with a particular ammonium content was significant. The conductivity of N-211 in the NH_4^+-form at 80°C decreased by a factor of 55 or 3 compared to that in the H^+-form at 30 %RH or 100 %RH, respectively.

The conductivity of a fresh membrane exposed to gas-phase ammonia was also studied under conditions similar to that of operating fuel cells. The conductivity of N-211 declined with TOS and reached the steady-state conductivity over the entire humidity range investigated (30-100%RH). The kinetics of ammonia adsorption onto the sulfonic groups at low humidity was much faster than at high humidity and the final steady-state conductivities of N-211 in the NH_4^+-form were significantly increased with an increase in

humidity. The experimental results suggest that operating PEMFCs at high relative humidity enhances their ammonia tolerance.

For further details about this study, please refer to:
"Influence of Ammonia on the Conductivity of Nafion Membranes," ***Journal of Power Sources*** 195 (2010) 30-38 (Kitiya Hongsirikarn, Jack Zhang, James G. Goodwin, Jr., Scott Greenway, and Stephen Creager).

References

Cheng, X.; Z. Shi, N. Glass, L. Zhang, J.J. Zhang, D.T. Song, Z.S. Liu, H.J. Wang, J. Shen, *Journal of Power Sources*, 165 (**2007**), 739.

Collier, A.; H.J. Wang, X.Z. Yuan, J.J. Zhang, D.P. Wilkinson, *International Journal of Hydrogen Energy*, 31 (**2006**), 1838.

Farrell, C.G.; C.L. Gardner, M. Ternan, *Journal of Power Sources*, 171 (**2007**), 282.

Halseid, R.; P.J.S. Vie, R. Tunold, *Journal of Electrochemical Society*, 151 (**2004**), A381.

Kundu, P.P.; A. Pal, *Reviews in Chemical Engineering*, 22 (**2006**), 125.

Slade, S.; S.A. Campbell, T.R. Ralph, F.C. Walsh, *Journal of Electrochemical Society*, 149 (**2002**), A1556.

Soto, H.J.; W.K. Lee, J.W. Van Zee, M. Murthy, *Electrochemical and Solid State Letters*, 6 (**2003**), A133.

Uribe, F.A.; S. Gottesfeld , T.A. Zawodzinski, *Journal of Electrochemical Society*, 149 (**2002**), A293.

Wei, Z.D.; H.B. Ran, X. A. Liu, Y. Liu, C. X. Sun, S. H. Chan, P. K. Shen, *Electrochimica Acta*, 51 (**2006**), 3091.

Xia, Z.T.; Q.P. Wang, M. Eikerling, Z.S. Liu, *Canadian Journal of Chemistry-Revue Canadienne De Chimie*, 86 (**2008**), 657.

4.2.2 Effect of Ammonium Ion Distribution on Nafion® Conductivity

4.2.2.1 Motivation

It has been found previously that the conductivities of Nafion® membranes decrease with an increase in ammonium ion composition in them [Uribe 2002; Soto 2003; Halseid 2004]. This is because the conductivity in the Nafion involves the transport of protons (H^+) and any proton-containing molecules (such as H_3O^+, H_2O, and NH_4^+), but the ionic mobility of NH_4^+ ions is lower than that of protons by ca. 75% [Halseid 2004; Hongsirikarn 2010a; Thakkar 2007].

Since ammonia, if present, is in the H_2 fuel stream at the anode, ammonia initially adsorbs on Nafion at the contacted interface before it penetrates into the bulk membrane. However, as the fuel cell operates, transport of ammonium ions from the anode to cathode can occur, causing a change in the non-uniformity of ammonium ion distribution in the membrane and catalyst layers. It is certainly true that initially, and potentially throughout its operation, NH_4^+ ions may be non-uniformly distributed throughout the

membrane, especially since adsorption of ammonia on Nafion is essentially irreversible. So far, no studies have been published addressing the effect of ammonium ion distribution on Nafion conductivity.

Preliminary results suggested proton conductivity in a Nafion membrane is affected not only by ammonium ion concentration (y_{NH4+}) but also by its distribution. The conductivities as a function of y_{NH4+} at 50 %RH and 80°C for uniformly and non-uniformly poisoned Nafion membranes are replotted in Figure 4.2.2-1. The uniformly poisoned case represents membranes pre-ion exchanged with solutions having known concentrations of NH_4Cl. The non-uniform case, on the other hand, represents membranes exposed to a He gas phase containing ppm levels of ammonia. Consequently, ammonia distributed non-uniformly in the membrane because ammonia first adsorbed on sites in the outer layers (being limited by the low concentration in the gas phase), and only later, after filling the more external sites, was able to diffuse in the gas phase further into the membrane. It can be seen in Figure 4.2.2-1 that the conductivity of a non-uniformly ammonium ion poisoned-membrane is different from that of a uniformly poisoned membrane, even though the membranes contain the same amounts of ammonium ions (overall values of y_{NH4+} being the same).

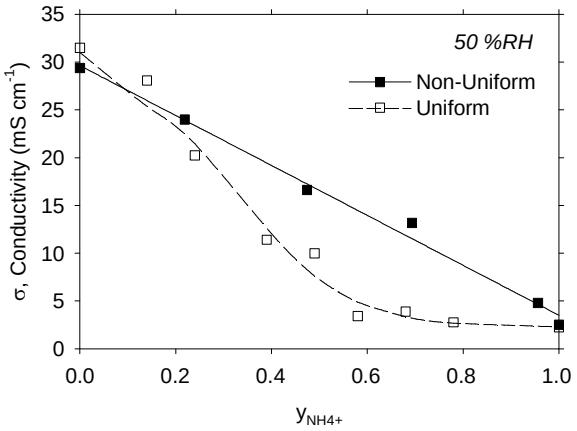

Figure 4.2.2-1: The conductivity at 50 %RH and 80°C of single N-211 membranes containing different NH_4^+ ion compositions with either uniform or non-uniform distributions. {Replotted from references [Hongsirikarn 2010a-b]}.

The objective of this work was to quantitatively investigate the influence of ammonium ion distribution on the conductivity of a Nafion membrane in a humidified gas stream at typical fuel cell conditions. The conductivities of two kinds of contaminated membranes having uniform and non-uniform ammonium ion distributions were studied. To simulate a membrane with a well-defined ammonium ion concentration profile, three individual Nafion membranes containing known amounts of ammonium ions were physically stacked together. The uniform and non-uniform cases represented membranes having 3 layers with the same y_{NH4+} or step changes in concentration, respectively.

4.2.2.2 Experimental

Commercial Nafion® 211 membranes (N-211, 1100 EW, 25 μm thick) were purchased from DuPont. In order to obtain the H^+-form of the N-211 membranes, rectangular samples of membranes (5.5x1 cm^2) were boiled separately in 3% H_2O_2, 0.5 M H_2SO_4, and deionized (DI) water for 1 h each. After that, the membranes were rinsed several times, immersed in DI water at room temperature (~25°C), and kept in the dark prior to an experiment.

In order to be able to investigate Nafion membranes with well defined and determined distributions, 3-layer composite membranes having various ammonium ion distributions were prepared by physically stacking together three membranes with known ammonium ion compositions (given by y_{NH4}+ which is the fraction of sulfonic sites ($-SO_3^-$) neutralized by ammonium ions). Each individual membrane was prepared by ion-exchanging the H^+-form of N-211 in standard solutions containing known concentrations of NH_4Cl and HCl at room temperature under constant shaking at 250 rpm for at least 7 days. All exchange solutions contained 0.1 M Cl^- and were changed periodically during equilibration to avoid any effect from differences in Cl^- concentration. Single membranes having different ammonium ion compositions in two separate longitudinal regions were also prepared by immersing each end of the membranes in separate exchange solutions contained in a two-compartment petri dish. The solutions in each compartment were also changed periodically, and the membranes were allowed to exchange in these static solutions at room temperature for at least 7 days.

Conductivity measurements were carried out using a two-probe ac technique. A potentiostat (Gamry Potentiostat Reference 600) was used for measuring the impedance of the membrane. Prior to conductivity measurements, each membrane sample having a given ammonium ion composition was taken out from the solution and rinsed several times with DI water to remove the excess exchange solution in the membrane. The membrane was then treated individually in a flow of 130 sccm He (UHP, National Specialty Gases) at 30 %RH and 80°C for 10 h in order to get rid of any weakly bound NH_4^+ ions in the Nafion clusters. For conductivity measurements in the gas phase of single membranes having different ammonium ion compositions in two separate regions or of 3-layer composite membranes with known ammonium ion distribution, the membrane was allowed to equilibrate in the impedance chamber (ID = 16 cm, H = 25 cm) at a given humidity and temperature for 4 h and the conductivity was measured. Composite membranes with $y^T_{NH_4^+}, y^M_{NH_4^+}, y^B_{NH_4^+}$ (where $y^T_{NH_4^+}, y^M_{NH_4^+}$, and $y^B_{NH_4^+}$ are the ammonium ion concentrations of the top, middle, and bottom layers of the composite membrane) were prepared by physically stacking three membranes together. For conductivity measurement in DI water, each membrane (5.5×1 cm^2) was re-equilibrated in DI water for 15 min before the conductivity was performed. Then, the three membranes with $y^T_{NH_4^+}, y^M_{NH_4^+}, y^B_{NH_4^+}$ were physically stacked together and allowed to equilibrate in DI water for 15 min prior to conductivity measurement in DI water.

For uniform ammonium ion poisoning (a 3-layer composite membrane with $y^{T}_{NH_4^+} = y^{M}_{NH_4^+} = y^{B}_{NH_4^+}$), the conductivity at 30 %RH of a composite membrane was measured until it was constant. After that, the humidity was increased in increments from 30 %RH to 100 %RH, and the conductivity was measured after equilibration at each humidity. It required ca. 3 h for the impedance chamber to stabilize at each new humidity. The dimensions of a composite membrane were determined at the end of the experiment. For non-uniform ammonium ion poisoning (a single membrane with different ammonium ion concentrations at each end or a 3-layer composite membrane with $y_{NH4}+$, 0, $y_{NH4}+$), the conductivity at a specific humidity of a membrane was measured. Then, the experiment was stopped and the dimensions of the single or the composite membrane were measured. After that, conductivity measurements at other humidities were made following the same procedure. The ionic conductivities of 3-layer composite membranes were analyzed in DI water at room temperature and the dimensions of the composite membrane were measured at the end of each experiment.

The ion exchange capacity of proton sites of the N-211 membrane was determined by titration. Samples (5.5x1 cm^2, ~30 mg) of the original H^+-form of N-211 were immersed in 0.005 M NaOH (Acros Organics) at room temperature under constant shaking at 250 rpm for 2 days. Then, the membranes were taken out and the liquid aliquot back-titrated with 0.005 M HCl (Acros Organics) using phenolphthalein as an indicator. The end point of titration determined by pH meter was at pH 7.

The ammonium ion compositions in each fraction of a single membrane and in each layer of a 3-layer composite membrane were investigated both prior to and after the conductivity measurements.

4.2.2.3 Results and Discussion

Ammonium Ion Composition in a 3-Layer Composite Nafion Membrane

Table 4.2.2-1 lists the average ammonium ion compositions of series of multi-layer composite membranes after conductivity measurements at different humidities. It shows that the ammonium ion distribution of non-uniformly poisoned membranes changed somewhat after the membranes were equilibrated at a particular humidity for 4 h before conductivity measurements. Since the time require for conductivity measurement was short (15 min), the change in ammonium ion distribution during measurement can be ignored.

Table 4.2.2-1: Ammonium ion composition of each layer in a 3-layer composite Nafion membrane equilibrated at 80°C.

Initial $y_{NH\,4+}^{Ini}$ [a]			Final $y_{NH\,4+}^{F}$ [b]		
Top	Middle	Bottom	Top	Middle	Bottom
0.00	0.00	0.00	0.00	0.00	0.00
0.51	0.00	0.51	0.42	0.18	0.42
0.69	0.00	0.69	0.56	0.27	0.56
1.00	0.00	1.00	0.80	0.37	0.83

[a] $y_{NH\,4+}^{Ini}$ is the average of initial ammonium ion composition in each membrane layer (before 3 membranes were physically stacked together) of a composite membrane.

[b] $y_{NH\,4+}^{F}$ is the average final ammonium ion content in each membrane layer of a composite membrane after conductivity measurements at a particular relative humidity. NH_4^+ ion analysis: error = ± 7 %.

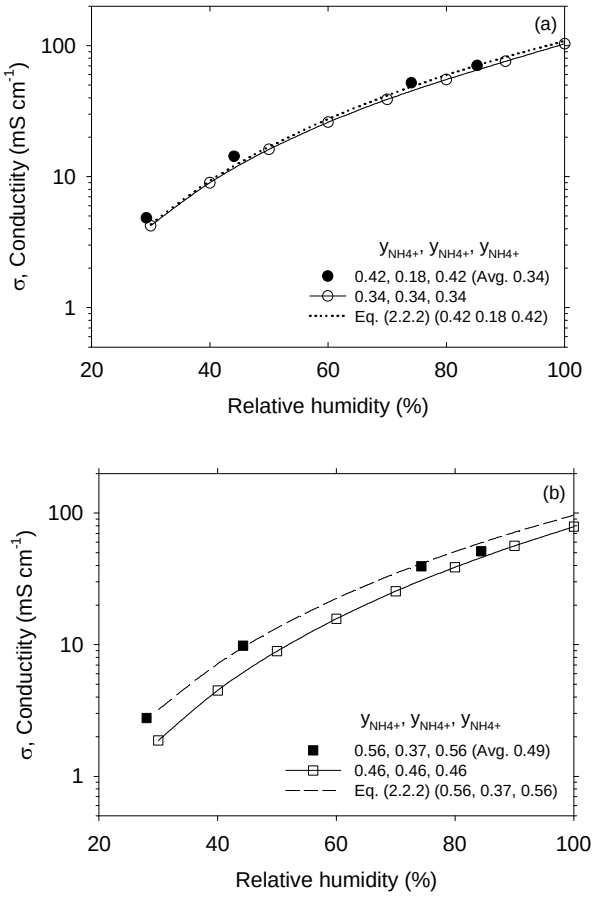

Figure 4.2.2-2: Conductivity at 80°C of composite membranes having homogeneously and non-homogeneously distributed ammonium ion concentrations with average y_{NH4+} of: (a) 0.34 and (b) 0.46.

Effect of Ammonium Ion Distribution on Gas-Phase Nafion Conductivity at 80°C

Figure 4.2.2-2(a-b) shows the conductivities of poisoned 3-layer composite membranes having similar overall ammonium ion compositions (y_{NH4+}), but different concentration profiles. The filled and unfilled symbols represent the conductivity of 3-layer composite membranes with non-uniform and uniform ammonium ion distributions, respectively. Solid lines represent a fit of data. It can be seen in Figure 4.2.2-2(a-b) that, at low y_{NH4+} ($y_{NH4+} \sim 0.34$), the effect of ammonium ion distribution of 3-layer composite membranes on the conductivity at relevant fuel cell conditions (30-100 %RH and 80°C) was minimal. However, as y_{NH4+} increased, the conductivity difference between the non-uniformly and uniformly poisoned composite membranes with equivalent ammonium ion contents became more significant. In Figure 4.2.2-2(a-b), the conductivities of non-homogeneous composite membranes with average y_{NH4+} of 0.34 and 0.49, respectively, were ca. 7-23% and 34-86% larger than those of homogeneously poisoned membranes with similar average y_{NH4+} values of 0.34 and 0.46, respectively. Thus, it can be seen that the conductivities under fuel cell operations of non-uniformly poisoned membranes were ca. 1.07–1.86 times larger than those of uniformly poisoned membranes depending on the relative humidity and ammonium ion distribution profile. The conductivity differences became smaller with an increase in humidity and ammonium ion distribution uniformity.

Also, in Figure 4.2.2-2(a-b), the dotted and dashed lines represent the predicted conductivities of non-uniformly contaminated membranes obtained from Eqs. (1-2) and based on the values of y_{NH4+} given in the parentheses for each layer in the legend.

$$\sigma_{RH,y_{NH_4^+}} = A_1\left(y_{NH_4^+}\right)^2 + A_2\left(y_{NH_4^+}\right) + A_3 \qquad (1)$$

$$\sigma_{3-layer} = \frac{1}{3}\left(\sigma_{RH,y^T_{NH_4^+}} + \sigma_{RH,y^M_{NH_4^+}} + \sigma_{RH,y^B_{NH_4^+}}\right) \qquad (2)$$

where $\sigma_{RH,y_{NH_4^+}}$ is the conductivity of a membrane having a composition of y_{NH4+} at a given %RH; parameters A_1-A_3 are given in reference [Hongsirikarn 2010e]; $\sigma_{3\text{-layer}}$ is the calculated overall conductivities of the 3-layer composite membranes at a particular humidity and 80°C, respectively; $\sigma_{RH,y^T_{NH_4^+}}$, $\sigma_{RH,y^M_{NH_4^+}}$, and $\sigma_{RH,y^B_{NH_4^+}}$ are the theoretical conductivities (based on the ammonium ion concentration measured for each layer of a 3-layer composite with $y_{NH4+} = y^T_{NH_4^+}, y^M_{NH_4^+}$, and $y^B_{NH_4^+}$ for the top, middle, and bottom layers, respectively and based on measurements of uniformly ammonium ion-poisoned composite membranes; Eq. (1)).

It can be seen in Figure 4.2.2-2(a-b) that these theoretical predictions (lines) correspond very well with the experimental results (filled symbols). This observation suggests that a conductivity model taking into account the non-homogeneity of ammonium ion concentration profile within a membrane or a catalyst layer would yield a more accurate prediction for a contaminated PEMFC performance. If the concentration profile is known, the overall conductivity ($\sigma_{overall}$) of a Nafion membrane and that of a Nafion's catalyst layer can be calculated as follows:

Nafion membrane:

$$\sigma_{overall,mem} = \int_{x_H}^{x_L} \sigma_{RH,y_{NH_4^+}}\, dx \quad (3)$$

Nafion catalyst layer:

$$\sigma_{overall,cat.layer} = \left(1-\varepsilon_{cat}\right)\left[1+\frac{\left(\varepsilon_{agg}-1\right)}{\left(1+\left(\delta/r_{agg}\right)\right)^3}\right]\int_{x_H}^{x_L} \sigma_{RH,y_{NH_4^+}}\, dx \quad (4)$$

where $x_H < x < x_L$ *and* $0 < y_{NH_4^+} < 1$

where $\sigma_{overall,\ mem}$ and $\sigma_{overall,\ cat.\ layer}$ are the estimated overall conductivities of a poisoned Nafion membrane (N-211) and a poisoned Nafion catalyst layer, respectively; $\sigma_{RH,y_{NH_4^+}}$ is the conductivity of an ammonium ion-contaminated Nafion polymer at a specific %RH with ammonium ion composition y_{NH4+} and it was obtained from Eq. (1); ε_{cat} and ε_{agg} are the volume fractions of the pores and of the Nafion in the catalyst layer, respectively; δ is the thickness of the Nafion film coating the agglomerate (multiple particles of Nafion on Pt/C support surrounded by Nafion thin film); r_{agg} is the radius of the agglomerate; x is the normalized distance from the catalyst layer/membrane interface in the thickness direction; and x_L and x_H are the normalized distances from the interface of the contaminated area having the lowest and the highest y_{NH4+}, respectively (generally, x_H = 0).

4.2.2.4 Conclusions

In this study, three membranes with known ammonium ion compositions were physically stacked together in order to ensure well-defined ammonium ion distribution within a 3-layer composite membrane. Under typical fuel cell condition, it was found that the conductivities of non-homogeneously ammonium ion-poisoned composite membranes with $y^T_{NH_4^+}, y^M_{NH_4^+}, y^B_{NH_4^+}$ were ca. 1.07-1.86 times larger than those of homogeneously poisoned composite membranes having the equivalent ammonium ion content, depending on humidity, level of contamination, and ammonium ion concentration profile in the membranes. This finding indicates that the effect of ammonium ion distribution on Nafion conductivity at typical fuel cell conditions can be significant. Results from this study also suggest that concentration gradients for other poisoning cations in membrane electrode assemblies (MEAs) may also have an effect on fuel cell operations.

For further details about this study, please refer to:
"Effect of Ammonium Ion Distribution on Nafion® Conductivity," ***Journal of Power Sources*** 196 (2011) 644-651(Kitiya Hongsirikarn, Thirapong Napapruekchart, Xunhua Mo, and James G. Goodwin, Jr.).

References

Halseid, R.; P.J.S. Vie, R. Tunold, *Journal of Electrochemical Society*, 151 (**2004**), A381.

Hongsirikarn, K.; J.G. Goodwin, Jr., S. Greenway, S. Creager, *Journal of Power Sources*, 195 (**2010**a) , 30.

Hongsirikarn, K.; X. Mo, J.G. Goodwin, Jr., *Journal of Power Sources*, 195 (**2010**b), 3416.

Hongsirikarn, K.; T. Napapruekchart, X. Mo, J.G. Goodwin, Jr., *Journal of Power Sources*, 196 (**2011**e), 644.

Soto, H.J.; W.K. Lee, J.W. Van Zee, M. Murthy, *Electrochemical and Solid State Letters*, 6.

Thakkar, R.; H. Patel, U. Chudasama, *Bulletin of Material Science*, 30 (**2007**), 205.

Uribe, F.A.; S. Gottesfeld , T.A. Zawodzinski, *Journal of Electrochemical Society*, 149 (**2002**), A293.

4.2.3 Effect of Metal Cation (Na^+, Ca^{2+}, Fe^{3+}) on the Conductivity of a Nafion® Membrane

4.2.3.1 Motivation

Poly(perfluorosulfonic acid) membranes, especially Nafion®, are attractive for the use in PEMFCs because of their high proton conductivity, high water uptake, and chemical, mechanical, and thermal stabilities [Li 2001]. However, during MEA preparation and/or fuel cell operation, the membrane can be contaminated by foreign cationic ions such as Na^+, Ca^{2+}, Fe^{3+}, etc. originating from the gas supply or coolant reagent, fabrication of the fuel cell, corrosion of materials, and other sources [Okada 1997; Okada 1999; Kelly 2005]. These metal cations are even worse than some impurities containing protons (e.g., ammonia) because they are not proton carriers and are harder to remove [Pivovar 2009]. To date, information about the effect of these cations on membrane conductivity under typical fuel cell conditions has been very limited.

In this study, conductivity measurements of Nafion membranes (N-211) in the binary-cationic form (H^+/M^{n+} form, M^{n+} = Na^+, Ca^{2+}, and Fe^{3+}) were performed both in the liquid phase and in the gas phase at typical fuel cell conditions (30–100 %RH and 80°C). The ionic conductivities of N-211 containing these nonproton cations were compared to the conductivities of N-211 with proton-containing cations (e.g., NH_4^+). Chloride-containing solutions were used to prepare various cationic compositions of N-211s in the H^+/M^{n+}-form (M^{n+} = Na^+, Ca^{2+}, and Fe^{3+}). The conductivity in the lateral direction was determined in a two-probe cell.

4.2.3.2 Experimental

Nafion® 211 membranes (DuPont Inc.) which are 25 µm thick and have an equivalent weight (EW) of 1,100 [g (mol $-SO_3^-)^{-1}$] were cut into 5.5 x 1 cm^2 rectangles and

sequentially pretreated for 1 hour at 90°C in solutions of: 3 % H_2O_2 (Fisher Scientific), 0.5 M H_2SO_4 (Acros Organics), and then DI water. Afterwards, the membranes were rinsed several times with DI water to remove all the residual acid and kept in the dark in DI water at room temperature prior to use.

Reagent-grade 1.0 M HCl (Fisher Scientific), 99.99 wt.% NaCl (Fisher Scientific), 96 wt.% $CaCl_2$ (Acros Organics), and 98 wt.% $FeCl_3$ (Acros Organics) were used to prepare various cationic compositions of N-211s in the H^+/M^{n+}-form (M^{n+} = Na^+, Ca^{2+}, and Fe^{3+}). The H^+-form of N-211 was allowed to ion-exchange in aqueous solutions containing various metal cation compositions with a total concentration of Cl^- ions of 0.1 M for at least 10 days at room temperature under continuous shaking. The contaminant-containing solutions were changed periodically during exchange equilibration.

Following membrane preparation and conductivity measurement in DI water and a He atmosphere, the ionic composition for Na and Ca ions in the membranes was determined using standard analytical chemistry methods. The compositional analysis of the Fe^{3+}-contaminated membrane in the dry state was determined by energy dispersive X-ray (EDX, SEM-Hitachi S-3400N) as used by Kelly et al. [6]. Although EDX is a surface technique, the elemental analysis of the bulk membrane in the H^+/Fe^{3+} form could be obtained assuming the composition of the bulk membrane was the same as that at the surface. This assumption should be valid because, in this study, the contaminated membranes were prepared by ion-exchange in aqueous solutions over a long period of time (at least 10 days). Thus, the distribution of Fe^{3+} in the membrane should be homogeneous. Inductively coupled plasma mass spectrometry (ICP-MS) elemental analyses (Na, Ca, and Fe), carried out by Galbraith Laboratories in Knoxville, Tennessee, were used to confirm the cationic composition of the membrane.

Conductivity measurement in DI water was done at room temperature (~25°C). The impedance of N-211 in the lateral direction was determined in a two-probe cell using an impedance analyzer (Gamry Potentiostat Reference 600) with 25 mV ac amplitude in a frequency range of 10^6 to 100 Hz. Conductivity measurement in the gas phase was carried out at 80°C. The membrane was put in a custom-made cell, placed in the gas phase chamber and allowed to equilibrate. The humidity was ramped from 30 %RH to 100 %RH to measure conductivity at various %RH with constant conductivity for 1 h being maintained before the %RH was changed.

4.2.3.3 Results and Discussion

Effect of Cations on the Conductivity of N-211 in DI Water at Room Temperature (25°C)

In Figure 4.2.3-1(a-b), the conductivities in DI water at room temperature of N-211 in the H^+/M^{n+} form (M^{n+} = Na^+, Ca^{2+}, and Fe^{3+}) and H^+/NH_4^+ form are shown. It was found that at very low cation compositions in the membrane (y_{H^+m} > 0.95), the effect of cations on the liquid-phase conductivity is minimal and is proportional to y_{H^+m}. The conductivities decreased in a similar linear fashion with the fraction of sites occupied by

protons (y_{H^+m}) and were essentially identical regardless of the nature of the second metal cation with H^+ in the membrane. Only NH_4^+/H^+ had a much higher conductivity for the same value of y_{H^+m} .

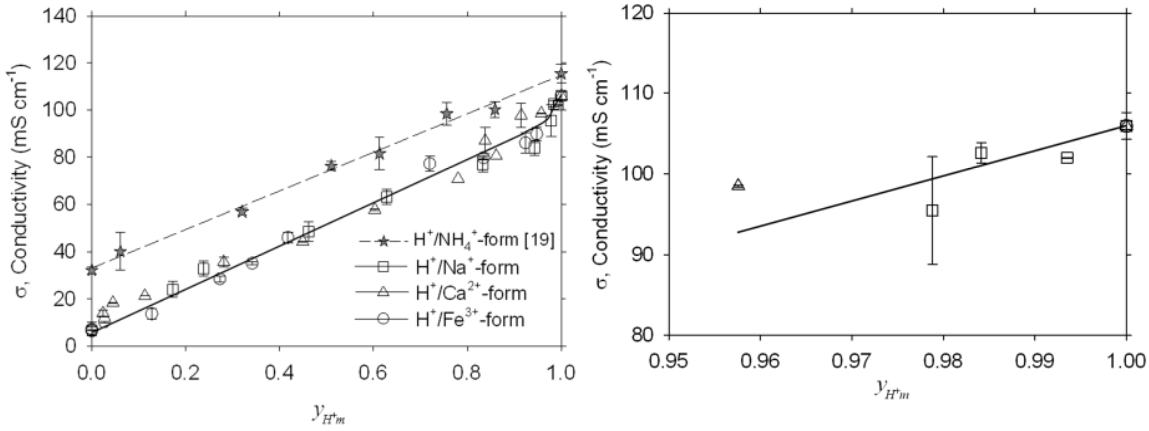

Figure 4.2.3-1: Conductivity in DI at room temperature for N-211 membranes containing various cation compositions: (a) for $0 \leq y_{H^+m} \leq 1$ and (b) for high y_{H^+m} region (very low cationic compositions).

Effect of Cations on the Conductivity of N-211 in the Gas Phase at 80°C

In Figure 4.2.3-2(a-c), the gas-phase conductivities of contaminated N-211 membranes are plotted against the membrane proton composition (y_{H^+m}). As expected, the effect of cations on the gas-phase conductivity of a membrane with trace amounts of cations ($y_{H^+m} > 0.98$) is fairly minimal, which corresponds very well with the conductivity results in DI water. The conductivity, however, decreases exponentially with y_{H^+m} . Under the same conditions and y_{H^+m} , the conductivities of N-211 membranes contaminated with monovalent cations (i.e., Na^+, NH_4^+) were similar, but were just slightly higher than those with higher valent cations (i.e., Ca^{2+}, Fe^{3+}). Thus, not including the NH_4^+ membrane, the conductivities of the H^+/M^{n+}-forms (M^{n+} = Na^+, Ca^{2+}, and Fe^{3+}) of the membrane at 80°C having the same y_{H^+m} were practically identical, in good agreement (all nearly identical, not in terms of absolute conductivities) with what was found in DI water as shown in Figure 4.2.3-1(a-b) for these contaminated membranes. In the fully metal cationic state, the gas-phase conductivity of the N-211 in the H^+/M^{n+}-form (M^{n+} = Na^+, Ca^{2+}, and Fe^{3+}) was ca. 6–125 less than that in the H^+-form, depending on humidity. The effect of the cationic ions on conductivity decreased as humidity increased.

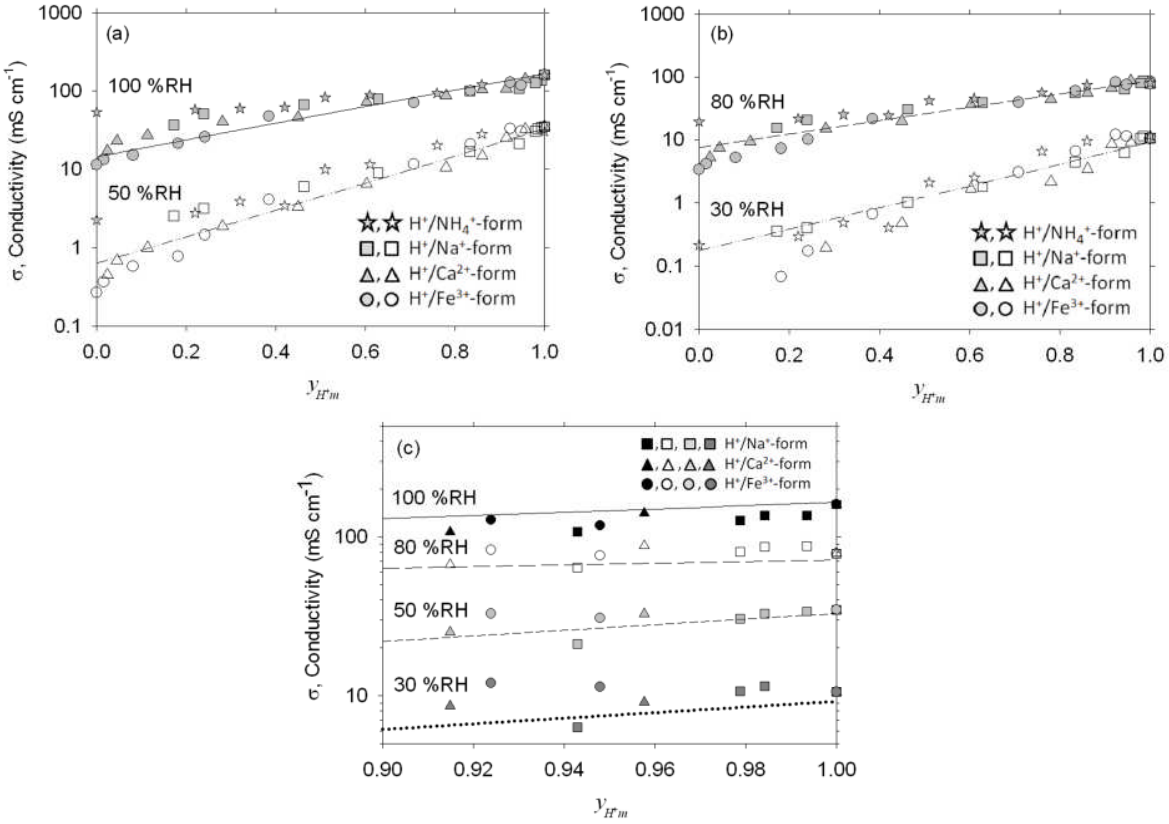

Figure 4.2.3-2: Conductivity of cationic-contaminated N-211 membranes at 80°C in the gas phase: (a) for 30 and 80 %RH, (b) for 50 and 100 %RH, and (c) at very low cationic compositions.

Comparison of Aqueous-Phase and Gas-Phase Ionic Conductivities

As shown in Figure 4.2.3-1(a-b) and Figure 4.2.3-2(a-c), foreign impurities have more a detrimental effect on gas-phase conductivities at 80°C than on liquid-phase conductivities at room temperature. The explanation for the different effect on conductivity in the liquid- and gas-phases is probably due to the dissimilarities of proton transport via the Grotthuss and vehicle mechanisms in these two phases. The conductivity of the membrane in the H^+-form in DI water at room temperature is mainly dominated by the Grotthuss mechanism, whereas, that measured at 80°C in the gas-phase is probably primarily governed by vehicle transport [Lott 2005; Kreuer 1998]. The results imply that the presence of the counter metal cationic ions in the Nafion structure significantly affected proton transport by reducing the connectivity of the water network in the ionic cluster, particularly in a membrane containing low water content (at 80°C) that caused a more rigid structure. Since the metal cation-water clusters were transported by the vehicle mechanism [Saito 2005], the experimental data suggest that the cation-water interactions at 80°C and 30–100 %RH (Figure 4.2.3-2(a-c)) severely influenced the

diffusion of the cation-water clusters more than the hopping of protons at room temperature in DI water through the cation-water network (Figure 4.2.3-1(a-b)).

4.2.3.4 Conclusions

The effect of monovalent and multivalent cation types on the conductivity of a Nafion membrane (N-211) under various conditions was studied. The ionic conductivities in DI water at room temperature (~25°C) of three different H^+/M^{n+}-forms (M^{n+} = Na^+, Ca^{2+}, and Fe^{3+}) of N-211 were found to be similar, but lower than those in the H^+/NH_4^+-form of N-211 having the same proton composition (y_{H^+m}). The aqueous-phase conductivities of all cationic-poisoned membranes decreased in a similar linear fashion with the y_{H^+m} . On the other hand, the gas-phase conductivities at 80°C of N-211 in various binary-metal cationic forms with identical y_{H^+m} were similar, but slightly lower than that in the NH_4^+-form, which was consistent with the results in DI water. Conductivity in the gas phase declined more dramatically with y_{H^+m} than that in an aqueous phase. The conductivity decreased exponentially with y_{H^+m} at a particular humidity and increased with the humidity. In liquid electrolyte (DI water) at room temperature, the conductivities of N-211 in the fully H^+-form were ca. 12 times higher than those in the fully metal cationic-forms. In humidified gas at 80°C, on the other hand, those in the fully metal cationic forms were lower by a factor of approximately 125 or 6 compared to those in the protonic form at 30 and 100 %RH, respectively.

For further details about this study, please refer to:
"Effect of Cations (Na^+, Ca^{2+}, Fe^{3+}) on the Conductivity of a Nafion Membrane," ***Journal of Power Sources*** 195 (2010) 7213-7220 (Kitiya Hongsirikarn, James G. Goodwin, Jr., Scott Greenway, and Stephen Creager).

References

Kelly, M.J.; G. Fafilek, J.O. Besenhard, H. Kronberger, G.E. Nauer, *Journal of Power Sources*, 145 (**2005**), 249.

Kreuer, K.D.; A. Fuchs, M. Ise, M. Spaeth, J. Maier, *Electrochimica Acta*, 43 (**1998**), 1281.

Li, T.; A. Wlaschin, P.B. Balbuena, *Industrial and Engineering Chemistry Research*, 40 (**2001**), 4789.

Lott, K.F.; B.D. Ghosh, J.E. Ritchie, *Electrochemical and Solid State Letters*, 8 (**2005**), A513.

Okada, T.; N. Nakamura, M. Yuasa, I. Sekine, *Journal of Electrochemical Society*, 144 (**1997**), 2744.

Okada, T.; Y. Ayato, M. Yuasa, I. Sekine, *Journal of Physical Chemistry B*, 103 (**1999**), 3315.

Pivovar, B.S.; B. Kienitz, T. Rockward, F.A. Uribe, F.H. Garzon, *Handbook of Fuel Cells*, Wiley, 6 (**2009**), 718.

Saito, M.; K. Hayamizu, T. Okada, *Journal of Physical Chemistry B*, 109 (**2005**), 3112.

4.2.4 Effect of H_2O_2 on Nafion® Properties and Conductivity at Fuel Cell Conditions

4.2.4.1 Motivation

Previous studies have shown that, even if a fuel cell is operated in neat H_2 fuel and oxidant streams, degradation of PEMFC performance can occur [Marrony 2008]. It is well-accepted that the performance is permanently decreased by degradation of the PFSA materials (e.g., Nafion) due to hydrogen peroxide (H_2O_2) formation at the anode or cathode (depending on the operating conditions) [Tang 2007; Aoki 2006; Qiao 2006; Vishal 2007]. The decomposition of H_2O_2, catalyzed by contaminating metal cations (i.e., Fe^{2+}, Pt^{2+}), generates highly active oxygen radicals (OH•, OOH•) that initiate the degradation of the ionomer [Vishal 2007; Xie 2007; Young 2010].

It has been previously reported that the H_2O_2 decomposition mechanism in Fenton's reagent {a solution of H_2O_2 with ppm level of metal contaminants (i.e., Fe^{2+}, Cu^{2+}, Pt^{2+}, etc.) [Chen 2007; Tang 2007; Endoh 2004; Jung 2007] is similar to that in typical fuel cell environments [Curtin 2004; Healy 2005; Schiraldi 2006]. The reactive species for Nafion decomposition appear to form as follows [Chen 2009; Kundu 2008; Maletzky 1999; Pozio 2003]:

$$Nafion - Fe^{2+} + H_2O_2 \longrightarrow Nafion - Fe^{3+} + OH\bullet + OH^- \quad (5)$$

$$H_2O_2 + OH\bullet \longrightarrow OOH\bullet + H_2O \quad (6)$$

$$Nafion - Fe^{3+} + OH^- \longrightarrow Nafion - (FeOH)^{2+} \quad (7)$$

$$Nafion - (FeOH)^{2+} \xrightarrow{h\nu} Nafion - Fe^{2+} + OH\bullet \quad (8)$$

where Nafion-Fe^{2+} and Nafion-Fe^{3+} represent the membrane having Fe^{2+} and Fe^{3+} ions neutralizing 2 and 3 sulfonate acid groups, respectively. In addition to enhancing degradation of the Nafion, the replacement of protons on the sulfonic groups by non-proton cations by themselves decreases Nafion conductivity [Hongsirikarn 2010abde; Okada 1999; Okada 1998; Okada 2002].

Previous results found that the degradation process of the ionomer in the membrane is faster than that in the catalyst layer and takes place in the proximity of the membrane-electrode interface [Chen 2007; Mittal 2006]. Consequently, characterization of the degraded membrane can potentially be a diagnostic approach to evaluate the impact of oxidation on the performance and to predict the lifetime of a PEMFC. However, up to the present, there is no detailed quantitative study reporting the effect of Nafion oxidation on conductivity (one of the most crucial factors for fuel cell performance) or the properties of degraded membranes at conditions relevant to practical PEMFC usage.

The purpose of this work was to provide more insight into the effect of oxidation on Nafion membranes under normal fuel cell conditions. The procedure for H_2O_2 treatment was slightly modified from that of other studies to provide more realistic results relative to a PEMFC. The membranes were first pre-ion exchanged with Fe^{2+} ions and then introduced to a freshly-prepared H_2O_2 solution to keep Fe content in the pretreated

membranes (Nafion-Fe^{2+}) constant over all H_2O_2 exposure times. Since metal cations on the sulfonic sites (SO_3^-) in the Nafion polymer arise during preparation or from very low concentrations of impurities in the gas streams, H_2O_2 decomposition during fuel cell operation proceeds primarily due to the presence of these metal cations in the Nafion instead of ions in solution. Therefore, this modification of the H_2O_2 pretreatment procedure yields a better replication of the degradation process in a typical fuel cell environment. The conductivity and physical and chemical characterizations of H_2O_2-treated membranes pretreated by this modified procedure were measured at conditions relevant to fuel cell environments (30-100 %R and 80°C). The quantitative results, reported in this study, should be more realistic than previous investigations using measurements in Fenton's reagent.

4.2.4.2 Experimental

Commercial Nafion 211 membranes (NRE-211, 25 μm nominal thickness, 1100 EW) were purchased from DuPont Inc. Nafion membranes (5.5 x 1 cm^2) were pretreated by a standard procedure. They were heated at 90°C for 1 hour each in aqueous solutions of 3 %vol. H_2O_2 (Fisher Scientific) to remove organic impurities, in 0.5 M H_2SO_4 (Fisher Scientific) to remove metallic impurities and to acidify the sulfonic sites, and in deionized (DI) water to remove residual acid solution. The subsequent acidified membranes were washed several times and kept in DI water prior to use.

For pre-ion exchange with Fe and H_2O_2 treatment of the Nafion-Fe^{2+} membranes, reagent grade solutions of 1 M $FeSO_4$, 1 M H_2SO_4, and 50 %vol. H_2O_2 were purchased from Fisher Scientific. Instead of following the general procedure for Fenton's reagent pretreatment by immersing acidified membranes in a freshly-prepared Fenton's reagent (ppm level of Fe^{2+} ions in H_2O_2 aqueous solution) , the procedure was modified for this study. The membrane samples were first ion-exchanged using a solution containing 20, 100, or 1,000 ppm of Fe^{2+} in 0.1 M H_2SO_4 at ambient temperature for 7 days under constant shaking to ensure exchange equilibration. Even trace amounts of Fe^{2+} ions in solutions results in a significant uptake of Fe in membranes, indicating that Fe^{2+} ions more preferentially adsorb on sulfonic sites than protons. The membrane samples are labeled corresponding to the proton composition in the membrane before H_2O_2 exposure (time = 0 h, M90 means 90% of $-SO_3^-$ groups neutralized with H^+ and 10% with Fe ions), since this parameter is one of the most crucial factors governing fuel cell performance. After Fe exchange, the ion-exchanged membranes were rinsed several times with DI water, dried at 80°C for 8 h, and weighted (W_0). Then, these Fe^{2+}-containing membranes were individually immersed in a freshly-prepared aqueous solution of 30 vol.% H_2O_2 at 80°C under constant shaking in amber glassware for a specific period of time. The H_2O_2 solution was changed every 4 h during the first 24 h and every 8 h afterwards to ensure essentially constant H_2O_2 concentration since the degradation tends to be almost stabilized after 24 h. The used solutions and treated membranes were separately allowed to cool to room temperature and were kept in amber glassware prior to fluorine analysis.

The ion-exchange capacities (IECs) are defined in this study as the concentration of proton sites available in the membranes and were determined by a standard acid-based titration technique using W_0 (original membrane sample weight) as the basis. This technique is widely considered to be a convenient and accurate method.

The F^- concentrations in the collected H_2O_2 solutions before and after Nafion degradation were determined using a fluoride ion selective electrode 9609BNWP (Thermo Scientific Orion). Conductivity, swelling, and weight change measurements were also made.

Conductivity measurements of the membranes in the lateral or in-plane direction at 30 %RH and 80°C were performed by a two-probe impedance analyzer (Gamry Potentiostat Reference 600) with ac amplitude of 50 mV until constant conductivity was obtained. After that, the relative humidity was raised in steps from 30 %RH to 100 %RH and the conductivity was measured after equilibration at each step in %RH. The membrane dimensions and weight ($W_{100\%RH}$) were obtained immediately after the conductivity measurements.

FTIR spectroscopy was performed to examine the change in chemical structure of the Nafion samples. The physical changes at the surfaces and over the cross-sections of Nafion membranes before and after treatment were investigated by SEM analysis (SEM-Hitachi S-3400N). Membrane cross-sections were prepared by a freeze-fracture technique. Elemental analyses (oxygen, fluorine, sulfur, and iron) of the membranes before and after H_2O_2 treatment were performed to confirm EDX results. Measurements were carried out by Galbraith Laboratories in Knoxville, TN.

4.2.4.3 Results and Discussion

Investigation of Changes in Nafion Morphology after H_2O_2 Treatment

After H_2O_2 treatment of Fe-containing membranes, remarkable physical changes (i.e., evolution of bubbles, significant change in the membrane's color from clear transparent to light yellow opaque, changes in membrane dimensions, etc.) were observed. The length and width of membrane changed only slightly after H_2O_2 exposure, but the thickness increased (ca. 1.5 times) due to the formation of bubbles. Figure 4.2.4-1 shows the change in morphology of the membrane with $y^0_{H^+-Fe}$ = 0.90 (M90). The membrane samples are labeled corresponding to the proton composition in the membrane before H_2O_2 exposure (time = 0 h, M90 means 90% of $-SO_3^-$ groups neutralized with H^+ and 10% with Fe ions), since this parameter is one of the most crucial factors governing fuel cell performance. It can be seen that the amount and size of bubbles increase and pinholes are observed as chemical degradation proceeds.

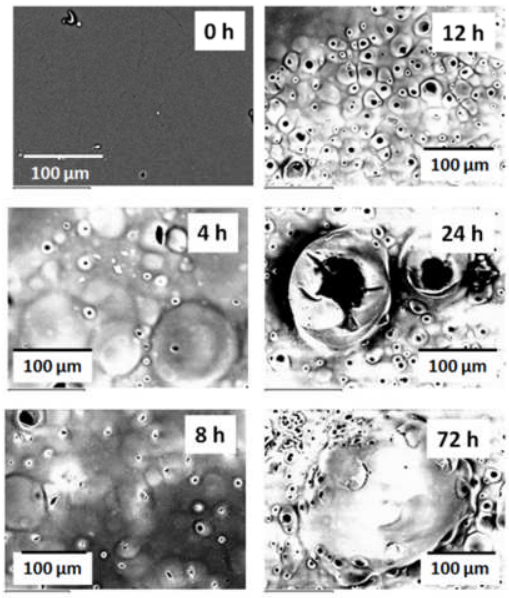

Figure 4.2.4-1: SEM images of the surface of a M90 membrane after various times of H_2O_2 treatment.

Effect of H_2O_2 Treatment on Nafion Decomposition

The degree of degradation of Fe ion-exchanged Nafion membranes by H_2O_2 was investigated by changes in ion-exchange capacity (IEC), weight, and fluorine content as measured by:

$$Ion\ exchange\ capacity\ \ fraction\ loss: X_{IEC} = \frac{y^0_{H^+-Fe} - y^t_{H^+-Fe}}{y^0_{H^+-Fe}} \qquad (9)$$

$$with\ y^0_{H^+-Fe} = \frac{IEC_{t=0}}{IEC_{original}},\ y^t_{H^+-Fe} = \frac{IEC_t}{IEC_{original}}$$

where X_{IEC} is the fraction of original proton composition lost by a degraded Nafion sample; $y^t_{H^+-Fe}$ is the fraction of original sulfonic sites in the membrane remaining after treatment time t; $IEC_{original}$ is the ion-exchange capacity of a Nafion membrane in the original proton form of the membrane [928 (µmol H^+) g^{-1}]; and $IEC_{t=0}$ and IEC_t are the ion-exchange capacities [(µmol H^+) g^{-1}] of Fe-containing membranes before and after treatment in H_2O_2 solutions for a period of time t, respectively.

$$Weight\ loss\ \ fraction: X_W = \frac{W_0 - W_t}{W_0} \qquad (10)$$

$$Fluorine\ loss\ \ fraction: X_F = \frac{[C_F]_t V_{H_2O_2}}{W_0 F_0} \qquad (11)$$

where X_W and X_F are the fractions of weight lost and of fluorine lost of a degraded Nafion sample, respectively; $[C_F]_t$ is the concentration of fluorine in the H_2O_2 solution at treatment time t [(mg F^-) cm^{-3}]; V_{H2O2} is the volume of H_2O_2 solution (cm^3); W_0 and W_t

are the dry weights (mg) of the Fe-contaminating membranes before and after H_2O_2 treatment for a period of time t; and F_0 is the initial weight fraction of fluorine in the Fe^{2+}-containing membranes at treatment time 0 with a value of 0.68 (results from elemental analysis).

These properties have been demonstrated to be important ones for evaluating degradation level and membrane stability. Figure 4.2.4-2 presents the fractions of y_{H^+-Fe}, weight, and fluorine lost for Nafion membranes (M90) with $y^0_{H^+-Fe}$ = 0.90 (10% of sulfonate sites neutralized with Fe^{2+} ions rather than H^+ ions) pretreated in a 30% H_2O_2 solution at 80°C for various periods of time. It can be seen that the fractional losses of IEC, weight, and fluorine followed the same trend, but the decomposition fractions of weight and fluorine lost were lower at all treatment times than that of IEC lost.

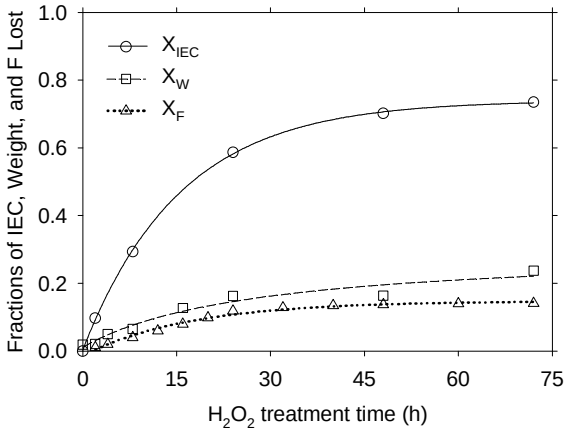

Figure 4.2.4-2: Fractions of ion-exchange capacity (IEC), weight, and fluorine lost from M90 membranes as a result of H_2O_2 treatment.

Figure 4.2.4-3 presents the kinetics of fluorine removal from the degrading membranes. It shows that the level of Fe^{2+} ions in the membrane significantly affects the degree and rate of Nafion decomposition. It is clear that the presence of Nafion-Fe^{2+} in the structure considerably enhances the membrane deterioration rate.

Effect of H_2O_2 treatment on Nafion conductivity at fuel cell conditions

Figure 4.2.4-4(a-d) demonstrates the effect of Nafion degradation and Fe composition on conductivity at typical fuel cell conditions (30-100 %RH and 80°C). The conductivities of all Fe-containing membranes prior to H_2O_2 exposure were consistent with the results from our previous study [Hongsirikarn 2010d]. It can be seen that, for the same Fe content, a lesser effect on the conductivity at higher humidities is observed, which is probably because of the higher water adsorption and a more flexible structure at higher humidities.

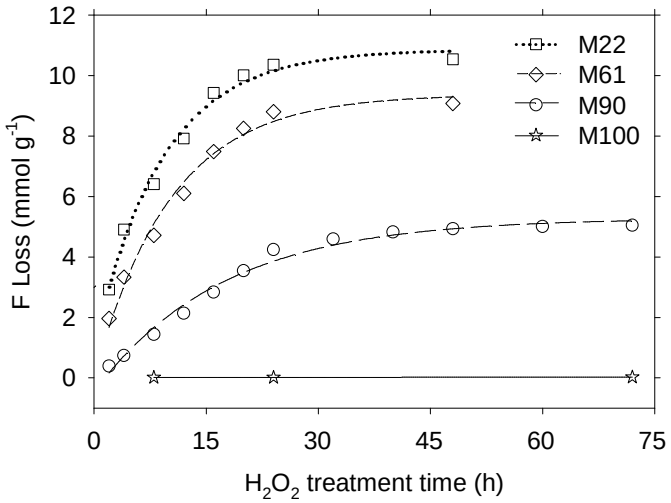

Figure 4.2.4-3: Fluorine loss (emission) of Nafion membranes with various levels of Fe content as a function of H_2O_2 exposure time.

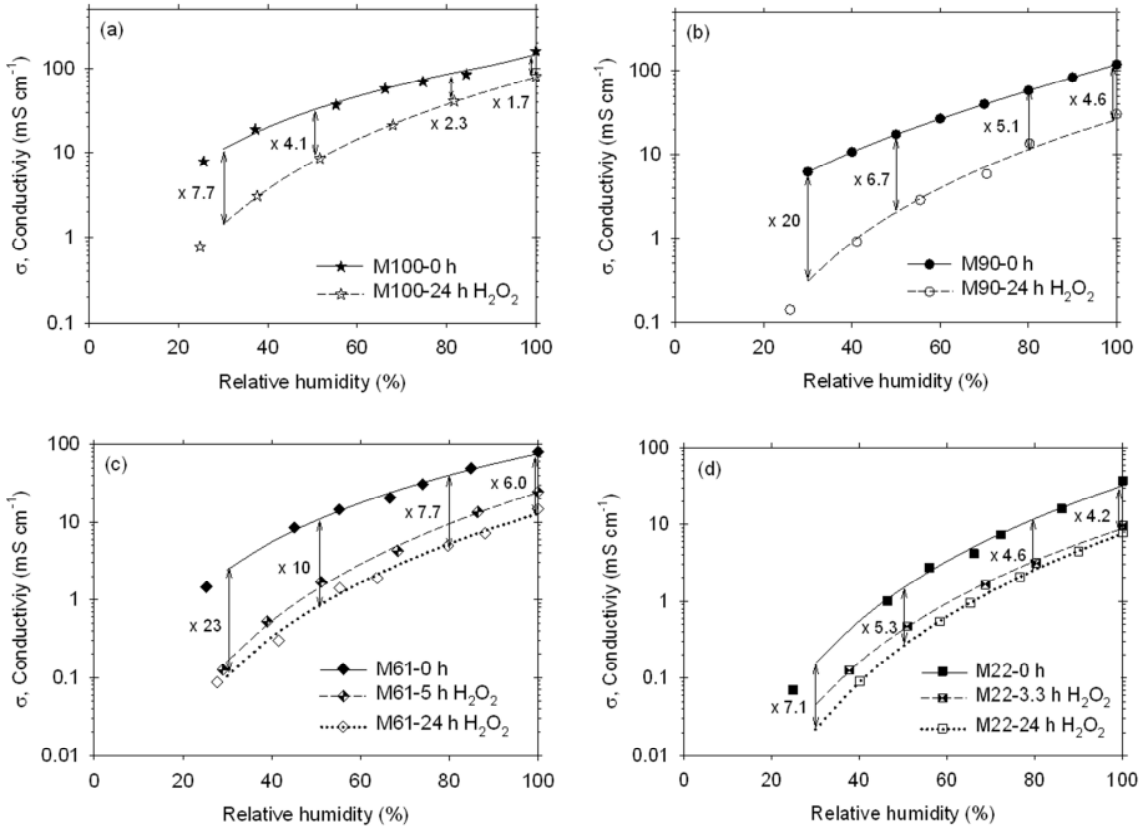

Figure 4.2.4-4: Conductivities at 80°C of Nafion membranes after various H_2O_2 exposure times: (a) M100, (b) M90, (c) M61, and (d) M22.

4.2.4.4 Conclusions

The effect of H_2O_2 on Nafion properties and conductivity at conditions relevant for fuel cell operation was quantitatively investigated for the first time in this study. After Fe-contaminated membranes were subjected to H_2O_2 solutions, major changes in physical morphologies and chemical properties of degraded samples were observed. The H_2O_2-treated membranes appeared to be more degraded and contained a lot of holes. In this study, the degree of degradation was measured by the fractional losses in ion-exchange capacity (X_{IEC}), weight (X_W), and fluorine content (X_F). It was found that plots of these losses vs. H_2O_2 treatment time for membranes with all Fe concentrations had similar trends, but the values for X_{IEC}, X_W, and X_F were higher for membranes with higher Fe content. However, the values for X_{IEC} were always higher than those of X_W and X_F for all Fe compositions. The conductivity of degraded Nafion membranes at normal fuel cell conditions was quantitatively examined. It was found that H_2O_2 treatment considerably decreases the conductivity of Nafion membranes by ca. 50% after exposure to H_2O_2 for 24 h, and the conductivity decreased by ca. 44-80% depending on H_2O_2 treatment time.

For further details about this study, please refer to:
"Effect of H_2O_2 on Nafion® Properties and Conductivity at Fuel Cell Conditions," ***Journal of Power Sources*** 196 (2011) 3060-3072 (Kitiya Hongsirikarn, Xunhua Mo, James G. Goodwin, Jr., and Stephen Creager).

References

Aoki, M.; H. Uchida, M. Watanabe, *Electrochemical Communication*, 8 (**2006**), 1509.

Chen, C.; G. Levitin, D.W. Hess, T.F. Fuller, *Journal of Power Sources*, 169 (**2007**), 288.

Chen, C.; T. F. Fuller, *Electrochimica Acta*, 54 (**2009**), 3984.

Curtin, D.E.; R.D. Lousenberg, T.J. Henry, P.C. Tangeman, M.E. Tisack, *Journal of Power Sources*, 131 (**2004**), 41.

Endoh, E.; S. Terazono, H. Widjaja, Y. Takimoto, *Electrochemical and Solid-State Letters*, 7 (**2004**), A209.

Healy, J.; C. Hayden, T. Xie, K. Olson, R. Waldo, A. Brundage, H. Gasteiger, J. Abbott, *Fuel Cells*, 5 (**2005**), 302.

Hongsirikarn, K.; J.G. Goodwin, Jr., S. Greenway, S. Creager, *Journal of Power Sources*, 195 (**2010**a) , 30.

Hongsirikarn, K.; X. Mo, J.G. Goodwin, Jr., *Journal of Power Sources*, 195 (**2010**b), 3416.

Hongsirikarn, K.; X. Mo, L. Zhiming, J.G. Goodwin, Jr., *Journal of Power Sources*, 195 (**2010**c), 5493.

Hongsirikarn, K.; J.G. Goodwin, Jr., S. Greenway, S. Creager, *Journal of Power Sources*, 195 (**2010**d) 7213.

Hongsirikarn, K.; T. Napapruekchart, X. Mo, J.G. Goodwin, Jr., *Journal of Power Sources*, 196 (**2011**e), 644.

Jung, U.H.; S.U. Jeong, K. Chun, K.T. Park, H.M. Lee, D.W. Choi, S.H. Kim, *Journal of Power Sources*, 170 (**2007**), 281.

Kundu, S.; L.C. Simon, M.W. Fowler, *Polymer Degradation and Stabilization*, 93 (**2008**), 214.
Okada, T.; S. Moller-Holst, O. Gorseth, S. Kjelstrup, *Journal of Electroanalytical Chemistry*, 442 (**1998**), 137.
Okada, T.; H. Satou, M. Okuno, M. Yuasa, *Journal of Physical Chemistry B*, 106 (**2002**), 1267.
Okada, T.; Y. Ayato, M. Yuasa, I. Sekine, *Journal of Physical Chemistry B*, 103 (**1999**), 3315.
Maletzky, P.; R. Bauer, J. Lahnsteiner, B. Pouresmael, *Chemosphere*, 38 (**1999**), 2315.
Mittal, V.O.; H.R. Kunz, J.M. Fenton, *Electrochemical and Solid-State Letters*, 9 (**2006**), A299.
Marrony, M.; R. Barrera, S. Quenet, S. Ginocchio, L. Montelatici, A. Aslanides, *Journal of Power Sources*, 182 (**2008**), 469.
Qiao, J.L.; M. Saito, K. Hayamizu, T. Okada, *Journal of Electrochemical Society*, 153 (**2006**), A967.
Schiraldi, D.A.; *Polymer Review*, 46 (**2006**), 315.
Tang, H.; S. Peikang, S.P. Jiang, F. Wang, M. Pan, *Journal of Power Sources*, 170 (**2007**), 85.
Vishal, O.M.; H.R. Kunz, M.F. James, *Journal of Electrochemical Society*, 154 (**2007**), B652.
Xie, T.; C.A. Hayden, Polymer, 48 (**2007**), 5497.
Young, A.P.; J. Stumper, S. Knights, E. Gyenge, *Journal of Electrochemical Society*, 157 (**2010**), B425.

4.2.5 Esterification as a diagnostic tool to predict proton conductivity affected by impurities on Nafion® components for PEMFCs

4.2.5.1 Motivation

In order to improve PEMFC performance and lifetime, fuller fundamental understanding of poisoning mechanisms must be obtained. However, research focusing on the specific impact of impurities and quantitative data about impurity coverage of the proton sites on individual electrolytes (membrane and catalyst ionomer layer for a PEMFC) are extremely limited. It has been found that under normal fuel cell operation in the absence of contaminants, proton transport limits fuel cell performance [Katsaounis 2005]. Thus, investigation of the effect of impurities on proton availability is extremely important.

Among commercial perfluorosulfonate ionomer (PFSI) electrolytes, Nafion shows the best performance in terms of durability, high proton conductance, and stability [Collette 2009; Li 2001]. Results from previous work directly suggest that the ionic conductivity of a Nafion membrane is proportional to the concentration of free proton sites [Hongsirikarn 2010a]. Thus, the conductivity of a Nafion membrane poisoned by ammonia or other impurities can be reasonably predicted by knowing the number of available proton sites.

The focus of this study was to develop an easy and convenient technique to quantitatively determine the number of available proton sites of electrolytes under fuel cell operation conditions. The approach was to use a simple characteristic acid-catalysed reaction, the gas-phase esterification of acetic acid with methanol, on Nafion components as used in PEMFCs under conditions similar to fuel cell operation (typically 80°C) to determine the surface coverage of impurities (e.g., ammonia) at the ppm level. The methanolysis reaction of acetic acid can take place at mild conditions (60–90°C, 1 atm) and is thermodynamically favorable (equilibrium conversion ~96% at 80°C) with 100% selectivity to methyl acetate. This reaction is possible to carry out using low concentrations of reactants. The results can be easily interpreted in terms of the number of proton/acid sites available because esterification, such as that of acetic acid with methanol (Eq. (12)),

$$CH_3OH + CH_3COOH \xrightarrow{H^+} CH_3COOCH_3 + H_2O \qquad (12)$$

is a simple acid-catalysed reaction between nonsterically hindered alcohols and acids. The reaction occurs on a single reaction site in solid Bronsted acid catalysts like Nafion [Liu 2006].

4.2.5.2 Experimental

In order to obtain the fully H^+-form, Nafion membrane samples (N-211, DuPont), having a nominal thickness of 25.4 μm (50 g m^{-2}), were acidified by pretreating at 90°C separately in aqueous solutions of: 3 wt.% H_2O_2 (Fisher Scientific), 0.5 M H_2SO_4 (Acros Organics), and deionized water for 1 h each. Then, the acidified membrane samples were rinsed and kept in deionized water at room temperature in the dark prior to the measurements. Reagent-grade 1.0 M HCl (Fisher Scientific) and 99.99 wt.% NaCl (Fisher Scientific) were used to prepare the cationic-forms (Na^+-form) of the Nafion®211 membrane (N-211).

Elemental analyses (sulfur, nitrogen, and chlorine) of samples were conducted by Galbraith Laboratory in Knoxville, Tennessee (USA). The concentrations of Bronsted acid sites on Nafion membranes (N-211, 5.5 x 1 cm^2, ~30 mg) were determined by titration. Nafion membranes (N-211s) exposed to ammonia for a certain time in the conductivity chamber/esterification reactor were ion-exchanged with 0.05 M HCl (Acros Organics) at room temperature under constant shaking at 200 rpm for at least 7 days. Then, the sample was removed from the aliquot. The amount of ammonium ions in the exchange solution was analyzed using an ion-selective electrode (ammonia electrode 9512 Thermo Scientific and Orion 4 star pH benchtop meter). Following the conductivity or esterification measurements, the Na^+ composition in the membrane was determined by immersing the membrane in 0.005 M NaOH aqueous solutions at room temperature under constant shaking for 2 days, allowing Na^+ to neutralize the remaining acid sites. The membrane was then removed and the excess NaOH solution was back-titrated with 0.005 M HCl using phenolphthalein indicator.

The only dimension change in the membrane during conductivity measurements was in the thickness. Thickness was measured immediately after conductivity measurement at 5 positions using a micrometer. The average of these measurements was used in the conductivity calculation.

The conductivity of the N-211 membranes in a humidified gas phase was measured in a specially designed chamber by a two-probe ac impedance spectroscopic technique using a Gamry Potentiostat Reference 600. The humidity was obtained via a flash chamber. The water was introduced into the chamber and the flow rate was controlled by a syringe pump (Genie pump, Kent Scientific Corporation). A He stream was introduced passing through the separate heated chamber mixing with the water vapor. The equilibrated "humidified" membrane was sandwiched at both ends between two platinum foils and two custom-made polyetheretherketone (PEEK) sheets, and placed in the conductivity chamber (ID = 16 cm, H = 25 cm) at the specific temperature and the same humidity as equilibration in a He atmosphere for 8 h. The conductivity was then measured until constant. After that, a given concentration of ammonia was introduced in a stream of He to the chamber, and the real time resistance measurement started. For a given study, the conductivity of a membrane exposed to ammonia in hydrogen flow was measured with time-on-stream (TOS) until a given time when the experiment was stopped. The membrane was then removed from the cell and the ammonium ion composition measured. The conductivity of pre-poisoned Na^+ Nafion membranes was also measured.

Methanol (99.9 wt.%), acetic acid (99.7 wt.%), and methyl acetate (99 wt.%) were purchased from Fisher-Scientific and used as supplied. Gas-phase esterification of methanol and acetic acid was carried out in a differential tubular reactor (ID = 0.7 cm) under various conditions. The Nafion membrane was pre-treated in-situ in a 100 sccm H_2 at specific humidity, 80°C, and 1 atm for 3 h. Afterwards, known quantities of acetic acid (HAc), methanol (MeOH), water vapor, and ammonia were introduced to the reactor. An equimolar ratio of MeOH:HAc was used in this study. The esterification was carried out at a given humidity, 80°C, and 1 atm under a total flow rate of 100 sccm H_2. In order to avoid condensation inside the differential reactor and to minimize competitive adsorption of reactants with ammonia, the partial pressures of the reactants were kept low (P_{MeOH}=P_{HAc}=0.009 atm). The concentrations of reactants (MeOH and HAc) and product (MeOAc) in the effluent stream were determined by a Varian CP-3380 GC equipped with an FID detector and a Varian CPWAX 52CB fused silica capillary column (60 m × 0.53 mm × 1 μm). For the comparison of the conductivity and esterification activity of a Nafion membrane as a function of ammonium ion composition in the membrane (y_{NH4+}), the membrane was taken out of the reactor to determine ammonium uptake after a specified ammonia exposure time and ion-exchanged with 0.05 M HCl. The activity of esterification of pre-poisoned Na^+ Nafion membranes was investigated after the membrane was pretreated at 0 %RH and 80°C for 3 h. Then, the humidity was raised by 15 %RH from 0 %RH to 95 %RH and the steady-state rate of methyl acetate (MeOAc) formation was measured at each humidity equilibration.

4.2.5.3 Results and Discussion

Effect of Ammonia Poisoning on Conductivity and Esterification Activity of Nafion Membranes at 50%RH and 80℃

The data points given in Figure 4.2.5-1(a) show the changes in real time conductivity and in the amount of adsorbed ammonia (in the form of NH_4^+) in the Nafion membrane (N-211) at 50 %RH, 80°C, and 1 atm for 20 ppm NH_3 in 100 sccm H_2. The amount of ammonia uptake (y_{NH4+}) and that of free proton sites (y_{H+}) are defined as follows:

$$y_{NH4+} = \frac{C_{NH4+}}{[C_{H+}]_0} \qquad (13)$$

$$y_{NH4+} + y_{H+} = 1 \qquad (14)$$

where y_{NH4+} and y_{H+} are the fraction of sulfonic acid sites occupied by ammonium ions and protons, respectively; C_{NH4+} is the concentration of ammonium ions interacting with the sulfonic groups in the Nafion membrane; and $[C_{H+}]_0$ is the proton concentration (IEC) of the N-211 in the fully H^+-form, respectively.

In Figure 4.2.5-1(a), the dotted line represents the ammonia uptake with time-on-stream (TOS) assuming 100% of ammonia introduced to the conductivity cell adsorbed on the membrane. It can be seen that the experimental data significantly deviates from the prediction because the flow characteristics inside an unstirred conductivity chamber (ID = 16 cm, H = 25 cm) are not efficient, allowing a lot of the ammonia to by-pass a membrane. For the actual data, as the amount of ammonia adsorption on the $–SO_3^-$-H^+ sites increased with time-on-stream (TOS), the conductivity decreased. Figure 4.2.5-1(b), on the other hand, presents the decrease in esterification activity and accessible free acid sites (y_{H+}) with TOS. The real time esterification activity was investigated on the same membrane, but the ammonia uptake was done on different samples under the exact same conditions. The dotted line shows the predicted esterification activity and ammonium ion composition assuming that all ammonia entering the reactor was absorbed by the membrane. It is evident the ammonia adsorption is much more efficient in the flow differential reactor than in the conductivity chamber. As expected, the esterification activity decreased accordingly with the decrease in proton composition (y_{H+}). It is evident that ammonia influences both conductivity and esterification activity in a similar manner under similar conditions.

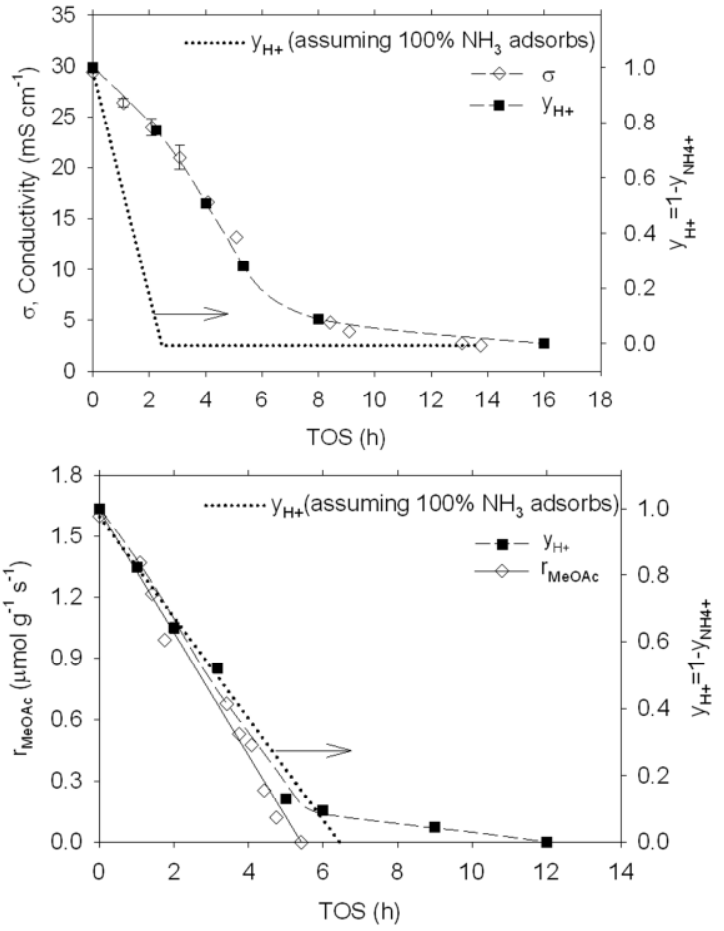

Figure 4.2.5-1: (a) Conductivity vs. proton composition (y_{H+}) and (b) esterification activity vs. proton composition (y_{H+}) of N-211 in the presence of 20 ppm NH_3 in flowing He at 50 %RH and 80°C as a function of TOS.

Effect of Humidity on Conductivity and Esterification Activity of Nafion Membranes in the Presence of 20 ppm at 50%RH and 80°C

Figure 4.2.5-2(a-b) show the effect of water vapor on the TOS conductivities and activities of N-211 in the presence of 20 ppm NH_3 at 80°C, and 1 atm, respectively. It can be seen in Figure 4.2.5-2(a) that the conductivity linearly decreased with TOS exposure to ammonia and reached the steady state. The kinetics of ammonia poisoning was slower and the steady-state conductivity was significantly increased with an increase in relative humidity. The results suggest that water is beneficial to proton migration because of three reasons: (1) water competitively adsorbs on the $-SO_3^-$ groups and protects the sites from ammonia; (2) water weakens the acid strength of the sulfonic sites and increases water mobility in the ionic domain; and (3) water increases the hydrophilic region of the Nafion matrix resulting in the enhancement of the connectivity throughout

the overall pore network. In Figure 4.2.5-2(b), on the other hand, the esterification activity decreased with TOS and the initial and steady-state activities declined with an increase in humidity. The results indicate that water is detrimental to esterification activity because (1) water molecules competitively adsorb with reactants (methanol and acetic acid) on the proton sites blocking them for reaction; (2) water vapor decreases the strength of the acid sites (acidity) by surrounding proton sites with fixed anionic charges [Hu 1993]; and/or (3) water vapor favors the hydrolysis reaction (re-forming acetic acid from methyl acetate).

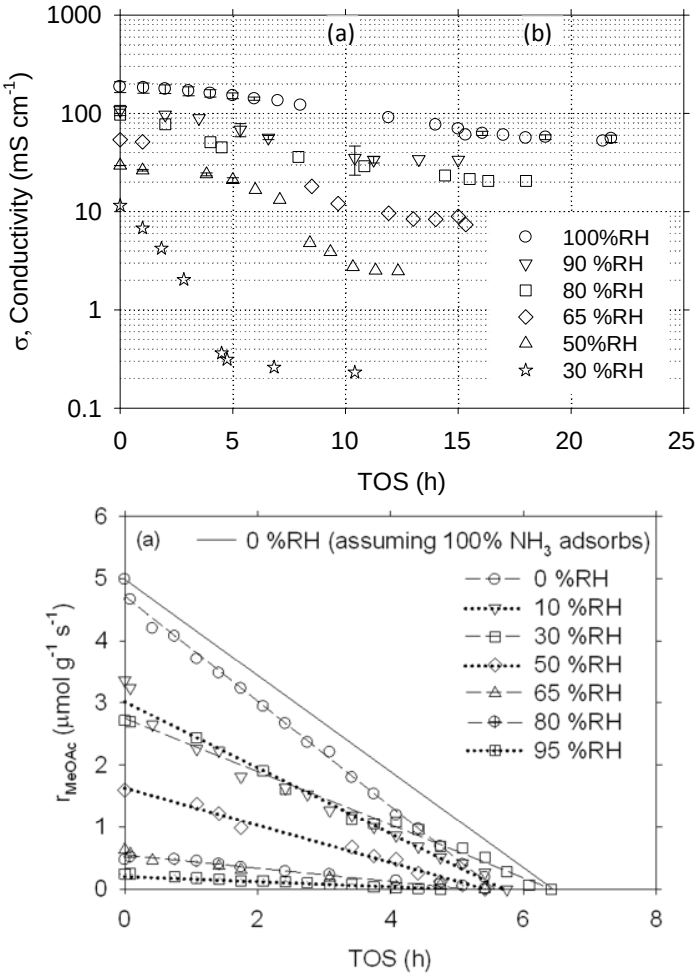

Figure 4.2.5-2: (a) Conductivity and (b) esterification of N-211 at different humidities and 80°C in the presence of 20 ppm NH_3 as a function of time-on-stream (TOS).

Relationship between the Conductivity and Esterification Activity of N-211

Since both esterification activity and proton conductivity are affected directly by proton concentration, a possible correlation exists between these two processes with some corrections for the different effects of water vapor and for the flow characteristics on the

two processes. While water vapor favors proton transport, it poisons esterification. Thus, the conditions, that yield the best ionic conductivity and esterification activity, are at 100 %RH and 0 %RH, respectively. Thus, normalized conductivity ($\sigma_{Norm.}$) and esterification activity ($r_{MeOAc,\ Norm.}$) should be plotted against %relative humidity and 100 - %RH, respectively. The expressions for the normalized values for σ and r_{MeOAc} are as follows:

Conductivity:

$$Normalized\ \sigma\ (\sigma_{Norm.}) = \frac{(\sigma_{y_{H+}=1} - \sigma_{y_{H+}})_{RH,80^oC}}{(\sigma_{y_{H+}=1} - \sigma_{y_{H+}})_{100\%RH,80^oC}} \quad (15)$$

Esterification:

$$Normalized\ r_{MeOAc}\ (r_{MeOAc,Norm.}) = \frac{(r_{MeOAc,y_{H+}=1} - r_{MeOAc,\ y_{H+}})_{RH,80^oC}}{(r_{MeOAc,y_{H+}=1} - r_{MeOAc,\ y_{H+}})_{0\%RH,80^oC}} \quad (16)$$

where $\sigma_{yH+=1}$ and σ_{yH+} are the conductivities of N-211 in the H^+-form and the mixed H^+/cations (NH_4^+ or other impurities) form, respectively; and $r_{MeOAc,\ yH+=1}$ and $r_{MeOAc,\ yH+}$ are the esterification activity of N-211 in the H^+-form and the mixed H^+/cations (NH_4^+ or other impurities) form, respectively.

Figure 4.2.5-3 shows the comparison of the normalized ionic conductivities and esterification activities of Nafion membranes (N-211) under a wide range of humidities at 80°C. After normalization, the $\sigma_{Norm.}$ (solid line) and $r_{MeOAc,\ Norm.}$ (dashed line) results essentially overlap. This observation provides further justification for using esterification to probe the number of free proton sites at various conditions.

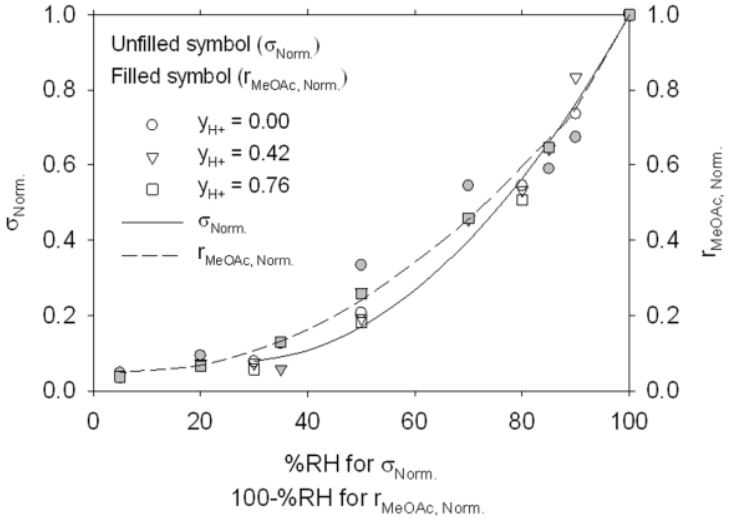

Figure 4.2.5-3: Comparison of the conductivity and esterification activity of N-211 poisoned with NH_3 at 80°C. ($\sigma_{Norm.}$ and $r_{MeOAc,\ Norm.}$ are normalized conductivity and normalized esterification activity obtained from Eqs. (15-16), respectively.)

To test the validity of this technique, the predicted steady-state conductivities of N-211 prepoisoned with Na^+ were calculated from the normalized esterification activity ($r_{MeOAc,\ Norm.}$) and compared with experimental results. The normalized esterification activities ($r_{MeOAc,\ Norm.}$) for the series of Na^+-contaminated membranes obtained from Eq. (16) were used to predict the normalized conductivity ($\sigma_{Norm.\ Predicted}$). The predicted conductivities (σ_{yH+}) for Na^+-contaminated membranes were obtained from Eq. (18):

$$\sigma_{Norm.,\ Predicted} \approx \frac{\left[\left(\sigma_{yH+=1}-\sigma_{yH+}\right)_{RH,80^oC}\right]_{Na^+}}{\left[\left(\sigma_{yH+=1}-\sigma_{yH+}\right)_{100\%RH,80^oC}\right]_{NH_4^+}} \quad (17)$$

$$\left[\left(\sigma_{yH+}\right)_{RH,80^oC}\right]_{Na^+} \approx \left[\left(\sigma_{yH+=1}\right)_{RH,80^oC}\right]_{Na^+} - \sigma_{Norm.,Predicted}\left[\left(\sigma_{yH+=1}-\sigma_{yH+}\right)_{100\%RH,80^oC}\right]_{NH_4^+} \quad (18)$$

Validity of Esterification Technique.

In Figure 4.2.5-4, the symbols and the solid lines represent the experimental and predicted conductivities of the N-211 membrane with different Na^+ concentrations and at different %RH. The agreement of prediction with experimental data shown in this study confirms that after normalization, the relative effect of foreign impurities on both ionic conductance and esterification is almost identical. On the other hand, impurities, that we have found to not affect ionic conductance of a Nafion membrane (e.g., CO_2, CO, HCOOH, C_2H_4, CH_3CHO, C_4H_8O (tetrahydrofuran), etc.), also do not affect esterification activity (data not presented here). This is because they do not adsorb on the anionic sulfonic charges and/or interfere with the strength of acid/proton sites.

This study validates the use of esterification as a powerful analysing technique to quantitatively analyse the number of active proton sites (directly related to esterification activity in the absence of mass transport limitations) and to predict ionic conductivity of the membrane over a wide range of humidity under operational fuel cell conditions.

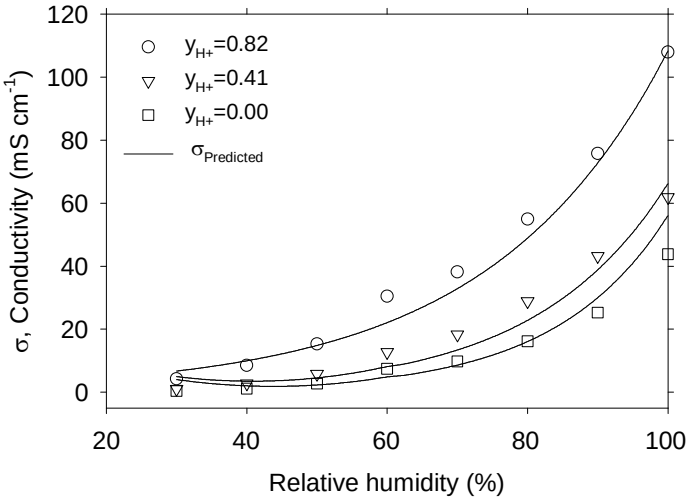

Figure 4.2.5-4: Experimental and predicted ionic conductivities of N-211 in the H^+/Na^+-form at 80°C.

4.2.5.4 Conclusions

In this study, the effect of impurity poisoning (such as by ammonia) on the proton availability of Nafion membranes at conditions typical of a fuel cell was investigated. The influence of ammonia on a Nafion membrane (N-211) was examined for the first time by making use of conductivity measurements, ammonia uptakes, and an acid-catalyzed reaction for Bronsted acid sites (esterification). It was found that in the presence of ammonia, the conductivity and esterification activity of N-211 decrease at 80^{o}C and all humidities in proportion to an increase in ammonia adsorption onto proton sites. This observation suggested that the ionic conductivity of Nafion membranes should be able to be plausibly predicted by knowing the proton compositions in them. This work proposes a convenient alternative technique to numerically investigate the number of acid sites during impurity exposure using a simple esterification reaction catalysed by the proton sites. Despite some dissimilarities between these two reactions, the normalization of the difference between the initial (or non-poisoned) and steady-state (or poisoned) conductivity and esterification activity allows us to establish a relationship between these two processes. The validity of this methodology was tested by predicting the conductivities of Na^{+}-contaminated membranes. It was found that the predicted conductivity was in good agreement with the experimental conductivity at all proton compositions (y_{H+}) and humidity ranges. These results justify the use of esterification as a diagnostic tool to quantitatively investigate the proton availability and predict the ionic conductivity of Nafion components in the presence of other contaminants at various conditions.

For further details about this study, please refer to:
"Esterification as a Diagnostic Tool to Predict Proton Conductivity Affected by Impurities on Nafion Components for Proton Exchange Membrane Fuel Cells," ***Journal of Power Sources*** 195 (2010) 3416-3424 (Kitiya Hongsirikarn, Xunhua Mo, and James G. Goodwin, Jr.).

References

Collette, F. M.; C. Lorentz, G. Gebel, F. Thominette, *Journal of Membrane Science*, 330 (**2009**), 21.

Hongsirikarn, K.; J.G. Goodwin, Jr., S. Greenway, S. Creager, *Journal of Power Sources*, 195 (**2010**a) , 30.

Hu, C.W.; M. Hashimoto, T. Okuhara, M. Misono, *Journal of Catalysis*, 143 (**1993**), 437.

Katsaounis, A.; S.P. Balomenou, D. Tsiplakides, M. Tsampas, C. G. Vayenas, *Electrochimica Acta*, 50 (**2005**), 5132.

Li, T.; A. Wlaschin, P.B. Balbuena, *Industrial and Engineering Chemistry Research*, 40 (**2001**), 4789.

Liu, Y.J.; E. Lotero, J.G. Goodwin, Jr., *Journal of Catalysis*, 242 (**2006**), 278.

4.2.6 Prediction of the effective conductivity of Nafion® in the catalyst layer of a PEMFC

4.2.6.1 Motivation

Previous studies have shown that in the absence of an impurity, fuel cell performance depends greatly on transport processes in the cathode catalyst layer [Song 2004]. However, under some circumstances, where the hydrogen fuel and/or oxidant streams contain contaminants, the rate of the HOR and the oxygen reduction reaction (ORR) on the active catalyst (typically Pt), or the rate of proton transport via the solid electrolyte (generally Nafion) in the ionomer layer and the membrane may be the main determining factor governing the performance of proton exchange membrane fuel cell (PEMFC). However, there is no detailed and quantitative study with experimental support on the effect of foreign cations on the ionic transport within the catalyst layer of a PEMFC due to the difficulty in conductivity measurement of the Nafion ionomer in a catalyst layer even in the absence of impurity. Up to the present, there is no experimentally measured proton conductivity for this layer that has been reported [Saab 2002]. The understanding of ionomer conductivity within the active layer is very important because the long-term durability and the performance of large-scale PEMFC operation, where commercial H_2 fuel and air streams contain some contaminant cations and material corrosion occurs, could be severely affected by proton starvation within the ionomer phase.

Previously, the use of a simple acid-catalyzed reaction, esterification, to quantitatively investigate proton availability and to predict the conductivity of a Nafion membrane (N-211) has been validated with experimental results. In this study, we further applied esterification to examine proton composition (y_{H+}) of supported Nafon (Nafion on a carbon support and on Pt/C, resembling the agglomerates that constitute the catalyst layer in a PEMFC) during impurity (ammonia) exposure. The quantity y_{H+}, determined under various conditions including ammonia poisoning, was used herein to estimate the effective ionic conductivity of the cathode catalyst layer using the well-known steady-state agglomerate model which was then compared to measurements in the literature.

4.2.6.2 Experimental

Two Nafion-containing materials were prepared for this study using the impregnation method. One material had components similar to the catalyst layer in a PEMFC (Nafion supported on Pt/C) and another material contained only Nafion on the carbon support for comparison purposes. The as-received Nafion ionomer solution (LQ-1105, DuPont, 5 wt.% Nafion) was impregnated on carbon black powder (Vulcan XC-72R, Carbot International) and a commercial 20 wt.% Pt/C (E-TEK) by incipient wetness, since this technique is believed to provide a better contact of the triple phase boundaries between the Nafion, Pt, and carbon support. The perfluorosulfonic acid ionomer content in the catalysts was fixed at ~30 wt.% because this Nafion loading has been found to be optimum for PEMFC applications. In this study, the ionomer content in the electrode catalyst is defined as: ionomer content (wt.%) = $(W_{ion}/W_{total}) \times 100$, where W_{ion} is the weight of dry ionomer, and W_{total} is the total weight of dry ionomer and support (carbon

or Pt/C). After impregnation, the 30 wt.% Nafion on the carbon support (designated as 30-Nfn/C) and the 30 wt.% Nafion on Pt/C (30-Nfn/Pt/C) were dried overnight in an oven at 80^{O}C in dynamic air flow. The resulting agglomerates were then crushed and screened between sieves (80-230 mesh) before being stored in the dark prior to use.

The total surface areas of supported Nafion (30-Nfn/C and 30-Nfn/Pt/C) were determined via the BET method utilizing a Micromeritics ASAP 2001 apparatus. The concentrations of proton/acid sites on 30-Nfn/C and 30-Nfn/Pt/C were examined by titration. Nafion on different supports (30-Nfn/C and 30-Nfn/Pt/C) after ammonia exposure for a certain period were ion-exchanged with 0.05 M HCl (Acros Organics) at room temperature under constant shaking for at least 7 days. Then, the sample was filtered out from the aliquot. The ammonium concentration in the exchange solution was examined by an ion-selective electrode (ammonia electrode 9512 Thermo Scientific and Orion 4 star pH benchtop meter).

Prior to gas-phase esterification, approximately 100 mg of 30-Nfn/C or 30-Nfn/Pt/C was placed between quartz wool plugs in the middle of a differential tubular reactor (ID=0.7 cm). The sample was pretreated in 100 sccm H_2 at a given humidity, 80^{O}C, and 1 atm for 3 h. Then, a known amount of reactants (acetic acid (HAc) and methanol (MeOH)), water vapor, and ammonia was introduced to the reactor. The esterification was carried out with an equimolar, low concentration mixture of MeOH and HAc (P_{MeOH}=P_{HAc}=0.009 atm) at a given humidity, 80^{O}C, and 1 atm in 100 sccm H_2. The concentrations of reactants (MeOH and HAc) and product (MeOAc) in the outlet stream were analysed by a Varian CP-3380 GC equipped with an FID detector and a Varian CPWAX 52CB fused silica capillary column (60 m × 0.53 mm ×1 μm).

4.2.6.3 Results and Discussion

Effect of Ammonia Poisoning on Esterification Activity of Supported Nafion at 50%RH and 80℃

In Figure 4.2.6-1(a–b), the esterification activities and the concentrations of free acid/proton sites (y_{H+}) of a Nafion component for the 30-Nfn/C and 30-Nfn/Pt/C materials in H_2 containing ppm NH_3 and 50 %RH at 1 atm and 80^{O}C are illustrated, respectively. It can be seen that the catalytic activity decreases with time-on-stream (TOS) accordingly to the decrease in proton concentration in the Nafion ionomer (y_{H+}) for both supported Nafion materials, consistent with the results for Nafion membranes reported in the previous study [Hongsirikarn 2010b]. The experimental results imply that in the presence of other materials (i.e., alloyed Pt, C support) and other impurities, the acid site/proton concentration of a Nafion polymer can be quantitatively investigated by this acid-catalysed reaction. Unlike a conventional titration method, which is a destructive technique, esterification allows us to study the effect of contaminants on the proton availability of a Nafion component in-situ and to continuously monitor using only a single sample the available proton composition during impurity exposure.

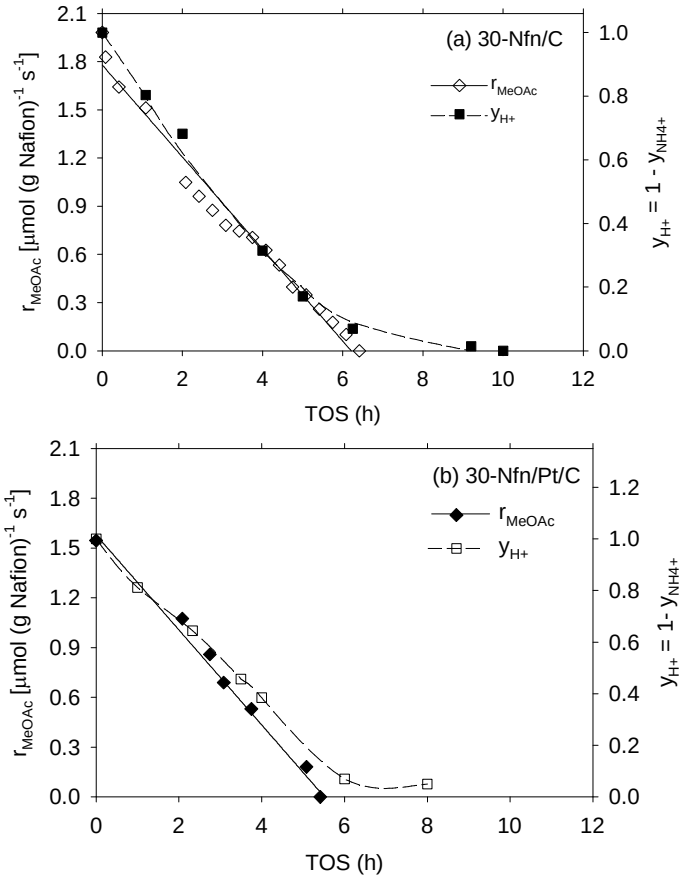

Figure 4.2.6-1: Relationship of esterification activity to proton fraction of: (a) 30-Nfn/C, and (b) 30-Nfn/Pt/C at 50 %RH in the presence of 20 ppm NH_3 and 80°C.

Modified Steady-State Agglomerate Model to Predict the Overall Conductivity of a Contaminated Catalyst Layer in a PEMFC

The effective protonic conductivity is crucial to the performance and optimization of the active layer in PEMFCs [Du 2004]. It is known that the agglomerate model is the most popular and the most theoretically based model to address proton transport in a catalyst layer (where three-phase contact exists between ionomer, catalyst, and carbon support). It matches very well with experimental data, especially for fuel cell operation [Jaouen 2002; Harvey 2008; Secanell 2007]. The effective proton conductivity in an active layer is as follows:

$$\sigma_{eff}^{cat} = \left(1-\varepsilon_{cat}\right)\left[1+\frac{\left(\varepsilon_{agg}-1\right)}{\left(1+\delta/r_{agg}\right)^{3}}\right]\sigma \qquad (19)$$

$$\sigma_{eff}^{cat} = C\sigma \qquad (20)$$

where σ_{eff}^{cat} and σ are the effective conductivity of the catalyst layer (active layer) and the bulk conductivity of the polymer (typically Nafion) fraction in the catalyst layer, respectively; ε_{agg} and ε_{cat} are the volume fractions of the polymer in the agglomerate and of the pores in the catalyst layer, respectively; r_{agg} is the agglomerate radius; δ is the thickness of the polymer film surrounding the agglomerate; and C is a factor depending on the operating conditions and physical properties of the metal(s), support, and ionomer used in the catalyst layer.

It can be seen in Eq. (20) that, in the absence of impurities, the effective conductivity is the product of a constant factor C and the bulk conductivity of the polymer. The factor C depends on the physical properties of the catalyst layer, for example, porosity, radius of the agglomerate, thickness of polymer surrounding the agglomerate, etc. Thus, the factor C can be considered to remain constant during exposure of the ionomer to impurities that do not affect these properties. For the ammonium-poisoned catalyst layer in this study, the factor C was assumed to be constant and the effective conductivity was able to be obtained by knowing the proton composition (y_{H+}). The correlation of the Nafion conductivity at typical fuel cell operation as a function of ammonium content has been reported in our previous study [Hongsirikarn 2010a]. Accordingly, the effective conductivity of an ammonium-poisoned catalyst layer can be estimated as follows:

$$\sigma_{eff}^{cat} = C\sigma_{yNH4+} \tag{21}$$

$$\sigma_{yNH4+} = \frac{A_3}{1+A_1\exp\left(A_2 y_{NH4+}\right)} + A_4 \tag{22}$$

where y_{H+} and y_{NH4+} are the concentrations of protons and ammonium ions in the Nafion polymer obtained from the esterification activity, respectively; σ_{yNH4+} is the conductivity of the Nafion polymer containing y_{NH4+} at 80°C; and parameters (A_1–A_4) are given in reference [Hongsirikarn 2010c]. The expression for σ_{yNH4+} given above is an empirical function that has been found to best fit the experimental data. The theoretical model of the relationship between the conductivity and y_{NH4+} has already been discussed in our previous work [Hongsirikarn 2010a].

Since ammonia is introduced at the anode as an impurity in H_2, ammonia adsorption on Nafion starts at the contacted interface before it is transported to the cathode, causing some potential gradients in ammonium composition within an MEA. If the ammonium distribution throughout an active catalyst layer is known, the overall effective conductivity ($\sigma_{overall\ cat}$) can be obtained by integrating the conductivity throughout that layer as follows:

$$\sigma_{overall\ cat} = \int_0^1 \sigma_{eff}^{cat}\, dx \tag{23}$$

$$assu\min g\quad \sigma_{eff}^{cat} = C\sigma_{yNH4+}\quad where\quad C = \left(1-\varepsilon_{cat}\right)\left[1+\frac{\left(\varepsilon_{agg}-1\right)}{\left(1+\delta/r_{agg}\right)^3}\right]$$

$$\sigma_{yNH4+} = F_1^n(y_{NH4+}) \quad (24)$$

$$y_{NH4+} = F_2^n(x) \quad (25)$$

$$\sigma_{overall\ cat} = (1-\varepsilon_{cat})\left[1+\frac{(\varepsilon_{agg}-1)}{\left(1+\delta/r_{agg}\right)^3}\right]\int_0^1 \sigma_{yNH4+}\,dx \quad (26)$$

where x is the normalized distance from the membrane interface/catalyst layer in the x-dimension; $F_1^n(y_{NH4+})$ is the correlation between the conductivity as a function of y_{NH4+} as shown in Eq. (22); and $F_2^n(x)$ is the ammonium distribution within the catalyst layer as a function of x.

The expression Eq. (26) can be used to estimate the overall conductivity of the active layer both at anode and cathode. In this study, we have demonstrated how to predict the overall conductivity of an ammonium-contaminated cathode layer at typical fuel cell conditions using the modified agglomerate model (Eq. (26)). A typical set of model parameters for the effective conductivity calculation at the cathode are given in reference [Hongsirikarn 2010c] and the expression for the overall effective conductivity ($\sigma_{overall\ cat}^{cathode}$, Eq. (19)) at the cathode operating at various humidities and 80°C can be simplified to:

$$\sigma_{overall\ cat}^{cathode} = 0.167\int_0^1 \sigma_{yNH4+}\,dx \quad (27)$$

Due to the lack of direct measurements of the conductivity of a poisoned catalyst layer, the accuracy of our predicted effective conductivity was validated using the experimental conductivity of an uncontaminated catalyst layer and the percentage of performance degradation of a fully ammonium-poisoned PEMFC. In Figure 4.2.6-2, the unfilled circles indicate the experimental conductivity at various humidities and 80°C of an uncontaminated catalyst layer determined by a hydrogen pump technique employed by reference [Iden 2009] and the dashed line represents a fit of their data. The solid line shows the predicted conductivity of the cathode catalyst layer ($\sigma_{overall\ cat}^{cathode}$) calculated from Eq. (27) using $y_{NH4+} = 0$. It can be seen that in the absence of impurities, the predicted values agree extremely well with experimental data. The estimated percentage decrease of the $\sigma_{ovrall\ cat}^{Cathode}$ of the fully ammonium-poisoned PEMFC (having a homogeneous ammonium ion concentration profile (constant $y_{NH4+} = 1$), dashed-dotted line in Figure 4.2.6-2) was compared with the results of performance testing reported by reference [Uribe 2002]. They studied the impact of ammonia on PEMFC performance, operating at 80°C. A PEMFC was exposed to 30 ppm of NH_3 for 15 h, which was enough for complete neutralization of the protonic sites of the MEA. They found that the cell voltage decreased ca. 49 – 77% at current densities of 0.2 – 0.4 A cm^{-2}. In this study, the estimated overall cathode conductivity ($\sigma_{ovrall\ cat}^{Cathode}$) of the Nafion ionomer in the fully

NH_4^+-form was ca. 64% lower than that of the fully H^+-form, which corresponds well with the performance loss in a PEMFC [Uribe 2002].

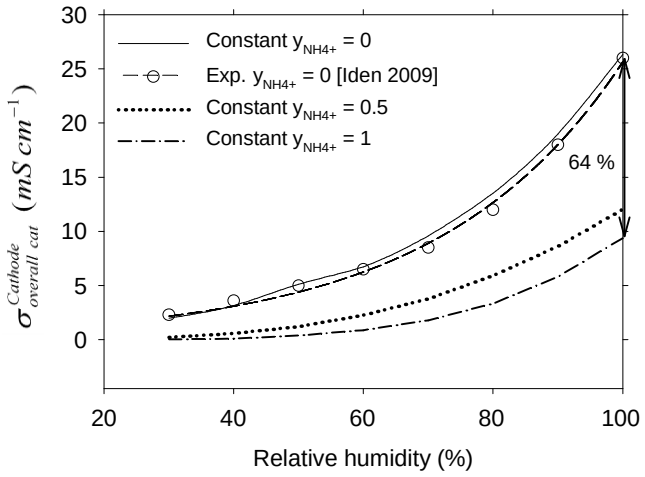

Figure 4.2.6-2: Predicted $\sigma^{Cathode}_{ovrall\ cat}$ of an NH_4^+-contaminated cathode catalyst layer having various NH_4^+ concentration profiles as a function of relative humidity at 80°C. ($\sigma^{Cathode}_{ovrall\ cat}$ was obtained from Eq. (27).)

Although only the estimated $\sigma^{Cathode}_{ovrall\ cat}$ and the estimated percentage decrease in $\sigma^{Cathode}_{ovrall\ cat}$ for the case of constant y_{NH4+} = 0 and 1 (i.e., uniform ammonium ion poisoning), respectively, can be shown to be matched with experimental results (due to the lack of appropriate experimental data in the literature), the overall conductivity at the cathode layer for other cases should be able to be reasonably predicted.

4.2.6-4 Conclusions

In this study, proton availability of Nafion impregnated on a carbon support and Pt/C (30-Nfn/C and 30-Nfn/Pt/C) as used in typical fuel cells was explored using the same characteristic acid-catalysed reaction (esterification of acetic acid with methanol) at various conditions (30 – 95% RH, 80^{O}C, and 1 atm). It was found that, under all the conditions studied, the esterification activity (r_{MeOAc}) on the supports was negligible and the esterification occurred only on the free proton/acid sites of the Nafion component. The results suggest that esterification can be used to quantitatively investigate the proton composition (y_{H+}) of a Nafion component during exposure to ammonia or other potential impurities. The information of y_{H+} gained from esterification was further used to estimate the overall conductivity of a catalyst layer using the modified agglomerate model and the correlation between conductivity and ammonium ion content (y_{NH4+}). The estimated effective conductivities of a cathode catalyst layer ($\sigma^{Cathode}_{ovrall\ cat}$) was validated with the available literature data at two extreme conditions (non-poisoned [Iden 2009] and fully ammonium-poisoned [Uribe 2002]) and found to be in good agreement at all humidity ranges. This study showed that the characterization reaction also has the potential to be applied to quantitatively examine the number of proton/acid sites of other

proton conducting materials impregnated on other supports (e.g., carbon, Pt/C, alloyed Pt/C) for a PEMFC under a wide range of conditions. The combination of the esterification technique and the modified agglomerate model proposed in this work should provide helpful information for future investigations of impurity resistance of all sorts of proton conducting electrolytes, catalyst layer optimization, and computation modeling of PEMFC performance.

For further details about this study, please refer to:
"Prediction of the Effective Conductivity of Nafion in the Catalyst Layer of a PEMFC," ***Journal of Power Sources*** 195 (2010) 5493-5500 (Kitiya Hongsirikarn, Xunhua Mo, Zhiming Liu, and James G. Goodwin, Jr.).

<u>References</u>

Du, C.Y.; P.F. Shi, X.Q. Cheng , G.P. Yin, *Electrochemical Communication*, 6 (**2004**), 435.

Harvey, D.; J.G. Pharoah , K. Karan, *Journal of Power Sources*, 179 (**2008**), 209.

Hongsirikarn, K.; J.G. Goodwin, Jr., S. Greenway, S. Creager, *Journal of Power Sources*, 195 (**2010**a) , 30.

Hongsirikarn, K.; X. Mo, J.G. Goodwin, Jr., *Journal of Power Sources*, 195 (**2010**b), 3416.

Hongsirikarn, K.; X. Mo, L. Zhiming, J.G. Goodwin, Jr., *Journal of Power Sources*, 195 (**2010**c), 5493.

Iden, H.; A. Ohma , K. Shinohara, *Journal of Electrochemical Society*, 156 (**2009**), B1078.

Jaouen, F.; G. Lindbergh , G. Sundholm, *Journal of Electrochemical Society*, 149 (**2002**), A437.

Saab, A.P.; F.H. Garzon , T.A. Zawodzinski, *Journal of Electrochemical Society*, 149 (**2002**), A1541.

Secanell, M.; B. Carnes, A. Suleman , N. Djilali, *Electrochimica Acta*, 52 (**2007**), 2668.

Song, D.T.; Q.P. Wang, Z.S. Liu, T. Navessin, M. Eikerling , S. Holdcroft, *Journal of Power Sources*, 126 (**2004**), 104.

Uribe, F.A.; S. Gottesfeld , T.A. Zawodzinski, *Journal of Electrochemical Society*, 149 (**2002**), A293.

4.3 Fuel Cell Studies

4.3.1 Fuel Cell and Procedure

4.3.1.1 Cell Performance Testing

Fuel cell performance testing was followed by standard electrochemical measurements such as cyclic-voltametry and electrochemical impedance spectroscopy techniques using commercially available fuel cell test stations and MEA. Figure 4.3.1-1 (right image) shows the enclosure containing the environmental chambers that were used to set temperature and humidity conditions for the fuel cell. Gas pressures and gas mixtures were set using manometric gas manifolds and analytical spectroscopic techniques. Figure 4.3.1-1 (left image) shows the module providing the impurities to the fuel cell station. Impurities were provided by a KinTek® calibration gas generator. Figure 4.3.1-2 shows the experimental schematic of how the two systems were synchronized so that automated continuous operations were achieved.

Figure 4.3.1-1: Picture of the KinTek calibration gas generator (left image) that is connected to fuel cell testing station (right image)

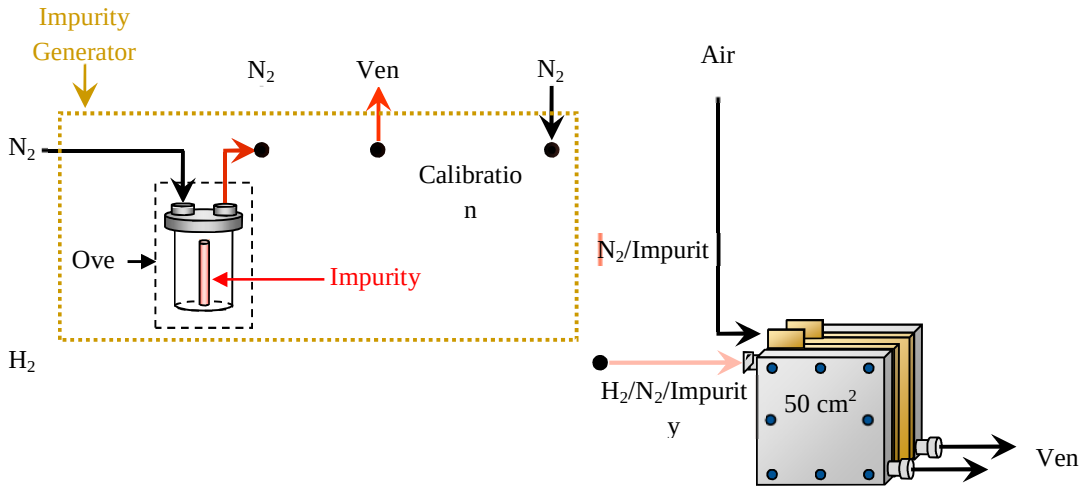

Figure 4.3.1-2: Experimental schematic of the impurity delivery system.

4.3.1.2 Experimental Techniques

All experiments were performed at 60°C with pressures of 101 kPa on the anode and the cathode. Each cell tested was "broken-in" at 60° C by maintaining a constant current of 0.6 A/cm^2 for a minimum of 24 hrs at 100% relative humidity (RH) with flow rates set to maintain a fixed stoichiometry of 1.2 and 2 for the anode and cathode, respectively. After the cell reached steady state performance, the humidifier temperatures were changed to maintain 100% and 50% RH in the anode and the cathode, respectively. The set of experiments included: (1) initial H_2/air voltage-current polarization scan to establish baseline performance of the cell, (2) cyclic voltammetry (CV) and electrochemical impedance spectroscopy (EIS) tests before poisoning the cell, (3) H_2/air potentiostatic polarization with impurity in the H_2 stream until the cell performance decayed to steady state, (4) H_2/air voltage-current polarization scan under poisoning conditions, (5) CV and EIS tests after poisoning the cell, and (6) H_2/air potentiostatic polarization with neat H_2 to test the cell recovery. In addition, galvanostatic polarization tests were performed (H_2 pump) in H_2/N_2.

The voltage-current polarizations were performed at constant cell voltage in a voltage range between the open circuit voltage (OCV) and 0.4 V. At each point, the voltage was maintained for 20 min and the average of the current during the last 5 min was recorded. The flows were set to maintain a fixed stoichiometry of 1.2 with a minimum flow of 84 sccm for the anode and 2.0 with a minimum flow of 347 sccm for the cathode. After a baseline was obtained the cell was held at 0.6 V for several hours. Then, the cell was exposed to PCE and the performance was monitored until it decayed to a steady state value.

CV and EIS measurements were performed using a Princeton Applied Research potentiostat/galvanostat model 2273 with a built-in frequency response analyzer and while flowing N_2 on the anode (working electrode) at 250 sccm and neat H_2 on the cathode (dynamic hydrogen reference electrode) at 250 sccm as well. The CV was measured between 0.05 V and 1.1 V for 2 cycles at a scan rate of 10 mV/s. The impedance spectrum was recorded using an amplitude of 14 mV around a bias potential of 15 mV above the open circuit and by sweeping the frequency in the range from 10 kHz to 1 Hz.

The H_2 pump test was performed while the cell was exposed to 30 ppm of PCE. The anode was fed with H_2 at a fixed stoichiometry of 1.2 with a minimum flow of 84 sccm and the cathode was fed with N_2 at 250 sccm. During the test, the polarization was measured by scanning the current between 0.2 and 1.4 A/cm^2 at a scan rate of 0.1 A/cm^2/min. Then the cell was held at 1.0 A/cm^2 for 26 min before another polarization scan started. The cycles continued until steady state conditions were reached.

In situ FT-IR experiments to detect PCE at the anode and cathode outlet of the fuel cell were performed using a Jasco FT-IR-6300 spectrometer at 0.5 cm^{-1} resolution. The spectrometer was equipped with a Specac Cyclone C10^{TM} gas cell with a path length of

10.6 m. The transmission line was maintained at 110°C and the gas cell to 100 ºC to avoid any water condensation. Measurements were performed under continuous gas flow at a constant pressure of 84.3 kPa, while hydrogen pump conditions were applied to the fuel cell. The PCE spectrum was monitored continuously and the final spectrum was obtained by averaging 10 scans after the signal reached steady state. In addition, experiments were conducted to calibrate the FT-IR signal by injecting known concentrations of PCE (0.5 – 200 ppm) directly to the gas cell.

A commercially-available MEA (Ion Power), 50 cm^2 active area with a total of 0.1 mg of Pt catalyst on the anode and 0.3 mg of Pt on the cathode, was tested at 60ºC in neat hydrogen and no back-pressure. The test sought to establish the baseline performance at different relative humidities. The selected conditions are believed to be representative of 2 major conditions which includes "dry" operations (automotive conditions, 50% RH/50% RH) and "wet" operation (normal laboratory conditions, 100% RH / 100% RH). The third case study was a combination of the first two cases, where the anode is run "wet" (100% RH) and the cathode is run "dry" (50% RH). Figure 4.3.1- shows the performance results for the three different case studies. As can be observed from the figure, the performance decreases as the relative humidity decreased. The effect was more pronounced at the intermediate current densities (between 0.2 to 1.0 A/cm^2), where the limitations of the cells are dominated by the membrane resistance.

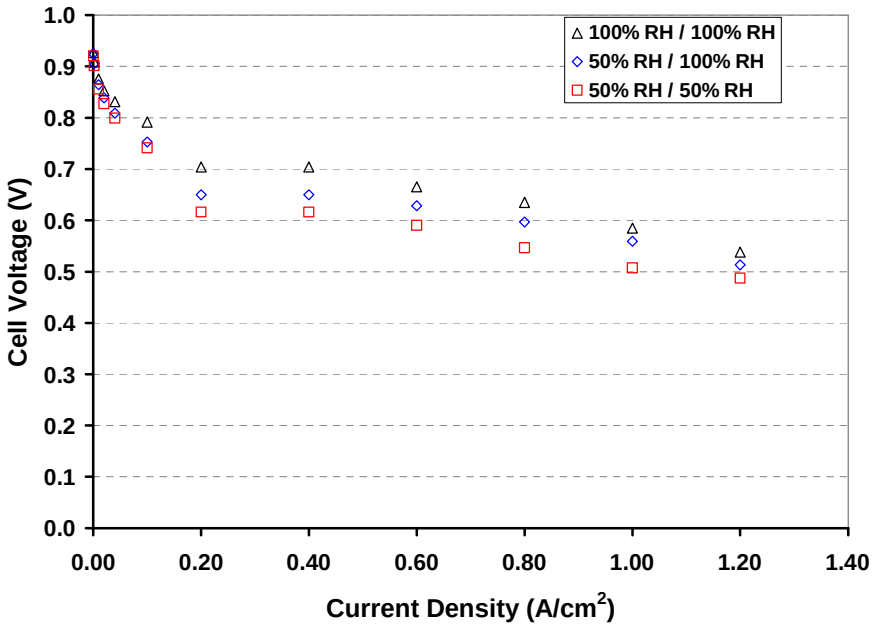

Figure 4.3.1-3: **Cell performance as a function of relative humidity of an Ion Power MEA at 60°C and no impurities.**

4.3.2 Effect of CO

CO poisoning experiments were performed to study the performance decay at International Office for Standardization (ISO) limits. Figure 4.3.2-1 shows the current decay at 0.6 V with time during the poisoning. The potentiostatic curve has been corrected for the typical degradation of the MEA observed before the poisoning. Notice that after 40 hrs the decay rate decreased indicating a steady state was reached. Although the concentration of CO is small, the performance decayed almost 10 % in a few hours. This decay is significant as it will immediately reduce the performance of the system by close to 10 % at the beginning of life. With other factors to consider such as other impurities and components degradation, the effects of CO at ISO limits are appreciable.

Figure 4.3.2-2 shows the polarization scan before and during exposure of CO, and after electrochemical oxidation of CO through cyclic voltammetry. As expected, electrochemical oxidation successfully removed all traces of CO and the MEA performance was recovered.

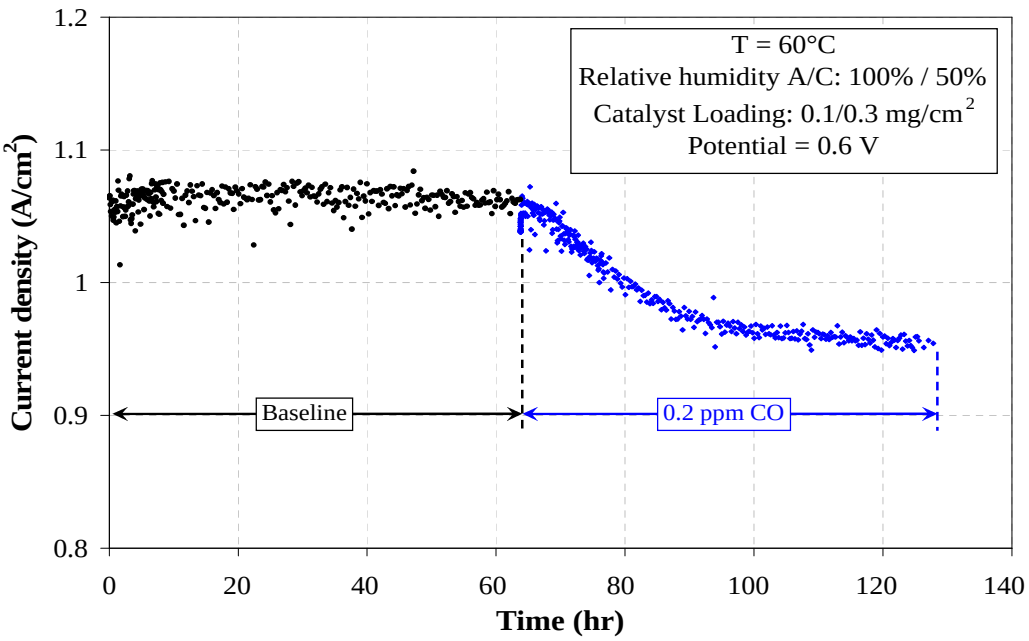

Figure 4.3.2-1: Current decay during 0.2 ppm CO poisoning of a 50 cm^2 Ion Power MEA with an anode Pt loading of 0.1 mg/cm2 at 60°C.

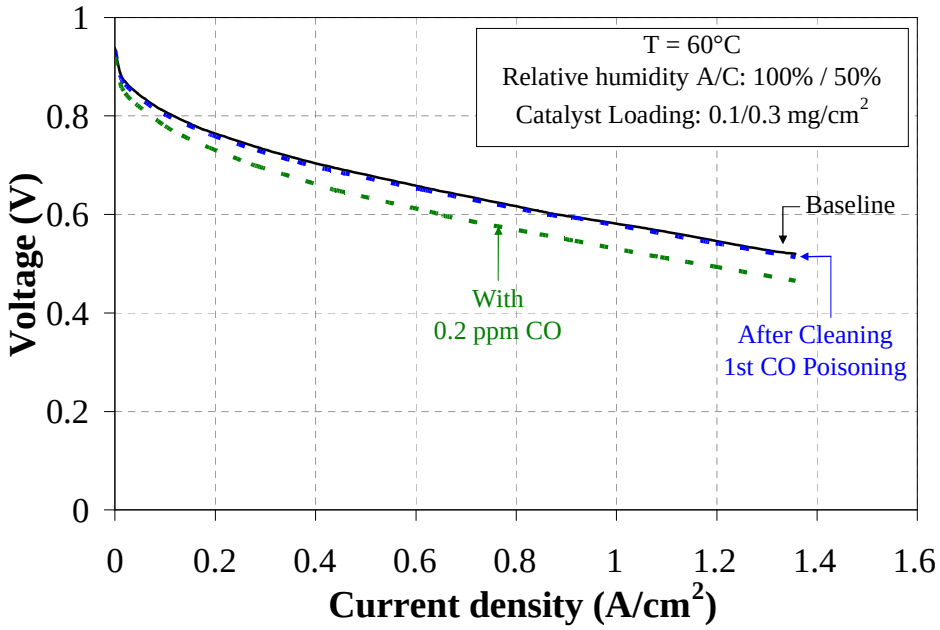

Figure 4.3.2-2: Polarization scan before, during and after electrochemical cleaning of the cell during the 0.2 ppm CO poisoning test of a 50 cm^2 Ion Power MEA with an anode Pt loading of 0.1 mg/cm2 at 60°C.

4.3.3 Effect of NH_3

4.3.3.1 Long Term Effect

Experiments were conducted to understand the impact of NH_3 on the fuel cell at the ISO fuel quality limit. A baseline and 0.1 ppm poisoning at 60°C and 50/50 %RH with an Ion Power MEA to determine the impact of NH_3 at the ISO limit were performed. Figure and Figure show the potentiostatic polarization for the baseline cell (under neat H_2) and the cell tested with a H_2 stream containing 0.1 ppm of NH_3, respectively. As the figures show, both the cells with and without ammonia exhibited a degradation rate of 15 mA/hr. This result indicates no appreciable degradation from the introduction of NH_3 at ISO specified level.

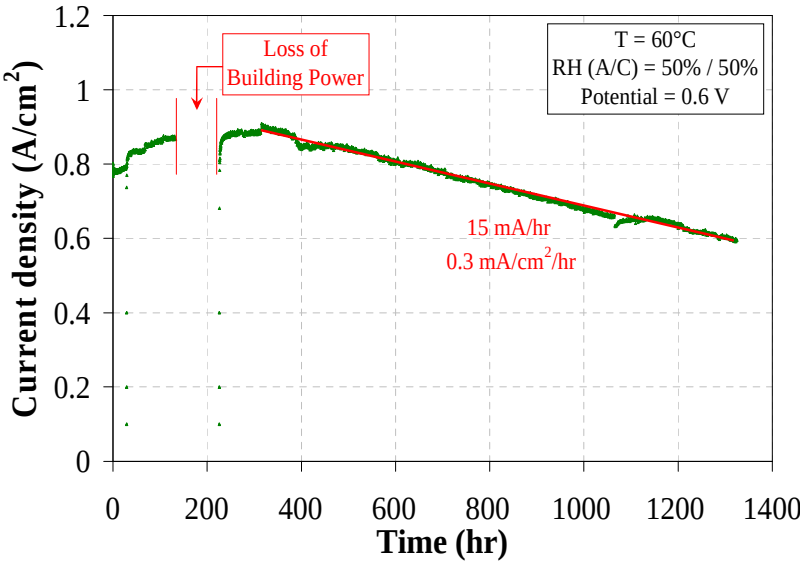

Figure 4.3.3-1: H_2/Air potentiostatic polarization baseline for an Ion Power MEA with 0.1/0.3 mg/cm^2 catalyst loadings at 60°C and 50%/50% RH.

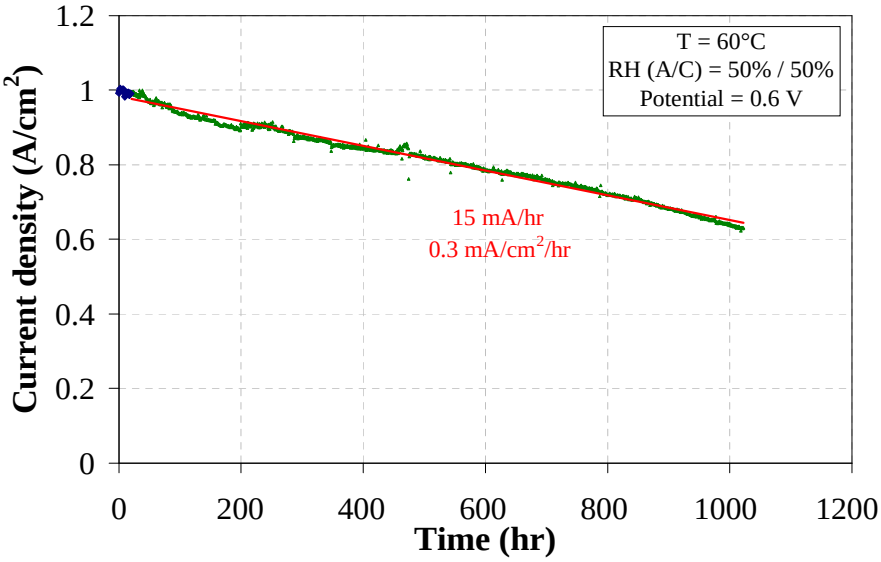

Figure 4.3.3-2: H_2/Air potentiostatic polarization baseline in the presence of 0.1 ppm NH_3 for an Ion Power MEA with 0.1/0.3 mg/cm^2 catalyst loadings at 60°C and 50%/50% RH.

4.3.3.2 H_2 Pump NH_3 Poisoning with NH_3 at 10 ppm

A hydrogen pump experiment was used to characterize changes in MEA properties during NH_3 poisoning. By performing the H_2 pump on a H_2 / N_2 system that is being poisoned at a current similar to an operating fuel cell, the kinetics of NH_3 poisoning of the membrane and ionomer can be measured. Figure shows the experimental set up and the experiment cycle parameters. In a typical cycle, hydrogen flowed to the anode and nitrogen to the cathode. Then a current was applied in order to oxidize the H_2 at the anode and reduce it at the cathode, just like in a typical fuel cell run. However, the oxygen reaction was avoided thus measuring the effects of only the ammonia on the hydrogen redox reaction. During an experiment, the cell was polarized by applying 50 A (1 A/cm^2) for 26 minutes, then a polarization curve was measured by scanning between 0.2 and 1.4 A/cm^2. The experiment was then cycled until steady state conditions were reached.

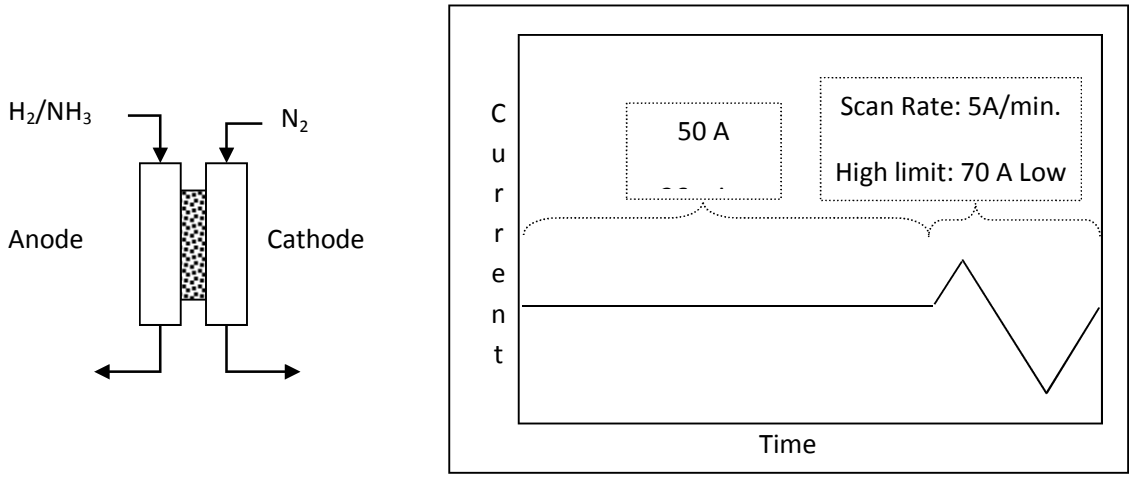

Figure 4.3.3-3: H_2 pump experiment set-up and cycle parameters.

Figure 4 shows the results of the 1 A/cm^2 section of the cycle. During the first 17 hours the cell ran with neat H_2, after that 10 ppm of NH_3 was injected along the hydrogen stream. As it can be seen in the figure, the introduction of NH_3 increased the overpotential of the H_2 oxidation reaction about 500 mV. The system quickly reached steady state in about 12 hours from the start of the poison.

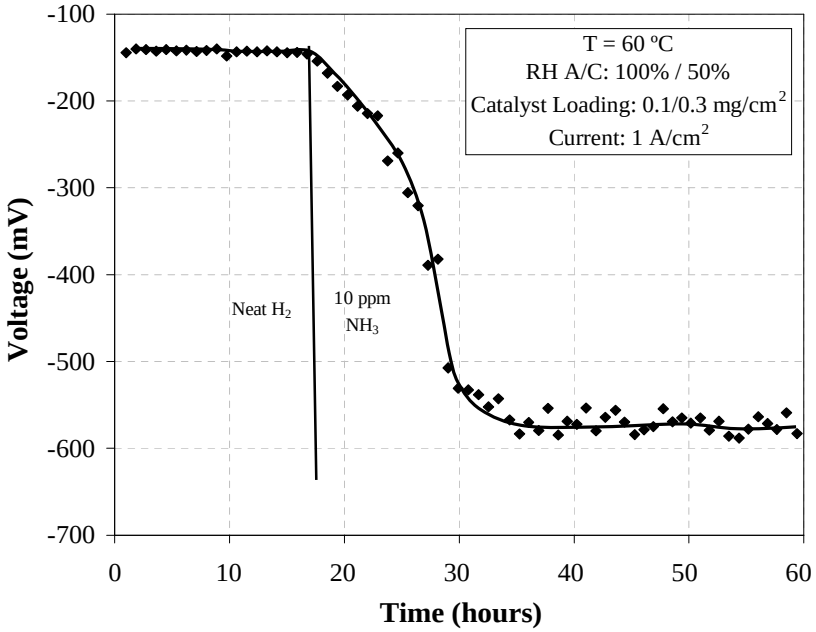

Figure 4.3.3-4: H_2/N_2 galvanostatic polarization in the presence of 10 ppm NH_3 for an Ion Power MEA with 0.1/0.3 mg/cm^2 catalyst loadings at 60°C and 100%/50% RH (A/C).

Figure shows some of the results from the polarization scan. From the experiment the slope of the curve can be related to the resistance of the cell. When neat H_2 flowed into the cell, a straight line was observed. As soon as NH_3 was introduced, the slope of the line started to increase and it was noted that the line starts to develop an inflection point and two slopes were observed. At current densities below around 0.75 A/cm^2, the rate of change of the slope tended to be slower than the rate of change of the slope at current densities higher than 0.75 A/cm^2. This difference in slope can be an indication of the effect of the NH_3 on the conductivity of the different regions inside the MEA.

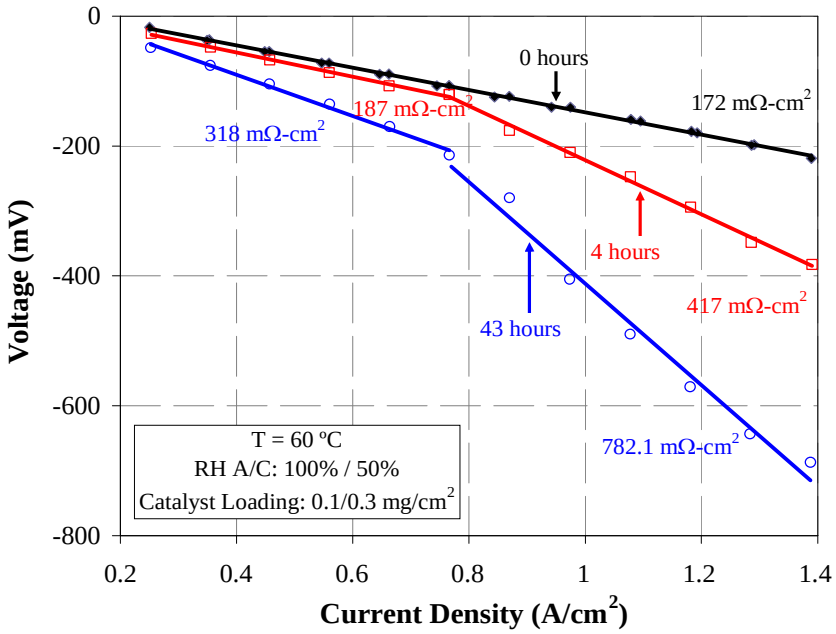

Figure 4.3.3-5: H_2/N_2 polarization scan in the presence of 10 ppm NH_3 for an Ion Power MEA with 0.1/0.3 mg/cm^2 catalyst loadings at 60°C and 100%/50% RH (A/C).

4.3.4 Effect of Halogenates

Impurity tests were performed with perchloroethylene (PCE, also called tetrachloroethylene) to characterize the performance effects that chlorinated cleaning agents can have on fuel cell performance. PCE concentrations of 30 ppm, 1 ppm, and 0.05 ppm were tested with anode/cathode relative humidities of 100%/50% RH. The 50 ppb concentration is the ISO total limit for halogenated compounds in the hydrogen stream. The current decay curves during the duplicate experiments are shown in Figure . SRNL will be working in the future with hydrogen producers to identify other halogenated compounds such as heat transfer fluids that should be studied as part of the evaluation of halogenated compounds for the ISO standard. It is likely that other chlorinated alkenes such as trichloroethylene, dichloroethylene, and chloroethylene would also need to have a reduced fuel quality limit.

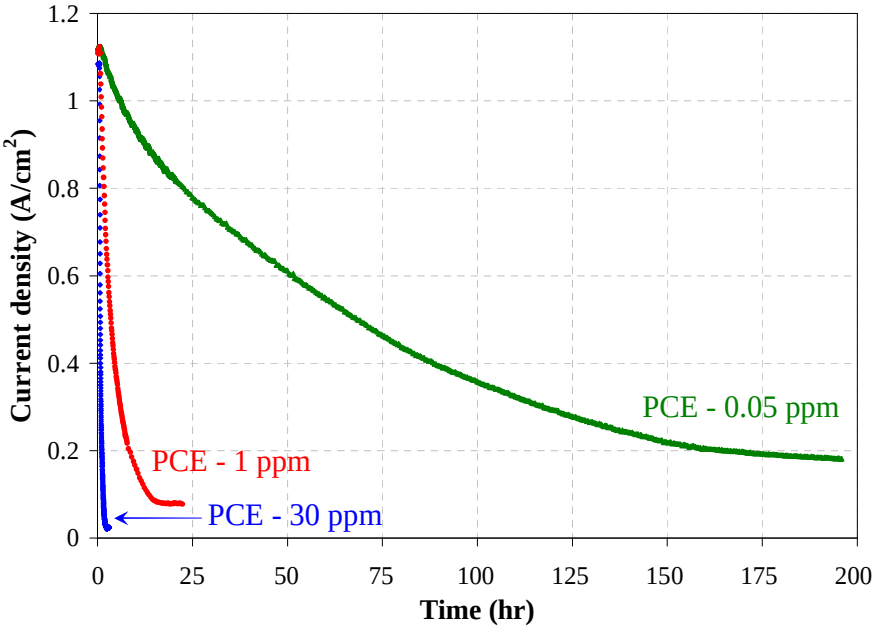

Figure 4.3.4-1: Effect of PCE concentration on PEM fuel cell performance at 60°C.

After poisoning the fuel cell, polarization curves were performed with PCE in the hydrogen stream to understand how PCE affected the system at different potentials. Figure shows the polarization curves with PCE in the hydrogen stream after the poisoning shown in Figure . As seen in previous experiments, the cell did not recover from poisoning during operation in neat hydrogen. However, the cell recovered after cyclic voltammetry on the anode.

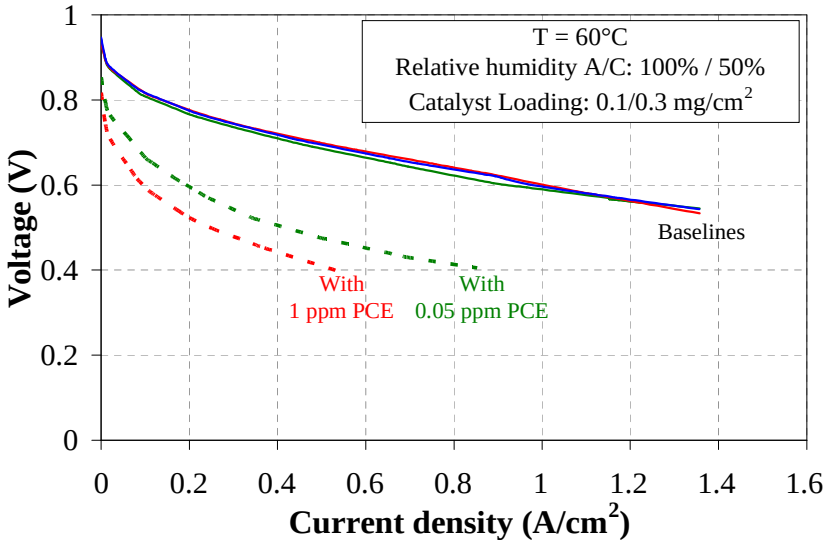

Figure 4.3.4-2: Polarization curves while poisoning with 1 ppm PCE and 0.05 ppm of PCE after steady state saturation has been reached.

To further investigate the effect of PCE, a hydrogen pump experiment was used to characterize changes in the anode and membrane during poisoning. By performing the H_2 pump on a H_2/N_2 system that was being poisoned at similar conditions to an operating fuel cell, results could be obtained without observing the effect of the cathode overpotential. Figure 3 (a) and (b) show the results from the polarization scan and the galvanostatic polarization at 1 A/cm^2, respectively, at different times in the presence of 30 ppm of PCE. The introduction of PCE showed no effect on the overpotential of the H_2 oxidation. Also, the slope of the curve in Figure 3 (a), which can be related to the resistance of the cell, showed no significant changes within the 4 hr period. This result seems to indicate that the detrimental effects of PCE are linked to the cathode side

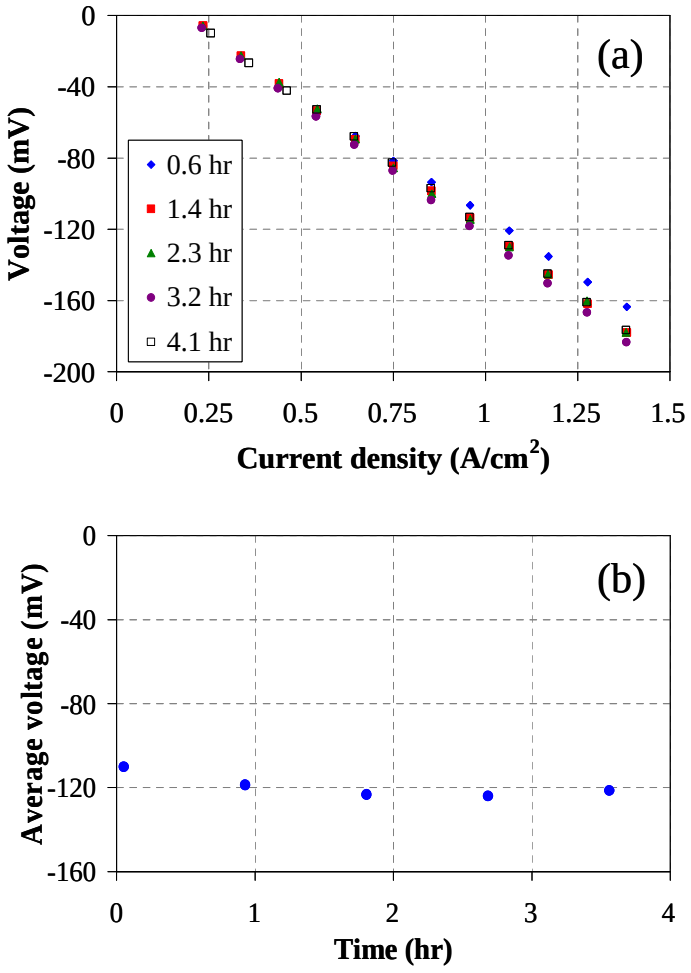

Figure 3: **H_2/N_2 galvanostatic polarization at 1 A/cm^2 in the presence of 30 ppm PCE showing (a) polarization scans; and (b) average polarization as function of time.**

EIS characterization was performed before and after the cell was poisoned with PCE. The results shown in Figure 44-4 reveal that the membrane resistance was unchanged from

the value before poisoning for the different concentrations tested. The difference observed at low frequencies for the 1 ppm curve before and after the cell was poisoned is likely related to a small transient change in the humidity at the catalyst layer. Small changes in humidity can cause a difference in the EIS spectra at these frequencies. However, this does not affect the results observed for the membrane resistance. This analysis further suggests that the detrimental effects of PCE are not related to an increase in membrane losses.

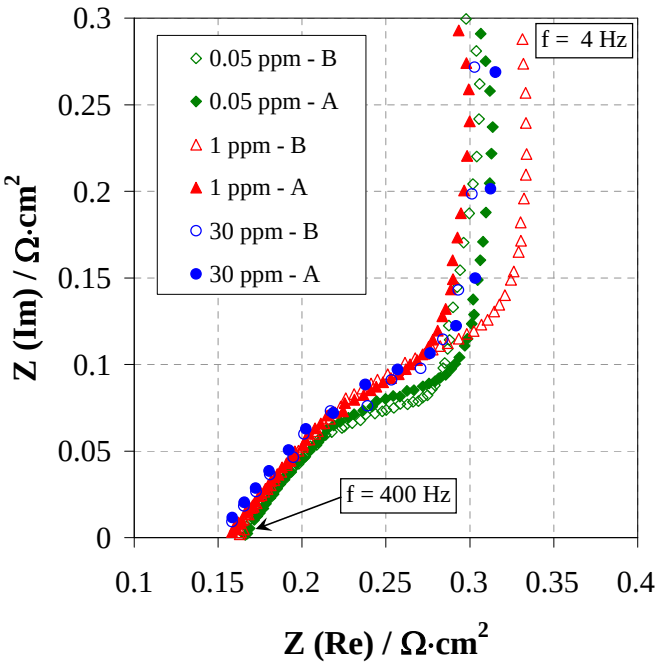

Figure 4: **EIS characterization before (B); and after (A) the cell was poisoned with various concentrations of PCE.**

A set of poisoning experiments were performed in order to identify the conditions at which a poisoning or a recovery is observed. Table summarizes the conditions and the results of these experiments. Step 1 shows the poisoning with 30 ppm PCE followed by the neat H_2 (step 2) while the cell was polarized to 0.6 V. After 6 hours an open circuit with N_2/H_2 in the anode/cathode respectively (step 3) was performed to simulate the conditions during CVs, but without the potential cycling. At this condition a full recovery was obtained. Note that during open circuit (step 3) the cell performance could not be observed. Consequently, the cell recovery obtained in step 3 was actually observed at the beginning of step 4 when the cell started from full performance with only a small linear decay in baseline current. It is believed that the slow decay obtained in step 4 after the cell was switched back to H_2/Air while polarized at 0.6 V is due to desorption of PCE from the gas lines. An increase in the gas stoichiometry (step 5) was performed for a short time to evaluate the effect of higher gas flow rates. However, only a temporary increase in current was observed attributed to better mass transport. The cell continued to degrade in this step. In step 6 an open circuit condition was performed, but this time with

Table 4.3.4-1: Summary of performance recovery studies.

Step	Voltage (V)	Anode				Cathode			Time at Specified Conditions (min)	Effect on Cell Performance
		PCE (ppm)	Gas	Stoich	Flow (sccm)	Gas	Stoich	Flow (sccm)		
1	0.6	30	H_2	1.2	-----	Air	2	-----	144	Rapid and complete degradation.
2	0.6	0	H_2	1.2	-----	Air	2	-----	198	About 14% recovery.
3	OCP (0.1)	0	N_2	-----	250	H_2	-----	250	73	Full recovery.
4	0.6	0	H_2	1.2	-----	Air	2	-----	937	About 38% degradation due to residual PCE desorption from gas lines.
5	0.6	0	H_2	2.5	-----	Air	2.5	-----	124	No recovery. Degradation continues.
6	OCP (0.88)	0	H_2	1.2	-----	Air	2	-----	60	No recovery.
7	0.6	0	H_2	1.2	-----	Air	2	-----	52	No recovery. Degradation reaches steady state.
8	OCP (0.1)	0	H_2	-----	250	N_2	-----	250	57	Full recovery.
9	0.6	0	H_2	1.2	-----	Air	2	-----	1127	About 81% degradation due to residual PCE desorption from gas lines.
10	0.6	30	H_2	1.2	-----	Air	2	-----	80	Rapid and complete degradation.
11	OCP (0.73)	0	H_2	-----	250	Air	-----	250	60	No recovery.
12	0.6	0	H_2	1.2	-----	Air	-----	250	32	About 9% recovery.
13	OCP (0.74 - 0.6)	0	N_2	-----	250	Air	-----	250	61	No recovery.
14	0.6	0	H_2	1.2	-----	Air	2	-----	59	About 87% degradation due to residual PCE desorption from gas lines.
15	OCP (0.4 - 0.2)	0	N_2	-----	250	N_2	-----	250	60	Full recovery.
16	0.6	0	H_2	1.2	-----	Air	2	-----	92	About 75% degradation due to residual PCE desorption from gas lines.
17	0.6	30	H_2	1.2	-----	Air	2	-----	24	Cell performance decay quickly with time.
18	0.5	30	H_2	1.2	-----	Air	2	-----	8	Cell performance decay quickly with time.
19	0.4	30	H_2	1.2	-----	Air	2	-----	13	Cell performance decay quickly with time.
20	0.3	30	H_2	1.2	-----	Air	2	-----	16	Cell performance decay slightly with time.
21	0.2	30	H_2	1.2	-----	Air	2	-----	16	Cell performance recovers quickly with time.

H_2/Air. No recovery was observed. The cell was set back to the original condition of H_2/Air at 0.6 V (step 7) followed by an open circuit but with H_2/N_2 (step 8). Note that step 8 is similar to step 3, except that the gases are switched between the anode and the cathode. Again, at this condition a full recovery was obtained.

Between steps 9 and 16 the cell was poisoned for a second time with 30 ppm of PCE and tests were performed using different flow rates and gases combination in the anode and the cathode. In these steps only the use of N_2/N_2 at open circuit (step 15) resulted in full recovery of the cell. Subsequently, the effect of operating the fuel cell (H_2/Air) at lower voltages in the presence of PCE was tested (steps 17 – 21). When the cell was maintained at 0.3 V (step 20) only a slightly decay in performance was observed. However, when the cell was maintained at 0.2 V (step 21) a quick recovery of the cell performance occurred.

From Table it can be observed that the experiments that produce full cell recovery all have a voltage of 0.2 V or lower. These results are consistent with the lack of impact for PCE on hydrogen pump experiments that were discussed previously. These results suggest that PCE mostly affects the cell at high potentials and complete recovery can be obtained when the cell potential is below 0.2 V. The low potential can be achieved either by purging with inert gas or hydrogen on the cathode or by applying a load which causes the cell voltage to be below 0.2 V. This could explain why PCE was not detected during the CV experiments which were performed after the cell was purged with N_2 in order to switch from H_2/air to N_2/H_2 in the anode/cathode respectively. During this switch, the low potential created in the cell could have been causing the cell to recover immediately. A suggested cleaning and recovery procedure needs to be incorporated, such as purging, in order to allow all PCE to desorb from the system lines.

Further experiments were conducted by connecting an FT-IR spectrometer to the anode and cathode gas flow of the fuel cell. Figure 4-5 shows the results of the PCE concentration detected at different points in the fuel cell. The spectrum of gaseous PCE had three main peaks in the region between 700 and 1000 cm^{-1} [Silverstein 1991]. From this spectrum, the strong peak at 915 cm^{-1} (see insert of Figure) was used to monitor the PCE. This peak represents the symmetric stretching of the C-Cl_2 bonds [Bertrand 2005]. Accordingly, a concentration of 164 ppm of PCE was injected at the anode inlet. However, a substantial reduction to 41 ppm was detected at the anode outlet during open circuit. Moreover, after a current of 0.6 A/cm^2 was applied to the cell, the PCE concentration was further reduced to 5.4 ppm. No PCE was detected at the cathode outlet during any of the tests. In order to investigate if other species were forming during the injection of PCE to the anode, a wider IR region was used during the scan. In this test, 106 ppm PCE were introduced to the anode and detected by the FT-IR as shown in Figure . However, at OCV and at 100 mV the peak of C-Cl_2 disappeared almost completely and a new peak appeared between 2830 and 3095 cm^{-1}. This new peak most likely corresponds to the symmetric stretching of the C-H bonds [Den 2006]. These results suggest that PCE is decomposing in the fuel cell, possibly to a partially or fully hydrogenated hydrocarbon that leaves the anode side in the gas stream and a chlorinated compound that crosses the membrane over to the cathode and poisons the electrocatalysts inhibiting the oxygen reduction reation. The electrochemical results indicate that the chlorinated compounds at the cathode desorbs from the electrode at low potentials. However, more detailed studies are required to understand the poisoning mechanism of PCE, although the fundamental study in section 4.1.5 of this reports sheds some light on this.

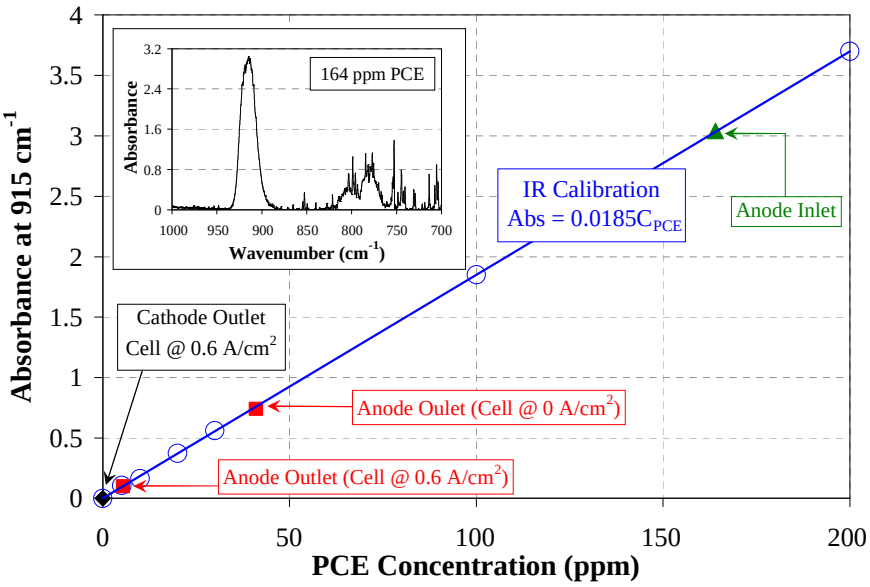

Figure 4.3.4-5: **FT-IR calibration and concentration detected during fuel cell operation for PCE using the absorbance band of the PCE gas phase spectrum (figure insert) at the frequency of 915 cm^{-1}.**

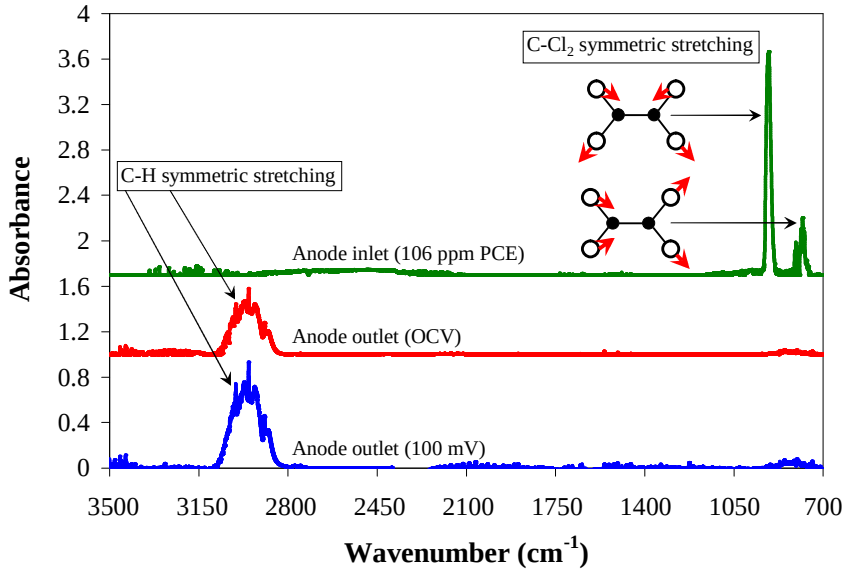

Figure 4.3.4-6: **FT-IR spectra of the anode gas inlet and outlet of the fuel cell when 106 ppm PCE is introduced in the anode.**

For further details about this study, please refer to:

"The Effect of Low Concentrations of Tetrachloroethylene on Performance of PEM Fuel Cells," ***Journal of the Electrochemical Society*** 158 (2011) 1-5 (Michael J. Martinez-Rodriguez, Elise B. Fox, William D. Rhodes, Christopher S. McWhorter, Scott Greenway, and Hector R. Colon-Mercado).

4.3.5 Effect of Hydrocarbons

Tetrahydrofuran (THF) was studied as a hydrocarbon model molecule. It was selected due to its wide use as a common solvent for many chemical syntheses. It is widely used for the production of hydrogen storage materials for the solid state storage of hydrogen for fuel cells. In this study, we tested 3 different concentrations in the hydrogen stream including concentrations at 0.5 ppm which corresponds to the hydrocarbon ISO limit of 2 ppm per carbon basis. While no effects have been observed on the ionic conductivity and during cyclic voltammetry, a large effect on the fuel cell performance was observed as indicated in the potentiostatic curve for a Gore MEA in Figure . As it can be observed, there was a drop in performance in the range of 42 % to 16 % for concentrations between 5 ppm and 0.5 ppm of THF, respectively. Even at the low concentration of 0.5 ppm the drop occurred fast, reaching steady state in approximately 25 hours. However the short term effects were only temporary since once the impurity was removed the fuel cell performance recovered.

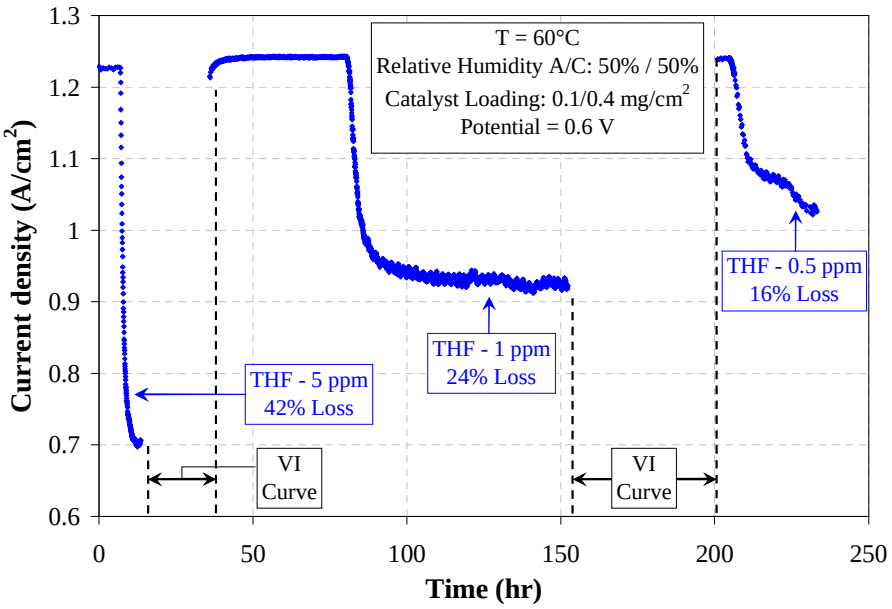

Figure 4.3.5-1: Potentiostatic (0.6 V vs. DHE) current decay and recovery during various concentrations of THF in the hydrogen stream in a 50 cm^2 Gore MEA with an anode Pt loading of 0.1 mg/cm2 at 60 °C and 50 % RH.

Figure shows the polarization before and during the THF poisoning, and after the recovery. This figure confirms the complete fuel cell recovery once the impurity is removed. Long term

fuel cell performance in the presence of THF will be studied in order to investigate if THF polymerizes inside the fuel cell electrodes.

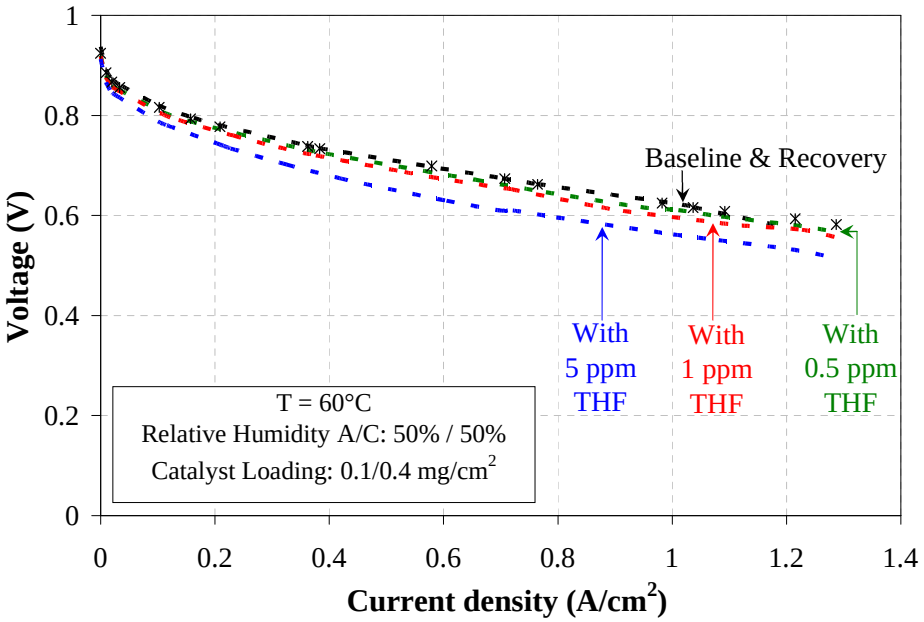

Figure 4.3.5-2: Polarization scan before, during and after recovery of the fuel cell during various concentrations of THF in the hydrogen stream in a 50 cm^2 Gore MEA with an anode Pt loading of 0.1 mg/cm2 at 60 °C and 50 % RH.

4.3.6 Effect of Diborane (B_2H_6)

Diborane (B_2H_6, DB) was being studied as a model molecule for hydrogen storage boron compounds. Diborane is the main impurity released during the dehydrogenation of many boron-based chemical and complex metal hydrides such as ammonia borane, which are being looked at as alternatives by the HSECoE (Hydrogen Storage Engineering Center of Excellence). In previous sections, we reported the effects of contaminants arising from the preparation and use of hydrogen storage materials such as THF and ammonia. These results indicate considerable performance degradation, affecting the membrane and ionomer (ammonia) and apparently the catalyst layer (THF).

In this DB study, we tested a concentration of 50 ppm in the hydrogen stream flowing into a Gore MEA with a Pt loading of 0.1/0.4 mg Pt/cm^2 (anode/cathode) and tested at 60ºC humidified at 50/50 %RH. The DB impurity was introduced in an Ar stream from a mixture in a specialty gas cylinder containing 160 ppm in Ar. While no effects were observed on the ionic conductivity and during cyclic voltammetry, a large effect on the fuel cell performance was observed as indicated in the potentiostatic curve for a Gore MEA in Figure . As it can be seen, there was a drop in performance of about 39% for a concentration of 50 ppm DB. While the effects seemed to be severe, the cell recovered as soon as the DB was removed from the stream.

However, the recovery took much longer and the recovery curve seemed to be linear, contrary to the poisoning curve which was exponential.

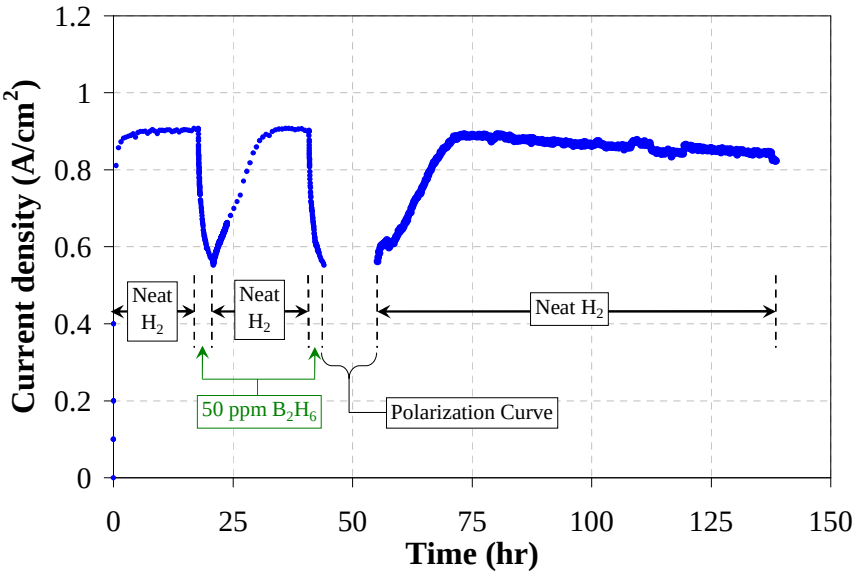

Figure 4.3.6-1: Potentiostatic (0.6 V vs. DHE) current decay and recovery during poisoning with 50 ppm of diborane in the hydrogen stream in a 50 cm^2 Gore MEA with an anode Pt loading of 0.1 mg/cm2 at 60 °C and 50 % RH.

Figure shows the polarization before, during and after recovery from the DB poisoning. The figure shows that the loss in performance arose mostly from the kinetic limited section (voltage drop in the low current area). While this behavior was observed during the polarization curves, no indication of catalyst poisoning was observed during cyclic voltammetry. After the DB poisoning, the cell recovered almost 100%.

4.3.7 Conclusions

Runs at ISO proposed concentration levels showed that some impurities, such as ammonia, do not cause degradation to the fuel cell. Other compounds, however, such as carbon monoxide, cause enough degradation at the ISO proposed concentration to compromise the overall total FC performance target, although the FC system can recover by following specific recovery procedures. Hydrocarbon and halocarbon compounds such as tetrahydrofuran and perchloroethylene can cause serious degradation. However, the degradation can be reversed. In the case of tetrahydrofuran, when the impurity is removed from the hydrogen stream the performance completely recovers. In the case of perchloroethylene the recovery involves flushing of the system with a gas combination that will lower the cell potential. As with tetrahydrofuran, the effects of diborane are temporary and complete recovery is observed after the impurity is removed from the system. This is the first time the effects of THF and diborane are documented in fuel cell research.

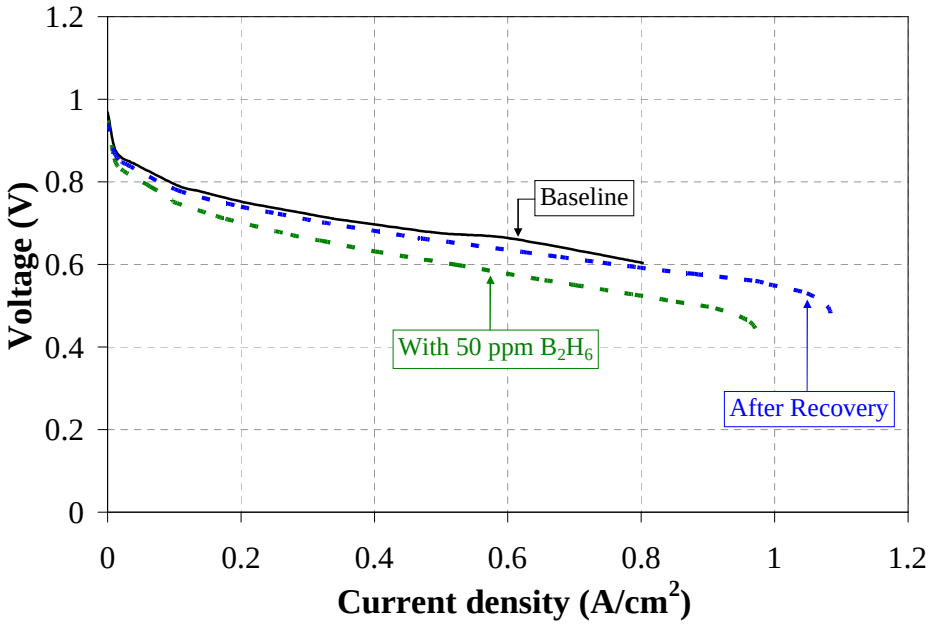

Figure 4.3.6-2: Polarization scan before, during and after recovery of the fuel cell during 50 ppm of diborane in the hydrogen stream in a 50 cm^2 Gore MEA with an anode Pt loading of 0.1 mg/cm2 at 60 °C and 50 % RH.

References

Bertrand, O.; G. Weber, S. Maure, V. Bernardet, J. P. Bellat and C. Paulin, Journal of Physical Chemistry B, 109 (**2005**) 13312.

Den, W.; V. Ravindran and M. Pirbazari, Chemical Engineering Science 61 (**2006**) 7909.

Silverstein, R.M: G. C. Bassler and T. C. Morrill, Spectrometric Identification of Organic Compounds, John Wiley & Sons, New York (**1991**).

5.0 STRATEGIES/MEANS TO REDUCE IMPACT OF IMPURITIES ON FUEL CELL PERFORMANCE

While the project primarily focused on investigating the effects of various classes of impurities on fuel cell operation, the following impurity mitigation strategies can be proposed based on the findings of this project:

- Use of higher %RH results in a smaller decrease in conductivity with NH_3 poisoning. Thus, a higher %RH is recommended for FC operation to increase the performance and lifetime when trace amounts of NH_3 are present in the fuel.

- Fuel cells can tolerate up to 0.1 ppm of NH_3 (maximum ISO specified level) for long periods of time.

- NH_3 poisoning can be partially reversed with time, however the impact of metal cations while similar, leads to an MEA that is essentially permanently degraded.

- Although water vapor does not appear to strongly affect CO poisoning at equilibrium, it does appear to increase the kinetics of recovery of the Pt surface in hydrogen. Thus, use of high humidity during regeneration after exposure to CO is suggested.

- Since it would be hard to eliminate the formation of H_2O_2 during fuel cell operation, it is absolutely imperative to minimize the presence of Fe and other metal ions to prevent greater degradation of the Nafion.

- Chlorine-containing impurities like PCE (perchloroethylene) can be detrimental to FC performance at even ppb levels. Their effect can probably be minimized and reversed by either imposing or changing the operating conditions so that the FC operates at low potentials.

- Tetrahydrofuran (400 ppm) and diborane (50 ppm) degrade fuel cell performance, but the effect seems to be reversible. For optimum performance, obviously these impurities should be minimized in the fuel/air streams.

Obviously, the actual materials and operational conditions chosen for use in a FC must be determined by an optimization of material properties, operation conditions, possible mitigation strategies to minimize the effect of impurities, and desired FC performance.

6.0 RECOMMENDATIONS FOR FUTURE WORK

Future work should include the study of the combined effects of multiple impurities on the performance of the fuel cell. It is expected that detrimental effects of some impurities on FC performance may be additive. In other cases, one will have the greater impact as each of the different impurities affect different critical components in the MEA.

Experiments using some of the techniques employed or developed in this project offer direct means to study impurity effects on the various active components in FC MEAs. This would allow rapid screening for impurity tolerance of new proton transport materials and catalysts, as well as an important way to investigate the mechanisms of impurity poisoning.

7.0 PUBLICATIONS

- "Influence of Ammonia on the Conductivity of Nafion Membranes," ***Journal of Power Sources*** 195 (2010) 30-38 (Kitiya Hongsirikarn, Jack Zhang, James G.Goodwin, Jr., Scott Greenway, and Stephen Creager).
- "The Effect of Low Concentrations of CO on H_2 Adsorption and Activation on Pt/C," ***Journal of Power Sources*** 195 (2010) 3060-3068 (Jack Z. Zhang, Zhiming Liu, and James G. Goodwin, Jr.).

- "Esterification as a Diagnostic Tool to Predict Proton Conductivity Affected by Impurities on Nafion Components for Proton Exchange Membrane Fuel Cells," ***Journal of Power Sources*** 195 (2010) 3416-3424 (Kitiya Hongsirikarn, Xunhua Mo, and James G. Goodwin, Jr.).
- "Prediction of the Effective Conductivity of Nafion in the Catalyst Layer of a PEMFC," ***Journal of Power Sources*** 195 (2010) 5493-5500 (Kitiya Hongsirikarn, Xunhua Mo, Zhiming Liu, and James G. Goodwin, Jr.).
- "Effect of Cations (Na^+, Ca^{2+}, Fe^{3+}) on the Conductivity of a Nafion Membrane," ***Journal of Power Sources*** 195 (2010) 7213-7220 (Kitiya Hongsirikarn, James G. Goodwin, Jr., Scott Greenway, and Stephen Creager).
- "Effect of Ammonium Ion Distribution on Nafion® Conductivity," ***Journal of Power Sources*** 196 (2011) 644-651(Kitiya Hongsirikarn, Thirapong Napapruekchart, Xunhua Mo, and James G. Goodwin, Jr.).
- "The Effect of Low Concentrations of Tetrachloroethylene on Performance of PEM Fuel Cells," ***Journal of the Electrochemical Society*** 158 (2011) 1-5 (Michael J. Martinez-Rodriguez, Elise B. Fox, William D. Rhodes, Christopher S. McWhorter, Scott Greenway, and Hector R. Colon-Mercado).
- "Effect of H_2O_2 on Nafion® Properties and Conductivity at Fuel Cell Conditions," ***Journal of Power Sources*** 196 (2011) 3060-3072 (Kitiya Hongsirikarn, Xunhua Mo, James G. Goodwin, Jr., and Stephen Creager).
- "Structure Sensitivity of Cyclopropane Hydrogenolysis on Carbon-Supported Platinum," ***Journal of Catalysis*** 280 (2011) 89-95 (Jack Z. Zhang, Yu-Tung Tsai, Khunya Leng Sangkaewwattana, and James G. Goodwin, Jr.).
- "The Effect of Low Concentrations of CO on H_2 Adsorption and Activation on Pt/C: Part 2 – in the Presence of H_2O Vapor," ***Journal of Power Sources*** 196 (2011) 6186-6195 (Jack Z. Zhang, Kitiya Hongsirikarn, James G. Goodwin, Jr.).
- "Effect and Siting of Nafion® in a Pt/C PEM Fuel Cell Catalyst," ***Journal of Power Sources*** 196 (2011) 7957-7966 (Jack Z. Zhang, Kitiya Hongsirikarn, and James G. Goodwin, Jr.).
- "The Effect of Low Concentrations of Tetrachloroethylene on H_2 Adsorption and Activation on a Pt Fuel Cell Catalyst," ***Journal of Power Sources*** 196 (2011) 8391-8397 (Jack Z. Zhang, Hector Colon-Mercado, and James G. Goodwin, Jr.).
- "The Effect of Low Concentrations of Ammonia on the Performance of PEM Fuel Cells," manuscript in preparation (Scott D. Greenway, Michael J. Martinez-Rodriguez, and Hector R. Colon-Mercado).
- "Effect of Tetrahydrofuran and Diborane on the Performance of PEM Fuel Cells," manuscript in preparation (Scott D. Greenway, Michael J. Martinez-Rodriguez, and Hector R. Colon-Mercado).

8.0 PRESENTATIONS

- "Effect of Impurities on Fuel Cell Performance and Durability," oral presentation, Dept. of Energy Office of Hydrogen, Fuel Cell, and Infrastructure Technologies New Fuel Cell Projects Kickoff Meeting, Washington, DC, Feb. 13-15, 2007 (James G. Goodwin, Jr.,

Jack Zhang, Kitiya Hongsirikarn, Zhiming Liu, William Rhodes, Hector Colon-Mercado, and Peter Finamoore).

- "Effects of Impurities on Fuel Cell Performance and Durability," poster, 2007 Annual Dept. of Energy Hydrogen Program Review Meeting, Washington, DC, May 15-18, 2007 (James G. Goodwin, Jr., Jack Zhang, Kitiya Hongsirikarn, Zhiming Liu, William Rhodes, Hector Colon-Mercado, and Peter Finamoore).
- "Effects of Impurities on Fuel Cell Performance and Durability," oral presentation, Fuel Cell Tech Team Meeting, Southfield, Michigan, November 2007 (James G. Goodwin, Jr., Jack Zhang, Z-M Liu, Kitiya Hongsirikarn, S. Creager, William Rhodes, Hector Colon-Mercado, Scott Greenway, and Peter Finamoore).
- "Effects of Impurities on Fuel Cell Performance and Durability," oral presentation, 2008 Annual Dept. of Energy Hydrogen Program Review Meeting, Washington, DC, June 9-13, 2008 (James G. Goodwin, Jr., Jack Zhang, Kitiya Hongsirikarn, Zhiming Liu, William Rhodes, Hector Colon-Mercado, Scott Greenway, and Peter Finamoore).
- "Effects of Impurities on Fuel Cell Performance and Durability," oral presentation, Fuel Cell Tech Team Meeting, August 2008 (James G. Goodwin, Jr., Jack Zhang, Z-M Liu, Kitiya Hongsirikarn, S. Creager, William Rhodes, Hector Colon-Mercado, Scott Greenway, and Peter Finamoore).
- "Esterification as a Diagnostic Tool to Investigate the Proton Activity of the Nafion Components of a PEMFC," poster presentation, Southeastern Catalysis Society 7th Annual Fall Symposium, Asheville, NC, September 28-29, 2008 (Kitiya Hongsirikarn, Jack Zhang[a], James G.Goodwin, Jr., and Scott Greenway).
- "The Effect of Low Concentration CO on H_2 Activation on Pt/C," poster presentation, Southeastern Catalysis Society 7th Annual Fall Symposium, Asheville, NC, September 28-29, 2008 (Jack Zhang and James G. Goodwin, Jr.).
- "Effects of Impurities on Fuel Cell Performance and Durability," oral presentation, 2009 Annual Dept. of Energy Hydrogen Program Review Meeting, Washington, DC, May, 2009 (James G. Goodwin, Jr., Jack Zhang, Kitiya Hongsirikarn, Hector Colon-Mercado, Scott Greenway, and Peter Finamoore).
- "The Effect of Low Concentrations of CO on H_2 Activation on Pt/C," poster presentation, 21th North American Meeting of the North American Catalysis Society, San Francisco, CA, June 5-10, 2009 (Jack Zhang, Kitiya Hongsirikarn, and James G. Goodwin, Jr.).
- "Influence of Ammonia on the Conductivity of Nafion Membranes," oral presentation, ACS National Meeting, Washington, DC, August 2009 (Kitiya Hongsirikarn, James G. Goodwin, Jr., and Scott Greenway).
- "Hydrogen Surface Coverage of Pt/C in Presence of CO," Southeastern Catalysis Society Annual Symposium, oral presentation, Asheville, NC, Sept. 27-28, 2009 (Jack Z. Zhang, Zhiming Liu, James G. Goodwin, Jr.).
- "Effects of Impurities on Fuel Cell Performance and Durability," oral presentation, Fuel Cell Tech Team Meeting, October 2009 (James G. Goodwin, Jr., Jack Zhang, Kitiya Hongsirikarn, Michael Martinez, Hector Colon-Mercado, Scott Greenway, and Peter Finamoore).
- "Effects of Impurities on Fuel Cell Performance and Durability," oral presentation, 2010 Annual Dept. of Energy Hydrogen Program Review Meeting, Washington, DC, June 7-11, 2010 (James G. Goodwin, Jr., Jack Zhang, Kitiya Hongsirikarn, Xunhua Mo, Hector Colon-Mercado, Scott Greenway, Michael Martinez, and Peter Finamoore).

- "Prediction of the Conductivity of Nafion® Components in a PEMFC Using an Acid-Catalyzed Reaction", oral presentation, Southeastern Catalysis Society 9th Annual Fall Symposium, Asheville, NC, Sept. 26-27, 2010 (Kitiya Hongsirikarn, Xunhua Mo, Zhiming Liu, and James G. Goodwin, Jr.).
- "Interaction of Nafion® with Pt in a PEM Fuel Cell Catalyst", oral presentation, Southeastern Catalysis Society 9th Annual Fall Symposium, Asheville, NC, Sept. 26-27, 2010 (Jack Z. Zhang, Kitiya Hongsirikarn, and James G. Goodwin, Jr.).
- "Fundamental Effects of Impurities on Fuel Cell Performance and Durability," oral presentation, Fuel Cell Tech Team Meeting, Southfield, Michigan, December 9, 2010 (J.G. Goodwin, Jr., Jack Zhang, K. Hongsirikarn, Xunhua Mo, Hector Colon-Mercado, Michael Martinez and Scott Greenway).
- "Effects of Impurities on Fuel Cell Performance and Durability," poster presentation, 2011 U.S. DOE Hydrogen Program Annual Merit Review and Peer Evaluation Meeting, Washington, DC, May 9, 2011 (James G. Goodwin, Jr., Jack Zhang, Kitiya Hongsirikarn, Hector Colon-Mercado, Scott Greenway, Michael Martinez, and Peter Finamoore).